

DESIGN OF A 10 MHZ TRANSIMPEDANCE LOW-PASS FILTER WITH SHARP
ROLL-OFF FOR A DIRECT CONVERSION WIRELESS RECEIVER

A Thesis

by

JAMES KEITH HODGSON

Submitted to the Office of Graduate Studies of
Texas A&M University
in partial fulfillment of the requirements for the degree of

MASTER OF SCIENCE

May 2009

Major Subject: Electrical Engineering

DESIGN OF A 10 MHZ TRANSIMPEDANCE LOW-PASS FILTER WITH SHARP
ROLL-OFF FOR A DIRECT CONVERSION WIRELESS RECEIVER

A Thesis

by

JAMES KEITH HODGSON

Submitted to the Office of Graduate Studies of
Texas A&M University
in partial fulfillment of the requirements for the degree of

MASTER OF SCIENCE

Approved by:

Chair of Committee,	Aydin Karsilayan
Committee Members,	Jose Silva-Martinez
	Frederick Strieter
	Philip Yasskin
Head of Department,	Costas Georgiades

May 2009

Major Subject: Electrical Engineering

ABSTRACT

Design of a 10 MHz Transimpedance Low-Pass Filter with Sharp Roll-Off for a Direct Conversion Wireless Receiver. (May 2009)

James Keith Hodgson, B. S., Texas A&M University

Chair of Advisory Committee: Dr. Aydin Karsilayan

A fully-differential base-band transimpedance low-pass filter is designed for use in a direct conversion wireless receiver. Existing base-band transimpedance amplifiers (TIA) often utilize single-pole filters which do not provide good stop-band rejection and may even allow the filter to saturate in the presence of large interferers near the edge of the pass-band. The designed filter is placed in parallel with an existing single-pole TIA filter and diverts stop-band current signals away from the existing filter, providing added rejection and safeguarding the filter from saturating. The presented filter has a bandwidth of 10 MHz, achieves 35 dB rejection at 50 MHz (25 dB in post-layout simulations), and can process interferers as large as 10 mA. The circuit is designed in Jazz 0.18 μm CMOS technology, and it is shown, using macromodels, that the design is scalable to smaller, faster technologies.

To my beautiful wife, ma chère, Courtney

ACKNOWLEDGEMENTS

I would like to thank the people who made this research project and thesis possible. First, I would like to express many thanks to my advisor Dr. Aydin Karsilayan, whose fine marketing skills convinced me during my time in his undergraduate engineering course to pursue a graduate degree in analog electronics. I would also like to thank him for all the insight and encouragement he provided in our many discussions and meetings.

I am also grateful to Dr. Jose Silva-Martinez for serving on my committee as well as for the technical knowledge he imparted to me in his classes and in our meetings. Special gratitude goes to Dr. Frederick Strieter and Dr. Philip Yasskin for taking time out of their busy schedules to serve on my committee. My peers in the Analog and Mixed Signal program deserve thanks for their helpful advice and encouragement. Specifically, I would like to thank Alfredo Perez for his ideas and collaboration on this design and Marvin Onabajo for his advice on the chip layout.

I am deeply indebted to my friends and family for all their support throughout this project. Great appreciation goes to my parents and my in-laws for all that they did to support and encourage my wife and me. I would like to thank my grandfather for his interest and unique insight into my design. Finally, I could not have done any of this without the never-ending love, support, and sacrifice of my wonderful wife. She has endured these past couple years with unbelievable patience and grace, and I dedicate this work to her.

TABLE OF CONTENTS

	Page
ABSTRACT	iii
DEDICATION	iv
ACKNOWLEDGEMENTS	v
TABLE OF CONTENTS	vi
LIST OF FIGURES	viii
LIST OF TABLES	xii
CHAPTER	
I INTRODUCTION.....	1
II THE BASIC TRANSIMPEDANCE FILTER	6
2.1 General Specifications	6
2.1.1 Gain	6
2.1.2 Frequency Response.....	7
2.1.3 Input Impedance	8
2.2 Existing TIA Filter	10
2.2.1 Specifications	10
2.2.2 Advantages	11
2.2.3 Drawbacks	14
III THE IMPROVED TRANSIMPEDANCE FILTER	15
3.1 Desired Response	15
3.2 Concept: The Impedance Shaper.....	15
3.2.1 Impedance to Be Shaped: R or C	20
3.2.2 Stability of Higher Order Filters	24
3.2.3 The Twin-T Network	29
3.3 Design of the Improved Transimpedance Filter.....	37
3.3.1 Design Procedure	39
3.3.1.1 The Minimum Value for C_{fb}	39
3.3.1.2 The Ratios C_x to C , C_{in} to C , and the Product RC	40
3.3.1.3 The Values C_x , C_{in} , C , and R	43
3.3.1.4 The Optimum Value of C_{TIA}	43

CHAPTER	Page
3.3.2 Macromodel Simulation Results	44
IV TRANSISTOR LEVEL DESIGN	49
4.1 Higher Order Effects	49
4.2 Filter Design	53
4.2.1 Filter Op Amp Folded-Cascode Gain Stage	55
4.2.2 Filter Op Amp Class AB Output Buffer	64
4.2.3 TIA Op Amp	71
4.3 Layout Considerations	74
4.3.1 Passive Components	75
4.3.2 Active Components	76
4.3.3 Chip Layout	77
V SIMULATION RESULTS	79
5.1 Schematic Level Simulation Results	79
5.2 Post-Layout Simulation Results	90
VI CONCLUSION	99
REFERENCES	101
APPENDIX A	103
APPENDIX B	106
APPENDIX C	108
VITA	120

LIST OF FIGURES

FIGURE	Page
1.1 A basic direct-conversion wireless receiver	2
1.2 Direct-conversion wireless receiver with current-mode passive mixer	3
2.1 The general TIA filter	7
2.2 A single-pole low-pass TIA filter.....	8
2.3 Fully-differential direct-conversion wireless receiver block diagram	11
2.4 Plot of input impedance $Z_{i,TIA}$ for the TIA filter in [4]	12
3.1 $Z_{i,TIA}$ for different GBW.....	16
3.2 The current divider concept.....	17
3.3 The high frequency capacitor C_{hf}	18
3.4 The Miller Effect.....	19
3.5 Impedance shaping of a resistor and a capacitor.....	21
3.6 Resistor thermal spot noise current power density.....	22
3.7 Resistor noise current amplified by the TIA	23
3.8 Impedance Z_{fb} in negative feedback with filter transfer function $H(s)$	25
3.9 Peaking in Z_i from equation (3.14) when Z_{fb} is a 20 pF capacitor	28
3.10 Ringing in input voltage for an input current step	29
3.11 The parallel LC network	30
3.12 The twin-T network.....	31
3.13 The twin-T network with input voltage and load.....	32

FIGURE	Page
3.14 The magnitude transimpedance of the twin-T network.....	33
3.15 AC output current magnitude of each branch of the twin-T network	34
3.16 AC output current phase of each branch of the twin-T network	34
3.17 Twin-T transimpedance for a sweep of R and C when RC product is fixed.....	35
3.18 RCR output current phase deviation for mismatch in one resistor	36
3.19 Twin-T AC output current for mismatch in one resistor.....	37
3.20 Existing transimpedance filter shown on the left hand side	38
3.21 Transimpedance gain.....	45
3.22 Total filter input impedance $Z_{i,tot}$	46
3.23 Transient response to 1 mA current step for all three GBW	46
3.24 Transimpedance gain for $GBW = 3$ GHz.....	47
3.25 Total filter input impedance $Z_{i,tot}$ for $f_{RC} = 65$ MHz, 85 MHz, and 110 MHz.....	48
3.26 Step response for $GBW = 3$ GHz	48
4.1 Effect of the zero created by R_o , dampened by R_z	50
4.2 Sweep of R_z for the circuit in Fig. 4.1	51
4.3 Transimpedance gain in TSMC 0.18 μm	52
4.4 Total filter input impedance, $Z_{i,tot}$, for sweep of C_{hf} from 20 pF to 50 pF..	52
4.5 Filter with component values	55
4.6 Simple NMOS differential pair with fully-differential PMOS load.....	56
4.7 Fully differential cascode op amp	59

FIGURE	Page
4.8 Fully differential folded-cascode op amp.....	60
4.9 Fully differential folded-cascode op amp with compensation	61
4.10 CMFB common-mode detector and error amplifier.....	63
4.11 Class B source-follower buffer	65
4.12 Crossover distortion in class B buffer	66
4.13 Class AB source-follower buffer.....	67
4.14 Class AB common source buffer	68
4.15 Buffer output resistance reduced by error amplifiers	69
4.16 Output buffer with single-ended error amplifiers	70
4.17 Fully-differential OTA from [4].....	72
4.18 Capacitors with common centroid.....	75
4.19 Multi-finger common centroid matched transistors with dummy elements.....	77
4.20 Filter layout in Jazz 0.18 μm	78
5.1 AC response of filter	80
5.2 Small signal input impedance of filter	81
5.3 Filter transient response to 1 mA current pulse.....	81
5.4 New filter response to 10 MHz 100 μA and 50 MHz 1 mA signals	82
5.5 Original filter response to 10 MHz 100 μA and 50 MHz 1 mA signals	83
5.6 New filter response to 10 MHz 100 μA and 50 MHz 10 mA signals	84
5.7 Original filter response to 10 MHz 100 μA and 50 MHz 10 mA signals ..	84
5.8 DFT for new filter 10 MHz 100 μA signal and 50 MHz 10 mA interferer	85

FIGURE	Page
5.9 DFT for original filter 10 MHz 100 μ A signal and 50 MHz 10 mA interferer	86
5.10 DFT of new filter response for 50 MHz and 90 MHz 5 mA signals.....	87
5.11 DFT of original filter response for 50 MHz and 90 MHz 5 mA signals....	87
5.12 New filter DFT for 9 MHz and 10 MHz 500 μ A signals	88
5.13 Original filter DFT for 9 MHz and 10 MHz 500 μ A signals	89
5.14 Input referred spot noise current density	90
5.15 Post-layout AC simulation results.....	91
5.16 Post-layout small signal input impedance	91
5.17 Post-layout transient step response	92
5.18 Post-layout transient response of new filter to 10 MHz 100 μ A and 50 MHz 1 mA signals.....	93
5.19 Post-layout transient response of original filter to 10 MHz 100 μ A and 50 MHz 1 mA signals.....	93
5.20 Transient input voltage waveform in the presence of 10 MHz 100 μ A and 50 MHz 1 mA signals.....	94
5.21 Post-layout transient response of new filter to 10 MHz 100 μ A and 50 MHz 10 mA signals.....	95
5.22 Post-layout transient response of original filter to 10 MHz 100 μ A and 50 MHz 10 mA signals.....	95
5.23 Post-layout DFT of response of new filter to 10 MHz 100 μ A signal and 50 MHz 10 mA interferer	96
5.24 Post-layout DFT of response of original filter to 10 MHz 100 μ A and 50 MHz 10 mA interferer.....	97
5.25 Post-layout simulation of input referred spot noise current density.....	98

LIST OF TABLES

TABLE	Page
3.1 Summary of Components in Macromodel Simulations	45
4.1 Folded Cascode Component Operating Points.....	62
4.2 Folded Cascode CMFB Transistor Operating Points	64
4.3 Output Buffer Transistor Operating Points	71
4.4 TIA Component Operating Points.....	73
4.5 TIA CMFB Transistor Operating Points.....	74
4.6 Amplifier Specifications	74
5.1 Noise Summary	89
5.2 Post-Layout Noise Summary	97

CHAPTER I

INTRODUCTION

Direct-conversion architectures are becoming much more popular in monolithic integrated wireless front-ends than are traditional super-heterodyne architectures for a couple of reasons. First, direct-conversion receivers translate radio frequency (RF) signals directly down to DC instead of to a non-zero intermediate frequency (IF) as is done in heterodyne systems. This avoids the heterodyne problem of generating an interfering image tone which must be filtered out by external circuitry. Second, since the desired base-band frequency is centered at $f = 0$ Hz, only low-pass filters are required in post-mixer blocks instead of other external band-pass elements such as SAW filters [1].

A basic direct-conversion receiver front-end architecture is shown in Fig. 1.1. In the first block, the RF signal coming from the antenna is amplified by a low-noise amplifier (LNA). This signal is then converted down to DC by a mixer with a local oscillator (LO) frequency equal to the desired RF channel. The DC centered signal from the mixer passes through a base-band low-pass filter which further amplifies the signal while rejecting interferers in neighboring channels. After the low-pass filter, the signal is passed to an analog-to-digital converter (ADC) which processes it in the digital domain.

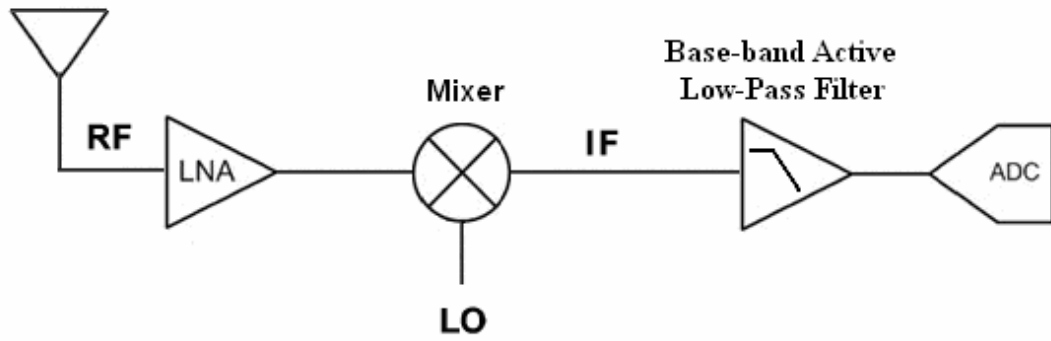


Fig. 1.1 A basic direct-conversion wireless receiver.

Noise is a critical parameter in analog front-ends because its reduction results in improved bit-error rate (BER) in the ADC. For direct-conversion systems, flicker noise is especially critical since the IF signal is located at a very low frequency. Since the mixer is the first block containing the IF signal, its flicker noise is the most important, and unfortunately, it is generally quite high. An empirical flicker noise formula is [2]:

$$v_{n,1/f}^2 = \frac{K_f I_{DS}^{af}}{C_{ox} L^2} \cdot \frac{1}{f^{er}} \quad (1.1)$$

K_f is the flicker noise coefficient, I_{DS} is the bias drain current, C_{ox} is the gate oxide capacitance per unit area, L is the transistor gate length, f is the frequency, and af and er are current and frequency exponents. One method of reducing mixer flicker noise is by utilizing a current-mode passive switching mixer [3]. Since there is effectively zero bias current in the switching devices, the flicker noise is substantially reduced. This

technique is found in the direct-conversion receiver designed in [4]. For a current-mode mixer, the LNA must be a transconductance (current-mode output) amplifier, and the base-band low-pass filter must be a transimpedance (current-mode input) amplifier (TIA). Fig. 1.2 shows the system described in [4] and displays the signal mode under each circuit node. The LNA and ADC inputs are still voltage mode, but LNA output and the low-pass filter input signals are current mode. The focus of the work in this thesis is on the TIA low-pass filter block.

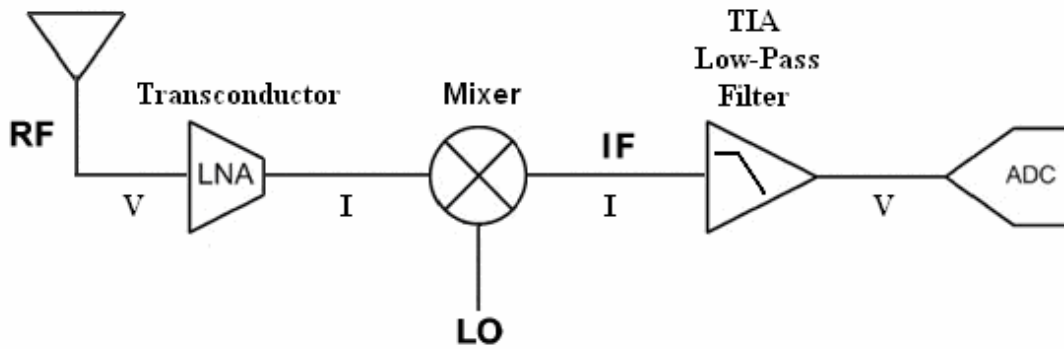


Fig. 1.2 Direct-conversion wireless receiver with current-mode passive mixer.

The purpose of the TIA filter is to amplify a small in-band current to a large output voltage, while rejecting (i.e. amplifying less) a large out-of-band current signal. Ideally, the filter has a “brick wall” response such that signals just outside the bandwidth are totally filtered while signals just within the bandwidth do not suffer any attenuation.

In addition to large gain and a sharp filter response, the TIA filter should ideally have zero input impedance; that is, the voltage swing at the input should always equal

zero no matter how large the incoming current signal. Having small input impedance is important to maintaining the linearity of both the TIA filter and the passive mixer. The input of the TIA is generally composed of a single CMOS differential pair whose input linear range is only about as large as the transistors' overdrive voltage. The mixer contains CMOS transistors operating in the triode region. As long as the drain-source voltage (V_{DS}) of the mixer transistors is small, the channel resistance is very linear. However, as V_{DS} increases, the transistors approach the saturation region and the channel resistance becomes very non-linear. While techniques such as floating-gates and source-degeneration may be employed to increase the input linear range of the TIA, no such techniques exist to linearize the mixer. The only way to achieve linear mixer channel resistance is to have a small voltage swing. This means the input impedance of the TIA must be small.

The TIA filter in [4] is a single-pole low-pass filter with a -3 dB bandwidth of 10 MHz. It provides 20 dB rejection at 100 MHz and only 14 dB rejection at 50 MHz. While this may be considered acceptable in some cases, the purpose of filtering in the analog domain is to relax the specifications of the ADC block. If the interferer level is reduced, then the required number of bits, and thus the complexity and cost, of the ADC can be reduced as well. Additionally, for typical supply voltages around 1 V, the existing filter will saturate if the interferer is greater than a few mA. For example, suppose the existing filter has a 1 V supply, a rail-to-rail output, and receives a 50 MHz interferer. The largest the interferer can be without saturating the amplifier is 5 mA. In practice, interferers up to 10 mA are expected, so additional filtering must be added.

The objective of this thesis is to introduce a filter which will increase the stop-band rejection of the TIA filter block while maintaining very low input impedance and good linearity. The new filter handles large 10 mA interferers without saturating, while at the same time minimizing added noise, area, and power consumption. The filter is designed and laid out in a mature technology (Jazz 0.18 μm CMOS), but it is also simulated using high-speed macromodel amplifiers to show that the filter concept will work in more advanced nanometer-scale technologies.

CHAPTER II

THE BASIC TRANSIMPEDANCE FILTER

While there are many drawbacks to the existing transimpedance filter in [4], a number of advantages exist as well. In order to rectify the weaknesses without sacrificing the benefits, it is necessary to understand the main parameters associated with TIA filters.

2.1 General Specifications

Transimpedance filters are a class of active filters. Active filters, which are composed of operational amplifiers and passive components (i.e. resistors and capacitors) are typically voltage-mode devices. Voltage-mode devices are those which have voltage-mode input and voltage-mode output signals. The two main specifications for active filters are pass-band gain and stop-band rejection. While these are also the basic parameters of TIA filters, they are measured differently because TIA filters receive current signals at the input instead of voltage signals. Other specifications, such as input impedance, are more important to TIA filters. The following sections discuss the specifications of the basic TIA filter.

2.1.1 Gain

The general TIA circuit is shown in Fig. 2.1. The transimpedance gain of the TIA is defined as the output voltage divided by the input current. Voltage divided by

current has units of Ohms (Ω), so it follows that the gain of the TIA is also in units of Ω . The gain of the filter in Fig. 2.1 is always equal to the value of the feedback impedance Z_{TIA} . For example, if Z_{TIA} is simply a 1000 Ω resistor, then the transimpedance gain is equal to 1000 Ω .

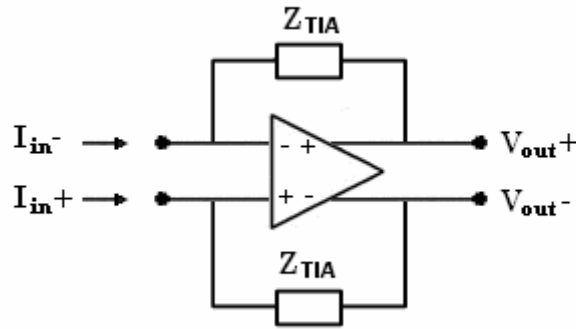


Fig. 2.1 The general TIA filter.

2.1.2 Frequency Response

The feedback impedance Z_{TIA} is generally a frequency dependent impedance, so the gain of the TIA is different at various frequencies. This implies that the TIA can operate as a filter. For instance, if the impedance of Z_{TIA} is large at low frequencies but small at high frequencies, then the overall TIA filter is characterized as a low-pass filter.

An example of a low-pass TIA filter is shown in Fig. 2.2, where Z_{TIA} from Fig. 2.1 is the parallel combination of resistor R_{TIA} and capacitor C_{TIA} . The low frequency gain is equal to R_{TIA} , but the high frequency gain is reduced because the impedance magnitude of C_{TIA} at high frequencies is much lower than the resistance of R_{TIA} .

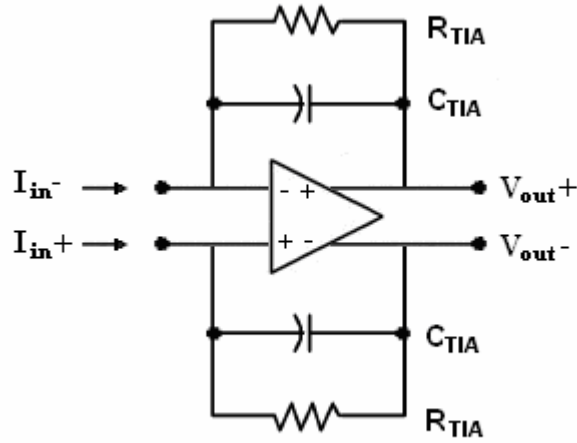


Fig. 2.2 A single-pole low-pass TIA filter.

The gain roll-off of the filter is -20 dB/decade after the corner frequency which is given by the equation:

$$\omega_{RC} = \frac{1}{R_{TIA} C_{TIA}} \quad (2.1)$$

2.1.3 Input Impedance

Ideally the filter's operational amplifier has infinite gain and infinite bandwidth. In this case, the voltage difference between the inputs of the op amp is always zero, meaning the input impedance of the circuit is also equal to zero. In reality, operational amplifiers have finite gain and bandwidth, so the voltage swing at the input, and likewise the input impedance, are small non-zero values. For an amplifier with constant voltage

gain A_v in a negative feedback configuration as in Fig. 2.1, the input impedance $Z_{i,TIA}$ of the circuit is given by the expression:

$$Z_{i,TIA} = \frac{Z_{TIA}}{1 + A_v} \quad (2.2)$$

A simple but fairly accurate model for an op amp open loop transfer function consists of amplifier DC gain A_v and dominant pole ω_p :

$$H(s) = \frac{A_v}{1 + \frac{s}{\omega_p}} \quad (2.3)$$

If the transfer function $H(s)$ in (2.3) is substituted for the constant gain A_v in (2.2), then the input impedance becomes:

$$Z_{i,TIA} = \frac{s(Z_{TIA}) + \omega_p Z_{TIA}}{s + \omega_p (1 + A_v)} \quad (2.4)$$

Examining (2.4) reveals that the DC input impedance reduces to the expression in (2.2). At the pole frequency ω_p , the input impedance is approximately twice the value in (2.2) if A_v is large, and at frequencies much higher than ω_p , the input impedance becomes equal to the feedback impedance Z_{TIA} .

An important figure of merit for the TIA filter op amp is the gain-bandwidth product (GBW). GBW is defined as the product of the DC gain and the dominant pole frequency; thus the GBW of an amplifier with the transfer function given in (2.3) is:

$$GBW = A_v \omega_p \quad (2.5)$$

For good phase margin, the first non-dominant pole is generally designed to be located at frequencies at or beyond the unity gain frequency (UGF), which means the gain bandwidth product and the unity gain frequency are approximately equal. At the unity gain frequency, the input impedance $Z_{i,TIA}$ is exactly half the feedback impedance Z_{TIA} .

2.2 Existing TIA Filter

2.2.1 Specifications

The TIA filter op amp in [4] is fabricated in a 90 nm CMOS process. It is a two stage op amp with a unity gain frequency of 2.8 GHz and a power consumption of 13 mW.

The TIA filter in Fig. 2.2 is the same design as the circuit that is employed as the base-band filter in the direct-conversion wireless receiver described in [4]. Fig. 2.3 shows the fully-differential direct-conversion receiver block diagram with the filter from Fig. 2.2.

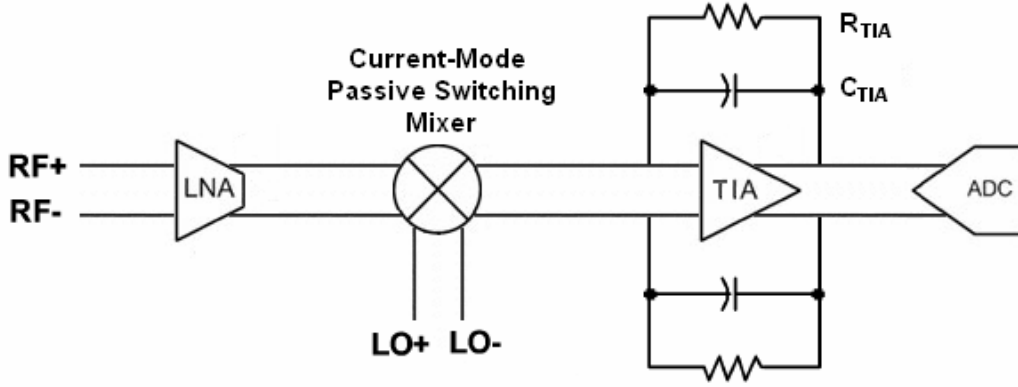


Fig. 2.3 Fully-differential direct-conversion wireless receiver block diagram.

In the receiver from [4], the DC gain of the TIA filter is 1 k Ω and the bandwidth of the down-converted signal is 10 MHz. This means the value of C_{TIA} is approximately 15.91 pF.

2.2.2 Advantages

The single most important advantage of the existing TIA filter over other topologies is its linearity, which is a direct consequence of low input impedance. The input impedance of the TIA filter is so low - well below 10 Ω - because the 2.8 GHz UGF of the amplifier open loop transfer function is far beyond the 10 MHz pole of the feedback network. The equation for the input impedance of the TIA filter with RC feedback is:

$$Z_{i,TIA} = \frac{s(\omega_{RC} R_{TIA}) + \omega_p \omega_{RC} R_{TIA}}{s^2 + s(\omega_{RC} + \omega_p (1 + A_v)) + \omega_{RC} \omega_p (1 + A_v)} \quad (2.6)$$

In equation (2.6), ω_{RC} is the -3 dB bandwidth found in (2.1). The effect of the limited GBW $A_v\omega_p$ is to increase the input impedance, while the effect of the feedback pole ω_{RC} is to reduce the impedance. Since the feedback pole frequency is so much lower than the amplifier UGF, the low impedance effect of the feedback network occurs first and tends to cancel out the effect of the increased impedance due to finite bandwidth. Fig. 2.4 shows a plot of the input impedance for the TIA filter along with the impedance of the filter without C_{TIA} ($Z_{i,TIA,noC}$) and the stand-alone impedance of the feedback network Z_{TIA} . It is assumed that the DC gain of the amplifier is 3000 and the dominant pole is 1 MHz, yielding $GBW = 3$ GHz. This is very close to the value of 2.8 GHz reported in [4].

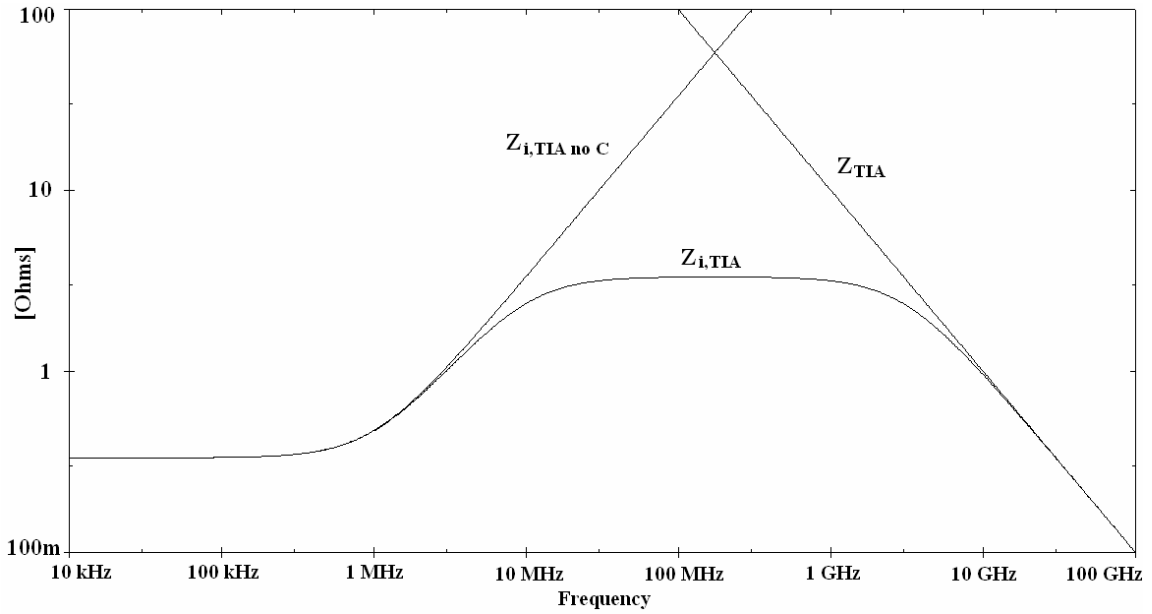


Fig. 2.4 Plot of input impedance $Z_{i,TIA}$ for the TIA filter in [4]. $Z_{i,TIA,no C}$ is the input impedance of the TIA filter with R_{TIA} but excluding C_{TIA} . Z_{TIA} is just the parallel impedance of R_{TIA} and C_{TIA} .

Notice in Fig. 2.4 that there is a hump in the input impedance whose center is located at the crossing of $Z_{i,TIA\ noC}$ and Z_{TIA} . If the GBW of the amplifier is increased, the crossing point is moved to higher frequencies and lower impedances. As a result, the width and height of the hump are also reduced.

The benefit of low input impedance is low voltage swing at the amplifier input. As previously stated, the linearity of the preceding passive mixer block is completely dependent on having a small voltage swing across the mixer transistors. As long as the drain-source voltage of a transistor remains far below the saturation voltage V_{DSAT} , then the transistor remains in the deep triode region and its on-resistance R_{on} is very linear. In Fig. 2.4, the maximum input impedance around 200 MHz is about 4 Ω . If a large 200 MHz 10 mA signal is received, then the voltage swing at the input is 40 mV. For transistors in the strong inversion region, V_{DSAT} is generally greater than 100 mV, so then even for this large signal, the mixer remains linear. The linearity of the TIA op amp is also improved by low voltage swing at the input. Like the mixer transistors, the linear range of a simple differential pair is less than V_{DSAT} . Though linearizing techniques such as source degeneration can increase the input linear range of a differential pair, it is more efficient in terms of power and complexity to use a simple differential pair.

Good linearity is crucial to the operation of the ADC block following the TIA filter. As long as the analog front-end is a linear system, incoming signals can be filtered post-ADC by a digital signal processor (DSP). However, if the analog system is not linear, harmonic distortions may be introduced that are indistinguishable to the DSP from true input signals, resulting in a loss of fidelity.

2.2.3 Drawbacks

While the linearity of the TIA filter may be acceptable, the filter suffers some major drawbacks. The main problem is that the filter rejection has only first order roll-off after the bandwidth ω_{RC} , so there is not a lot of attenuation of large interferers falling just beyond the pass-band. For instance, the DC gain of the filter is $1000\ \Omega$ (60 dB), and the bandwidth is 10 MHz. An interferer at 40 MHz has a gain of 48 dB or about $240\ \Omega$. This is 12 dB rejection from the DC gain and only 9 dB rejection from the gain at 10 MHz. While 9 dB rejection is not large, it may be sufficient if the ADC is good and the DSP can provide the rest of the filtering in the digital domain. However, this may not be enough rejection if the interferer is so large that it causes the filter to saturate.

The trend in modern wireless electronics is towards very low power devices operating with supply voltages around 1 V. If the filter receives a 10 mA signal at 40 MHz, the voltage swing at the output is 2.4 V which will saturate the amplifier. Even the receiver in [4], which operates at 2.3 V to allow extra headroom for large interferers, will saturate in the presence of such a large signal. If the signal is saturating in the analog front-end, there is no way it can be accurately recovered by the succeeding digital blocks. Thus it is critical for the TIA filter to achieve enough attenuation in the near stop-band so that interferers cannot saturate the amplifier.

CHAPTER III

THE IMPROVED TRANSIMPEDANCE FILTER

The disadvantages of the existing TIA filter are very problematic. Due to the saturation of large interferers, simply using traditional cascaded filters to increase rejection cannot be used because they would only serve to filter an already badly distorted signal. Also, since input impedance must remain very low for the mixer to remain linear, no additional filtering can be placed in series with the TIA input. The problem of saturation must be solved by modifying the existing TIA filter block.

3.1 Desired Response

The improved filter must increase the rejection of the existing TIA filter and protect against saturation without sacrificing input impedance and without increasing the area or power consumption too much. Ideally, the filter should have a brick wall low-pass response; that is, constant gain throughout the bandwidth and then an immediate drop to zero gain at the edge of the stop-band. While a perfect brick wall response is impossible to achieve in practice, it is possible to realize sharp roll-off and good attenuation using a limited number of components.

3.2 Concept: The Impedance Shaper

The input impedance of the TIA filter increases as the gain of the filter op amp decreases. Fig. 3.1 shows the input impedance of the existing TIA filter configuration

for various op amp GBW. The first observation is that larger GBW results in lower input impedance. Second, for all cases, the input impedance starts low and then begins to rise after the dominant pole, which is located at 1 MHz. Then at 10 MHz, the pole in the feedback network begins to level off the curve and then eventually reduces the input impedance.

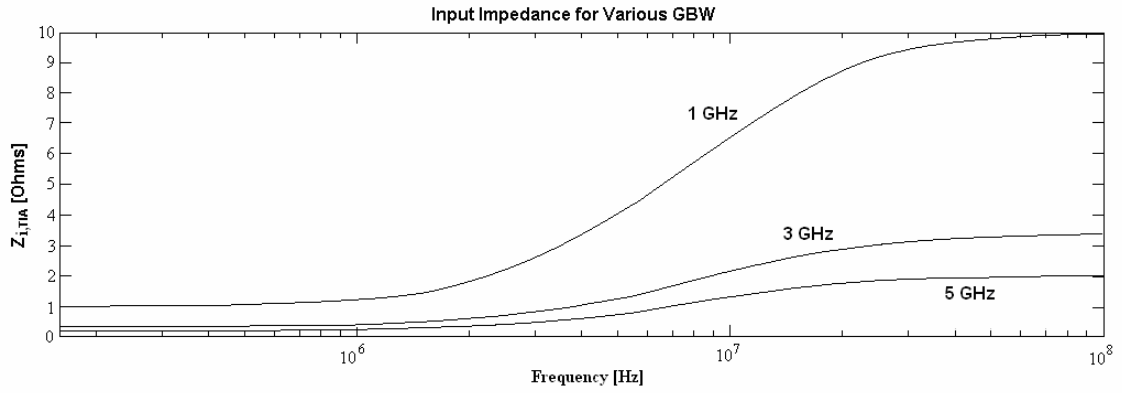


Fig. 3.1 $Z_{i,TIA}$ for different GBW. The amplifier dominant pole is at 1 MHz, and the DC gains are 1000, 3000, and 5000. $C_{TIA} = 15.91$ pF, $R_{TIA} = 1$ k Ω .

The basic concept behind the improved filter is a current divider as shown in Fig. 3.2. The current I_{in} is split into two currents I_1 and I_2 between impedances Z_1 and Z_2 , respectively. The current I_2 is given by the expression:

$$I_2 = I_{in} \frac{Z_1}{Z_1 + Z_2} \quad (3.1)$$

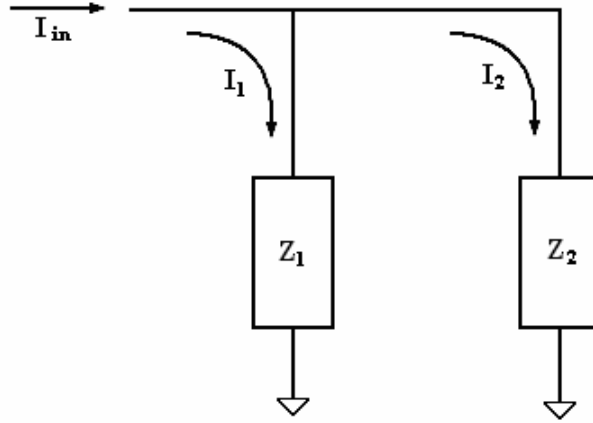


Fig. 3.2 The current divider concept.

If Z_2 is much smaller than Z_1 , then almost all the input current I_{in} passes through Z_2 . On the other hand, if Z_1 is much smaller than Z_2 , almost all the current is routed through Z_1 and Z_2 receives almost none. If the impedance Z_2 is replaced with the input impedance $Z_{i,TIA}$ of the TIA filter, and Z_1 is much larger than $Z_{i,TIA}$ at low frequencies and much smaller at high frequencies, then all current passes through the TIA filter at low frequencies, but is diverted to Z_1 at high frequencies. This concept is actually already exploited in the filter in [4] where Z_1 is a capacitor C_{hf} as shown in Fig. 3.3.

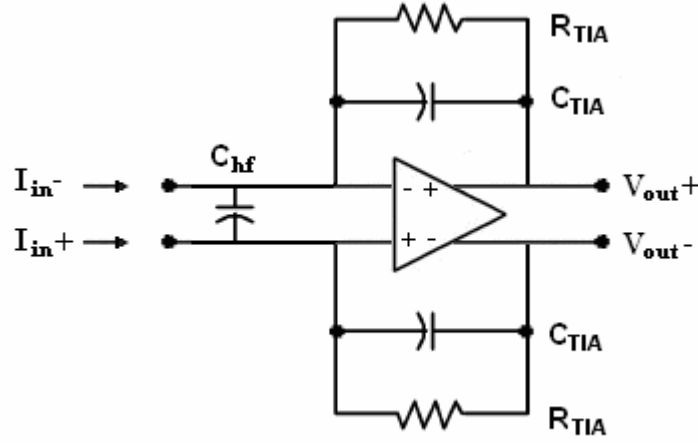


Fig. 3.3 The high frequency capacitor C_{hf} .

The size of an on-chip capacitor C_{hf} cannot be very large, with maximum values being no more than about 100 pF. If $Z_{i,TIA}$ is modeled as a constant $10\ \Omega$ resistance, then the added corner frequency (i.e. the point at which the impedance of C_{hf} and $Z_{i,TIA}$ are equal) is around 160 MHz. This is a best case scenario since in reality $Z_{i,TIA}$ will probably be lower than $10\ \Omega$ as shown in Fig. 3.1, and the capacitor C_{hf} will probably be smaller than 100 pF. So the additional filtering from C_{hf} will not occur until frequencies much higher than 160 MHz. This is fine for filtering signals in the GHz range, but it does not solve the problem of large interferers occurring near the edge of the stop-band.

It has already been stated that small input impedance is necessary for good linearity, so it would be a bad idea to purposely increase $Z_{i,TIA}$ just so that C_{hf} could filter lower frequencies. On the other hand, besides the large area consumption, having a very large capacitor at the input is not detrimental at all. In fact, it is possible using the Miller Effect to effectively multiply the actual capacitor value [5]. Shown in Fig. 3.4, the

Miller Effect, which was first reported by John Miller in 1920 in experiments using vacuum tube amplifiers, states that the effective capacitance C_M seen at the input of an inverting amplifier of gain A_v with a capacitor C in negative feedback configuration is:

$$C_M = C(1 + A_v) \quad (3.2)$$

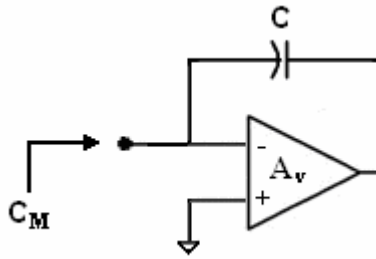


Fig. 3.4 The Miller Effect.

If C_{hf} is a more reasonable size like 10 pF and the amplifier gain A_v is 160, then the effective capacitance seen at the input is 1.6 nF. Assuming $Z_{i,TIA}$ is still a constant 10 Ω , then the corner frequency is around the filter bandwidth 10 MHz. This is the lowest corner frequency desired since anything lower will attenuate signals within the bandwidth.

It is important to note that the Miller Effect is not limited to capacitors. Any impedance in a negative feedback configuration is subject to the Miller Effect. In general, an impedance Z is transformed to the Miller impedance Z_M by the equation:

$$Z_M = \frac{Z}{(1 + A_v)} \quad (3.3)$$

Equation (3.3) shows that the Miller impedance is equal to the feedback impedance reduced by the factor $1+A_v$.

A large Miller capacitor may be useful for additional filtering, but it still only adds an extra -20 dB/decade roll-off in the stop band, which may not be enough if there are large interferers below 100 MHz. Additionally, the open loop gain of an operational amplifier usually features a low-pass response, which means the Miller capacitor appears larger at low frequencies and smaller at high frequencies. This shaping of the Miller capacitor has the opposite effect desired, attenuating in-band signals while failing to reject stop-band interferers. It follows from this problem, then, that instead of using a simple operational amplifier, a high-pass filter may be used to shape the Miller capacitor so that the capacitance appears smaller at low frequencies but much larger at high frequencies.

3.2.1 Impedance to Be Shaped: R or C

If a high-pass filter is used instead of an op amp, then the feedback impedance does not necessarily have to be a capacitor. For example, assume that instead of a capacitor, a 100 Ω resistor is put in feedback with a first order high-pass filter amplifier with unity gain up to a 1 MHz corner frequency. The impedance of this network at

frequencies greater than 1 MHz is the same as that of the 10 pF in feedback with the op amp with gain of 160. Fig. 3.5 shows the two equivalent filters next to each other.

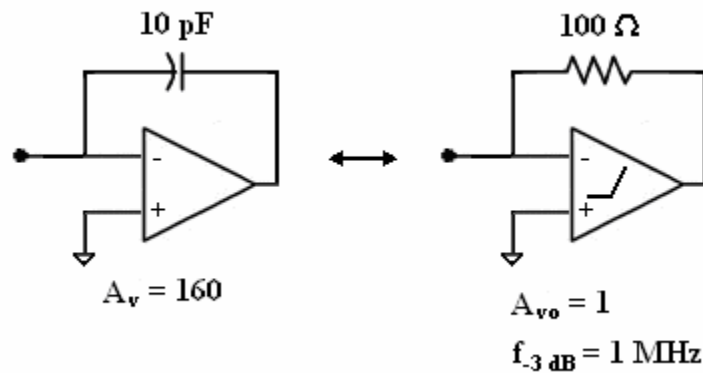


Fig. 3.5 Impedance shaping of a resistor and a capacitor. Input impedances are similar for frequencies greater than 1 MHz.

There is no reason the capacitor should be confined to use with a constant gain amplifier, and it could just as easily be placed around a high pass filter like the resistor. In fact, the capacitor provides more attenuation at high frequencies than the resistor when the same high-pass filter is used because of its inherent low-pass impedance characteristic. Thus a capacitor that is shaped by a first-order high pass filter exhibits an impedance roll-off equal to -40 dB/decade. While this is an advantage of the capacitor, the resistor is not far behind as it only needs a second-order filter to achieve the same roll-off. In fact, the resistor also has an advantage over the capacitor because it generally occupies much less silicon area than the capacitor. It may seem that there is no clear winner and that the designer has the option of deciding whether a resistor or a capacitor

suits the application best. However, the problem of noise in the resistor makes it an unacceptable choice for the feedback impedance.

The thermal noise current of a resistor is modeled as a current source in parallel with the noiseless resistor as shown in Fig. 3.6:

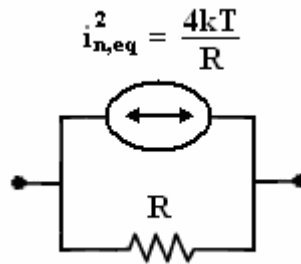


Fig. 3.6 Resistor thermal spot noise current power density.

The average thermal spot noise current power density of the resistor shown in Fig. 3.6 is given by the equation:

$$\bar{i}_{n,eq}^2 = \frac{4kT}{R} \quad (3.4)$$

The value k is Boltzmann's constant and T is the absolute temperature. The product kT is approximately 26 mV at room temperature. The value in (3.4) has units of $\frac{A^2}{Hz}$, which implies that the numerical solution to (3.4) is the squared average noise current in a 1 Hz

bandwidth. To find the total noise over a certain bandwidth, equation (3.4) must be integrated over that bandwidth.

From (3.4) it is observed that the noise current becomes larger as R becomes smaller. In the application of the TIA filter, the resistor must be larger than the in-band impedance $Z_{i,TIA}$, but small enough that an amplifier of modest gain will be able to reduce it to an impedance much smaller than $Z_{i,TIA}$ as shown in equation (3.3). If $Z_{i,TIA}$ is less than $10\ \Omega$, then R should be no smaller than about $50\ \Omega$ but no larger than about $100\ \Omega$. This situation is bad for two reasons. First, R is much smaller than R_{TIA} which is $1\ \text{k}\Omega$, so the noise current of R is at least 10 times as much as that of R_{TIA} . Second, since R is much larger than the in-band $Z_{i,TIA}$, almost all of its in-band noise current will pass into the transimpedance filter input instead of back through R . As shown in Fig. 3.7, this causes the noise to be amplified at the filter output.

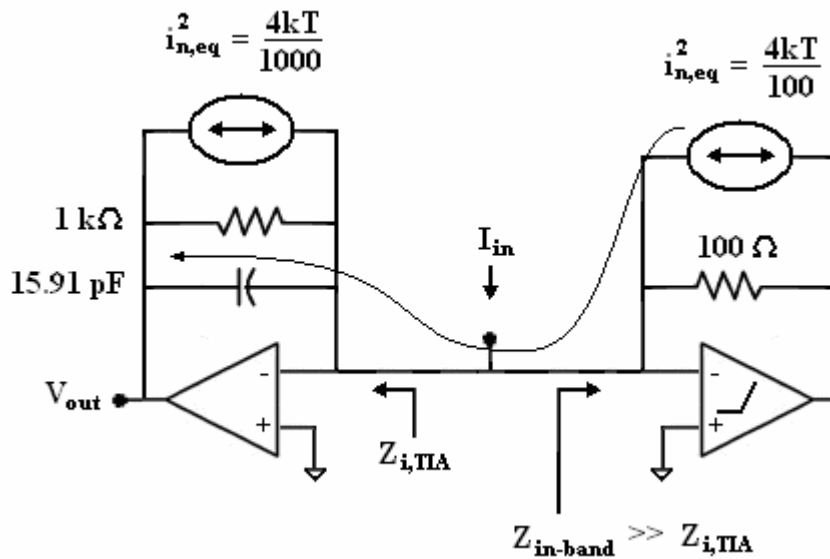


Fig. 3.7 Resistor noise current amplified by the TIA.

While the noisy resistor may increase the overall noise of the filter block by a factor of 10 (20 dB), the capacitor is ideally a noiseless component. A capacitor may allow some high frequency noise from the amplifier or high-pass filter components to be fed back to the TIA filter, but in-band noise is the only concern in this application since the ADC and DSP will filter out high frequency signals and thus their associated noise components. The size of the capacitor is important to consider also. A larger capacitor will allow more low frequency signals to leak back to the filter input, so for noise considerations, a small capacitor is desirable. In conclusion, it is not possible to use a resistor as the impedance to be shaped because of its noise characteristics. A capacitor is the only plausible choice because it is a noiseless device.

3.2.2 Stability of Higher Order Filters

A capacitor whose impedance is shaped by a first-order high pass filter exhibits an impedance roll-off equal to -40 dB/decade. Likewise a capacitor with a second-order high pass filter has -60 dB/decade impedance roll-off. It seems then that the problem of increased rejection can be solved simply by choosing an arbitrarily high ordered filter.

Unfortunately, stability becomes an issue when the filter is of high order. The first-order filter in Fig. 3.3 is stable, but if the filter order is any higher, effects such as transient ringing or even oscillations can occur. Fig. 3.8 shows the general configuration with feedback impedance Z_{fb} and a high-pass filter with transfer function $H(s)$.

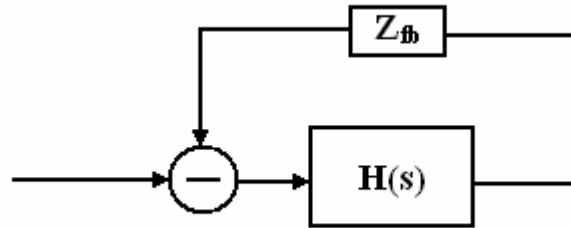


Fig. 3.8 Impedance Z_{fb} in negative feedback with filter transfer function $H(s)$.

For a high-pass transfer function $H(s)$ of the form:

$$H(s) = -\frac{(Gain)s^n}{s^n + (a_2)s^{n-1} + \dots + (a_n)s + (a_{n+1})} \quad (3.5)$$

Then the closed loop input impedance is:

$$Z_i = \frac{Z_{fb}}{1 - H(s)} = \frac{Z_{fb}(s^n + (a_2)s^{n-1} + \dots + (a_n)s + (a_{n+1}))}{(Gain + 1)s^n + (a_2)s^{n-1} + \dots + (a_n)s + (a_{n+1})} \quad (3.6)$$

For stability, the gain must not be too large such that there are positive real roots in the denominator. To check for stability, the Routh table for the denominator is found to be:

$$\begin{array}{c|cccc}
s^n & Gain+1 & a_3 & a_5 & a_7 \\
s^{n-1} & a_2 & a_4 & a_6 & a_8 \\
s^{n-2} & X & & & \\
s^{n-3} & & & &
\end{array} \quad (3.7)$$

where:

$$X = \frac{- \begin{vmatrix} Gain+1 & a_3 \\ a_2 & a_4 \end{vmatrix}}{a_2} = \frac{-((Gain+1)a_4 - a_3a_2)}{a_2} \quad (3.8)$$

For the system to avoid instability, the first column of the Routh table must not have any changes of sign. If all values of a are positive, then the inequality $(Gain+1)a_4 < a_3a_2$ must hold for the system to be stable. Thus a condition for stability is:

$$Gain < \frac{a_3a_2}{a_4} - 1 \quad (3.9)$$

A 3rd order Butterworth 20 MHz high-pass filter with a gain of 100 has the transfer function:

$$H(s) = -\frac{100s^3}{s^3 + 2.513e8s^2 + 3.158e16s + 1.984e24} \quad (3.10)$$

If this 3rd order filter is put in feedback with impedance Z_{fb} , then the input impedance is given by:

$$Z_i = \frac{Z_{fb}}{1 - H(s)} = \frac{Z_{fb} (s^3 + 2.513e8s^2 + 3.158e16s + 1.984e24)}{101s^3 + 2.513e8s^2 + 3.158e16s + 1.984e24} \quad (3.11)$$

Equation (3.11) does not satisfy the criteria of (3.9) and thus is unstable. In fact, (3.9) is not satisfied unless the gain of the filter in equation (3.10) is less than or equal to 3. This maximum gain value is not nearly large enough to reduce the impedance Z_{fb} enough for this filter to be practical.

A similar second order Butterworth filter has the transfer function:

$$H(s) = -\frac{100s^2}{s^2 + 1.777e8s + 1.579e16} \quad (3.12)$$

If this 2nd order filter is put in feedback with impedance Z_{fb} , then the input impedance is given by:

$$Z_i = \frac{Z_{fb}}{1 - H(s)} = \frac{Z_{fb} (s^2 + 1.777e8s + 1.579e16)}{101s^2 + 1.777e8s + 1.579e16} \quad (3.13)$$

The second order Butterworth filter is stable, but it is susceptible to peaking in the frequency domain as shown in Fig. 3.9, which translates to ringing in the transient step response as in Fig. 3.10.

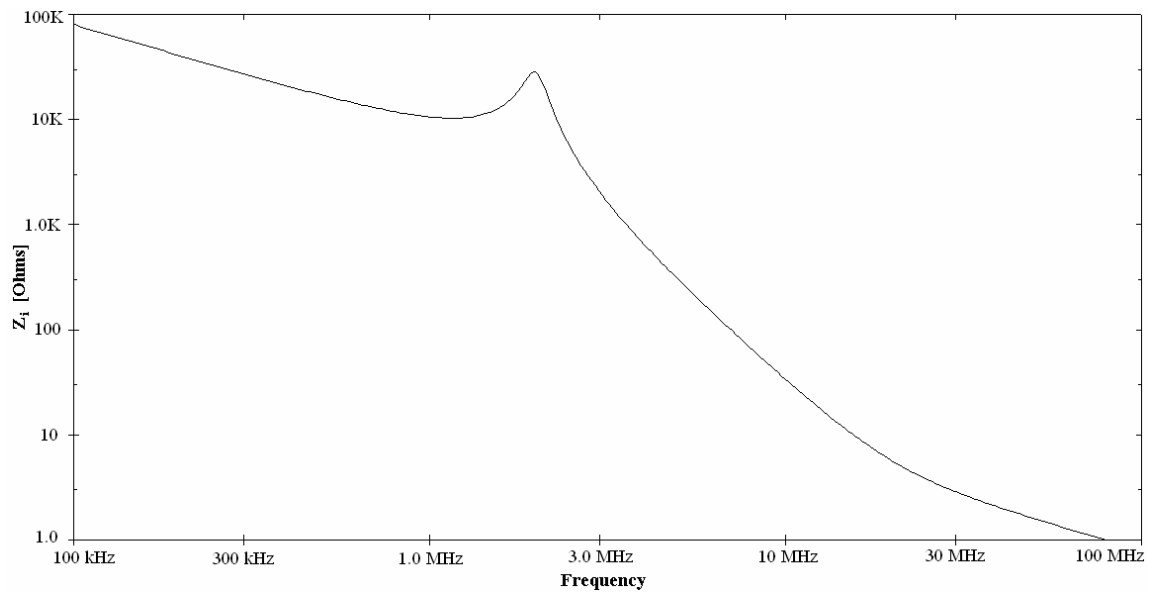


Fig. 3.9 Peaking in Z_i from equation (3.14) when Z_{fb} is a 20 pF capacitor.

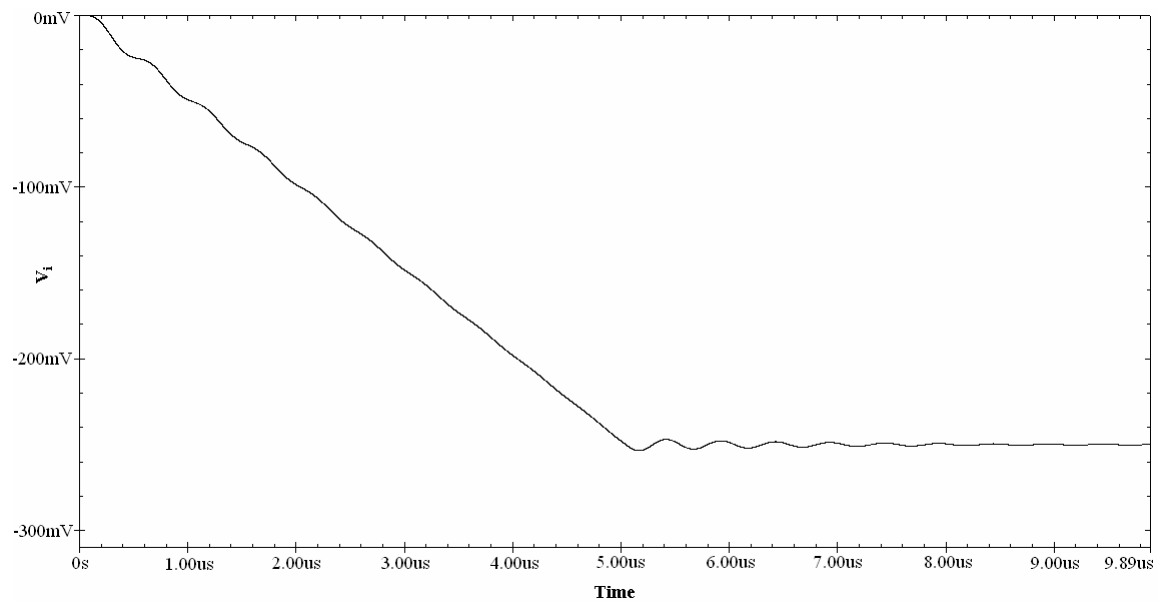


Fig. 3.10 Ringing in input voltage for an input current step.

In addition to Butterworth filters, other filter classes such as Chebyshev and elliptic filters can also be shown to be unstable when they are 3rd order or higher and possess large gain. In summary, arbitrarily high order filters cannot be used to increase the impedance roll-off of passive devices in the negative feedback configuration. Though this limits the overall roll-off in impedance, it can be shown that small regions of steep roll-off can still be achieved using other filtering techniques.

3.2.3 The Twin-T Network

One way to achieve sharp change in the frequency response of a system is to introduce a notch. A notch or transmission zero is achieved when the terms in a transfer function cancel each other out. A famous notch network, shown in Fig. 3.11, is the LC network.

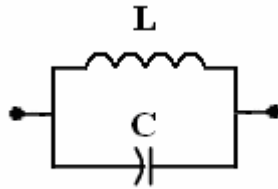


Fig. 3.11 The parallel LC network.

The impedance of the parallel LC shown in Fig. 3.11 is given by:

$$Z_{LC} = \frac{s(L)}{s^2(LC) + 1} \quad (3.14)$$

The impedance Z_{LC} is small at very low and very high frequencies, but increases to infinity at the frequency:

$$\omega_{notch,LC} = \sqrt{\frac{1}{LC}} \quad (3.15)$$

At the notch frequency, the impedances of the inductor and capacitor are equal and opposite, and they produce a real zero in the denominator of (3.14). While this circuit could be used to create a notch for shaping a feedback impedance, it is advisable to avoid using inductors in integrated circuits because they can be expensive, consume large surface area, and can be difficult to properly design.

Another circuit that behaves similarly to the parallel LC is the RC twin-T network. The twin-T, composed of two RC T-bridges, is shown in Fig. 3.12. Only two component values, R and C , are required to characterize the twin-T network. The path with the series capacitors and the shunt resistor is the CRC path, and the path with the series resistors and shunt capacitor is the RCR path.

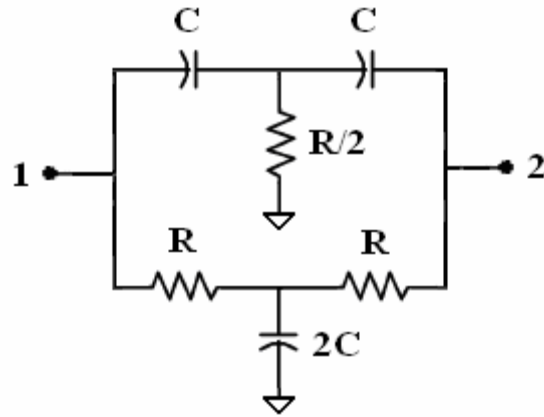


Fig. 3.12 The twin-T network.

If terminal 2 of the network is connected to a load and an AC voltage input is applied to terminal 1 as shown in Fig. 3.13, the network transadmittance, that is, the output current divided by input voltage, is given by:

$$Y_m = \frac{i_2}{v_1} = \frac{s^2(R^2C^2) + 1}{s(2R^2C) + 2R} \quad (3.16)$$

The reciprocal of (3.16) is the network transimpedance:

$$Z_m = \frac{v_1}{i_2} = \frac{s(2R^2C) + 2R}{s^2(R^2C^2) + 1} \quad (3.17)$$

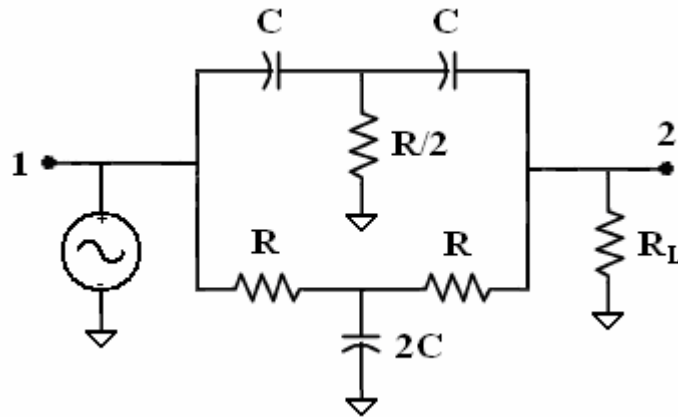


Fig. 3.13 The twin-T network with input voltage and load.

From (3.17), the DC transimpedance is equal to $2R$, and the high frequency transimpedance is equal to the impedance of a capacitor equal to $C/2$. The transimpedance goes to infinity at the frequency:

$$\omega_{RC} = \frac{1}{RC} \quad (3.18)$$

Equation (3.18) has units of radians/second. The equivalent equation in units of Hz is:

$$f_{RC} = \frac{1}{2\pi RC} \quad (3.19)$$

The general plot of $|Z_m|$ from (3.17) is shown in Fig. 3.14.

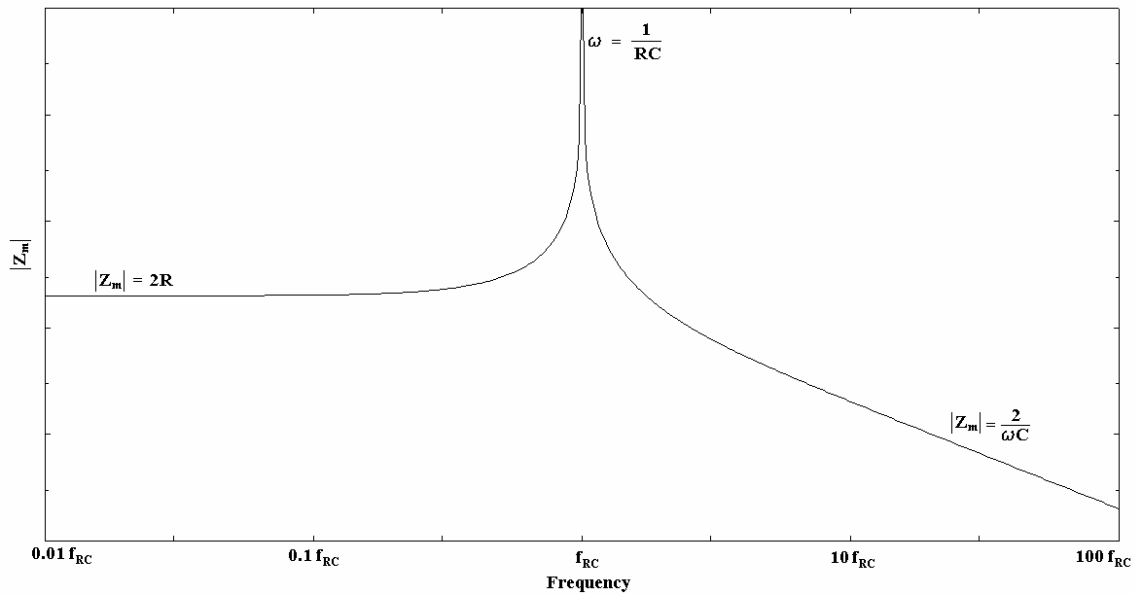


Fig. 3.14 The magnitude transimpedance of the twin-T network.

To gain an intuitive understanding of the twin-T, one must realize that the notch effect of the twin-T network is based on the principle of phase cancellation. As long as the values and ratios of R and C are precise, the AC current phase difference through each path at the output is always equal to 180° . The CRC path behaves as a high-pass filter and the RCR path as a low-pass. At the frequency in which their magnitudes are equal, the currents cancel each other out completely and no current flows to the load. Fig. 3.15 shows the output current magnitude through each branch on a log-scale plot and the point at which the magnitudes are equal. Fig. 3.16 shows that the AC current phase difference of the two paths is a constant 180° at all frequencies.

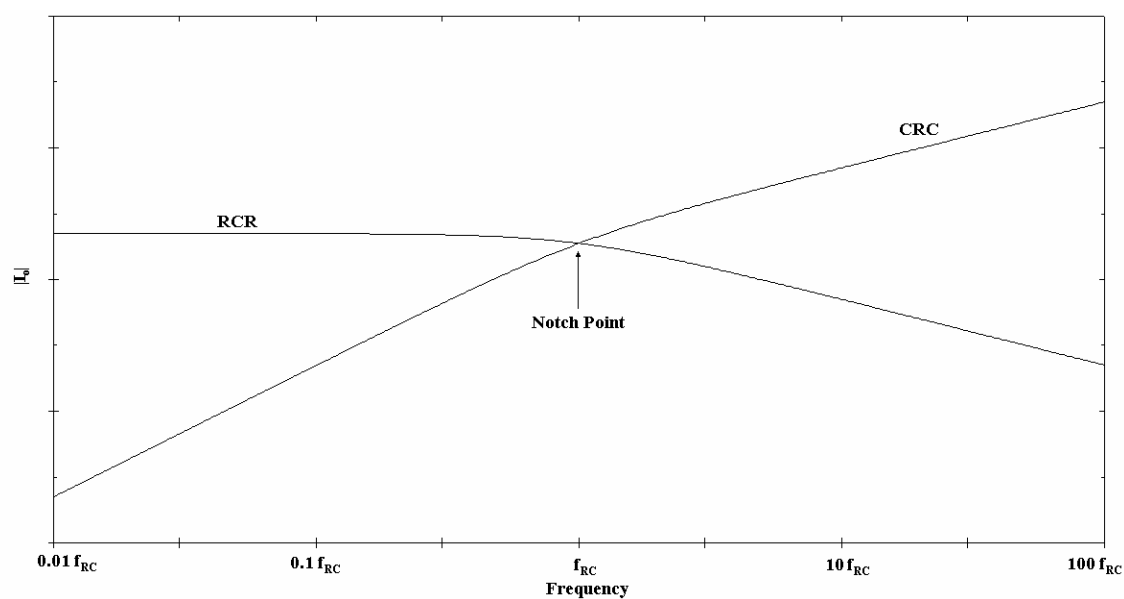


Fig. 3.15 AC output current magnitude of each branch of the twin-T network.

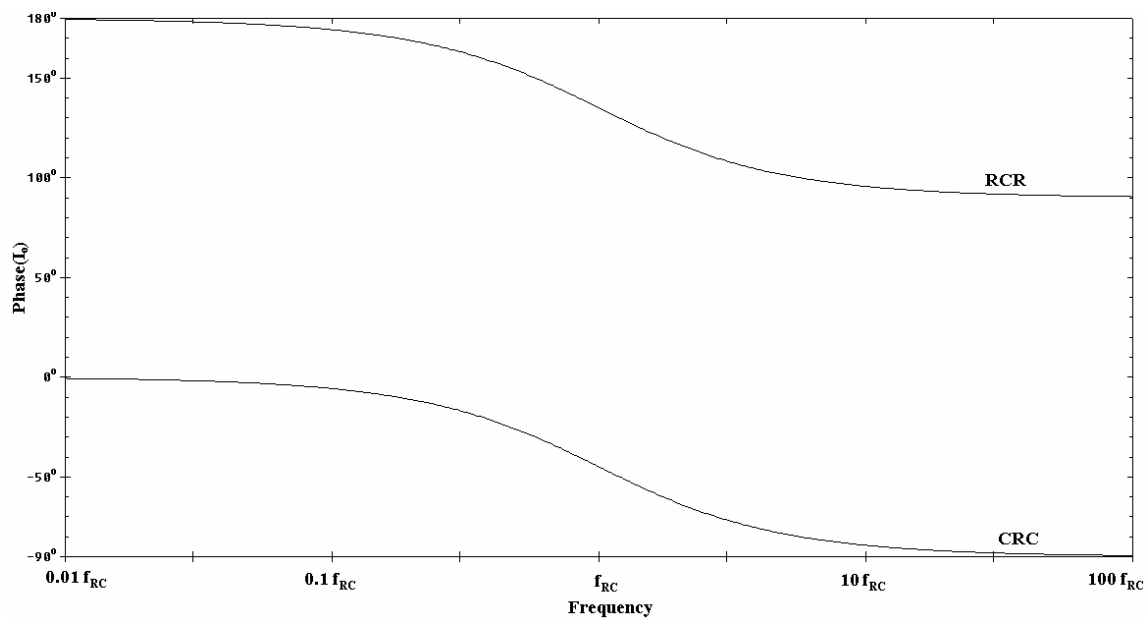


Fig. 3.16 AC output current phase of each branch of the twin-T network.

The absolute values of R and C in the twin-T network are not highly sensitive parameters, as they mostly influence the filter in the asymptotic regions as was shown in Fig. 3.14. In Fig. 3.17, a logarithmic sweep of R and C is shown for a constant RC product. Notice that the notch frequency is not affected, even as R and C are swept over 2 orders of magnitude.

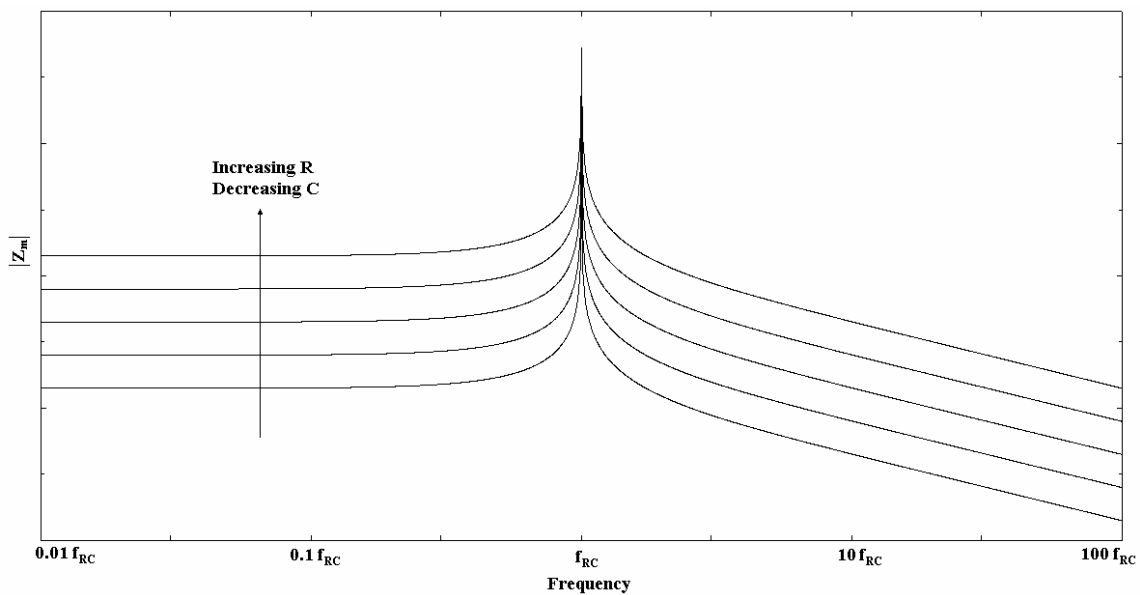


Fig. 3.17 Twin-T transimpedance for a sweep of R and C when RC product is fixed.

On the other hand, the precision of the component matching is very important to the notch functionality of the twin-T because of the constant phase difference requirement. As a consequence of the topology of the twin-T, the phase difference at frequency extremes always approaches 180° , no matter what the component values are. Unfortunately, the notch occurs at the midpoint of the phase change, which is also when the rate of change is the highest. Thus any variation in the phase plot of either branch

will result in a large deviation from the constant 180° difference at the intended notch frequency. Fig. 3.18 shows the deviation in output AC current phase through the RCR branch when one of the resistors is varied by 10%, 25%, and 50%.

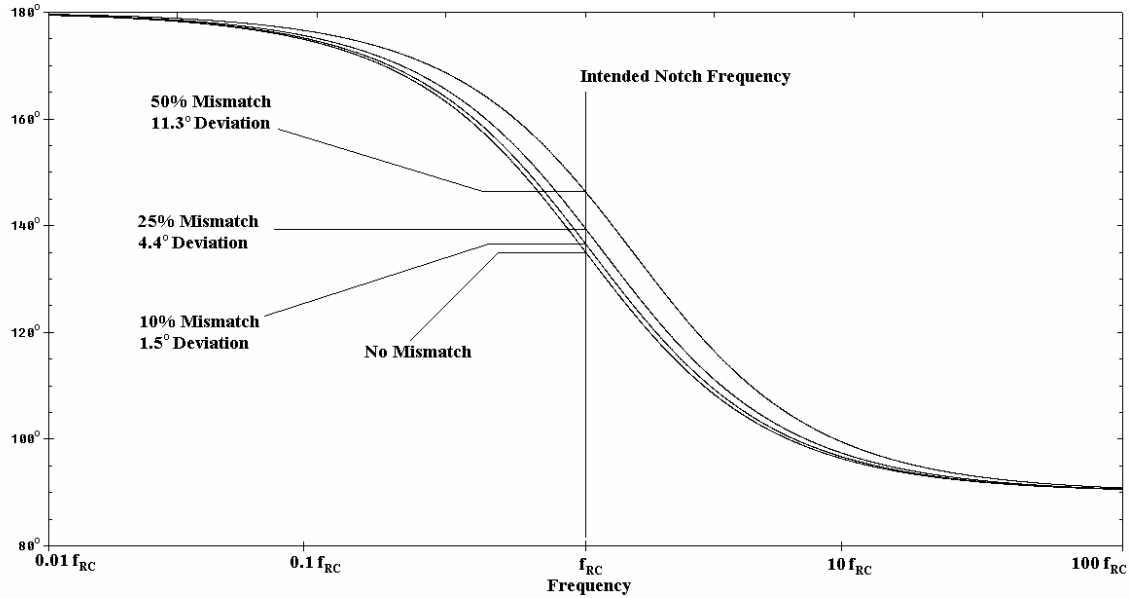


Fig. 3.18 RCR output current phase deviation for mismatch in one resistor.

Fig. 3.19 shows on a log-scale how the phase deviation from Fig. 3.18 affects the response of the overall network. Notice that the notch depth is severely reduced with only 10% mismatch in one component. At 50% mismatch, the notch is hardly present, and the local minimum drifts to higher frequencies.

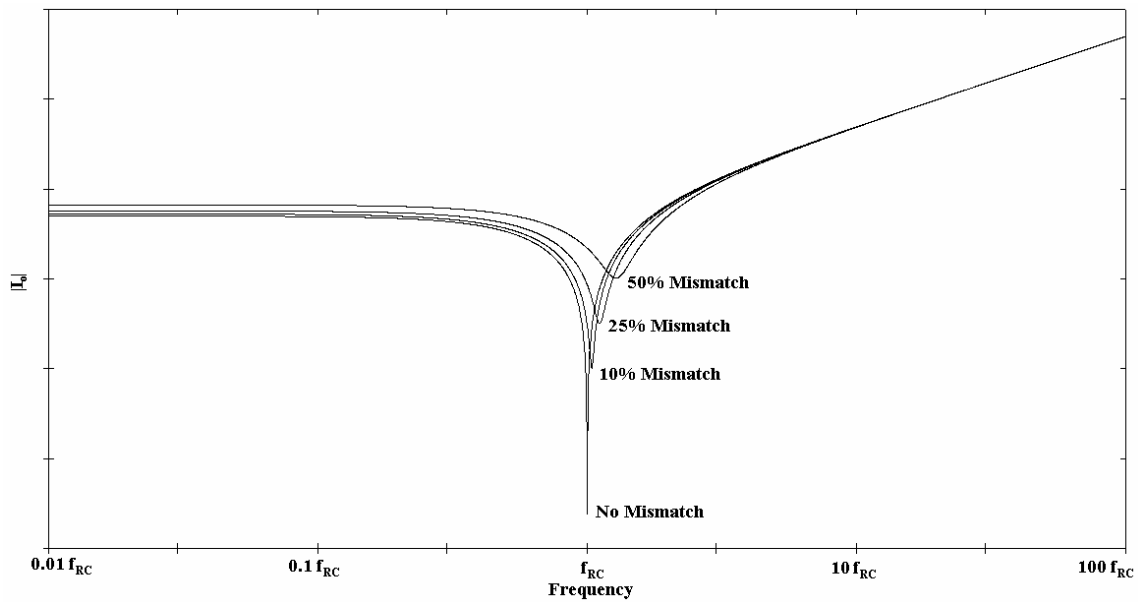


Fig. 3.19 Twin-T AC output current for mismatch in one resistor.

3.3 Design of the Improved Transimpedance Filter

The notch that is created by the twin-T network is useful for creating a locally sharp change in AC response without the need for high order filters. This characteristic is utilized in an active network to create an impedance shaper that can improve the rejection of the existing TIA low-pass filter utilized in [4]. The concept of the current divider, illustrated earlier in Fig. 3.2, is the basis of the improved filter design.

The proposed baseband transimpedance filter design achieves extra attenuation of interfering signals near the edge of an existing filter's bandwidth. The new filter is placed in parallel with the existing single-pole low-pass transimpedance filter as shown in Fig. 3.20.

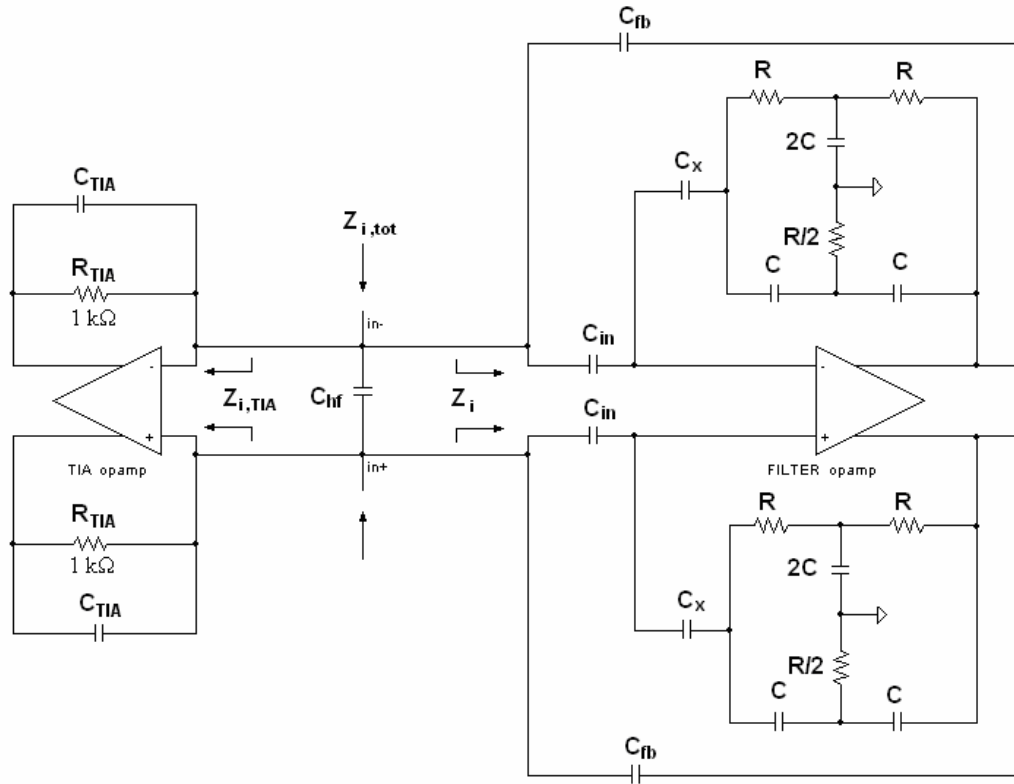


Fig. 3.20 Existing transimpedance filter shown on the left hand side. On the right is the proposed additional filter, an impedance scaler for which $Z_i \gg Z_{i,TIA}$ for in-band frequencies and $Z_i \ll Z_{i,TIA}$ in the stop-band. The ideal shape of Z_i is that of a low-pass notch where the notch is generated by the twin-T RC feedback network and is designed to give sharp roll-off in the stop-band.

The new filter is designed to have relatively large impedance within the bandwidth, but quickly change to low impedance in the stop-band; thus it diverts high frequency current signals away from the main filter. The impedance of the additional filter is shaped around a real capacitor C_{fb} . The impedance of the capacitor C_{fb} should be significantly larger than the in-band TIA input impedance $Z_{i,TIA}$ to avoid attenuation of desired signals. Just beyond the edge of the pass-band, C_{fb} is effectively multiplied to a value such that it has much lower impedance than the out-of-band $Z_{i,TIA}$.

The additional filter's amplifier, which does the scaling, must have a large enough GBW so that it has sufficient gain in the stop-band of interest (i.e. up to a certain frequency, at which point a real capacitor such as C_{hf} in Fig. 3.20). There is no maximum requirement on the existing TIA op amp bandwidth, and the minimum bandwidth is set by requirements for mixer linearity. The TIA gain-bandwidth product, which determines $Z_{i,TIA}$, sets a maximum value on the low-frequency scaled C_{fb} . The minimum C_{fb} is set by the largest anticipated interfering current signal and the available voltage swing. Once C_{fb} is chosen, the optimum values of C_{in} , C , R , and C_x can be selected.

3.3.1 Design Procedure

3.3.1.1 The Minimum Value for C_{fb}

Interfering current signals are filtered out by sinking them through C_{fb} . The lowest-frequency interferer to be rejected and its largest anticipated value determine the minimum value for C_{fb} . For a given voltage swing V_{sw} and interferer amplitude I_{int} at frequency ω_{int} , the minimum value for C_{fb} can be determined by the following equation:

$$C_{fb,min} = \frac{I_{int}}{\omega_{int} V_{sw}} \quad (3.20)$$

For example, for a 50 MHz 10 mA interferer and a maximum voltage swing of 1 V, the smallest C_{fb} is roughly 32 pF. Chip area limitations may force the designer to use $C_{fb,min}$

for the value for C_{fb} . However, if area can be spared, it may be helpful to increase C_{fb} beyond $C_{fb,min}$ to relax the required values of other components and the specifications of the filter amplifier. The maximum value for C_{fb} to avoid any attenuation of in-band signals is discussed in the next design step. However, for very fast technologies which have very low $Z_{i,TIA}$ up to the edge of the pass-band, the maximum value of C_{fb} can range anywhere from 100 pF to greater than 1 nF. These values are generally considered too large to design on-chip anyway.

3.3.1.2 The Ratios C_x to C , C_{in} to C , and the Product RC

The impedance Z_i is shaped by using C_{fb} to close the loop around a high pass filter. The closed loop impedance is given by the general equation:

$$Z_i \approx \frac{1}{\frac{sC_{fb}}{1-H(s)}} \quad (3.21)$$

Equation (3.21) is a specific case of the general impedance transformation function found in equation (3.2). $H(s)$ is the filter's open loop voltage transfer function when C_{fb} is not present. In this design, $H(s)$ has a high pass characteristic with a spike and is calculated in Appendix B. The high-pass spike causes the shape of Z_i to look like a low-pass notch which is designed to give sharp roll-off of the input impedance just beyond the edge of the pass-band. The impedance transfer function Z_i is:

$$Z_i = \frac{s^2(RC)^2 + 1}{s^3(R^2C^2C_{fb}(C + N(C + 2C_x))) + s^2(2RC_{fb}N(2C + C_x)) + s(C_{fb}(N + 1))} \quad (3.22)$$

where the notch frequency is determined by the twin-T RC product and is found in equations (3.18) and (3.19), and where:

$$N = \frac{C_{in}}{C_x} \quad (3.23)$$

Note that the notch frequency in (3.18) and (3.19) is only accurate if the additional filter amplifier has high gain over all frequencies. In reality, as the amplifier gain reduces because of bandwidth limitations, the actual location of the notch (or local minimum) tends to drift to lower frequencies than f_{RC} . This effect can be compensated for by preemptively increasing the value of f_{RC} .

Equation (3.23) is the factor by which C_{fb} is multiplied at low frequencies; that is, $C_{fb,eff}$ at low frequencies is equal to $(N+1)C_{fb}$. Thus, the impedance Z_i for in-band frequencies is given by the equation:

$$Z_{i,lf} = \frac{1}{s(N+1)C_{fb}} \quad (3.24)$$

The value of $Z_{i,lf}$ in (3.24) must be at least 10 times larger than the largest in-band value of $Z_{i,TIA}$ to avoid attenuation of desired signals. The graph in Fig. 3.1 shows $Z_{i,TIA}$ for

various TIA GBW. Once the largest in-band value of Z_{TIA} is determined, C_{fb} and N should be selected so that $Z_{i,lf}$ is much larger than Z_{TIA} at the edge of the pass-band. For example, for $GBW = 1$ GHz from Fig. 3.1, the input impedance around 10 MHz is about 7Ω . This means the impedance of $Z_{i,lf}$ should be at least 70Ω at 10 MHz. As a result, the maximum allowable $C_{fb,eff}$ is about 225 pF. For a minimum $C_{fb} = 32$ pF from the example in the first design step, the maximum value for N is roughly 7.

From (3.22) it can be shown that the high frequency impedance $Z_{i,hf}$ is:

$$Z_{i,hf} = \frac{1}{s(1 + N + 2M)C_{fb}} \quad (3.25)$$

where:

$$M = \frac{C_{in}}{C} \quad (3.26)$$

Observing (3.25) reveals that the effective capacitance $C_{fb,eff}$ at high frequencies is equal to $C_{fb}(1+N+2M)$. From the standpoint of large rejection and low overall input impedance $Z_{i,tot}$, it is desirable to have a large value for $(1+N+2M)$ in (3.25). However, transient effects like ringing and overshoot, as well as the noise of resistors in the twin-T network must also be taken into consideration when determining N and M . These effects are highlighted in the next design step.

3.3.1.3 The Values C_x , C_{in} , C , and R

The absolute values of the components are relevant when considering noise, area consumption, and power efficiency. The resistors in the twin-T network add noise which is fed back to the TIA input through the relatively large capacitor C_{fb} . Minimizing R can reduce in-band noise contribution, but there are a number of things to consider when decreasing the value of R . First, small resistor values require the capacitors C , C_x , and C_{in} to increase and so consume larger area. Second, as R gets smaller, perhaps in the range of $100\ \Omega$ to $1\ \text{k}\Omega$, the noise contribution of the new filter block may be dominated by the noise of the filter amplifier rather than the resistors. Finally, as R gets smaller and the capacitors get larger, more current must be fed back through the twin-T network and C_x , causing the filter consume more power and operate less efficiently.

3.3.1.4 The Optimum Value of C_{TIA}

It is observed that the additional filter produces bandwidth extension, with the new -3 dB frequency occurring as high as twice the original bandwidth. This extended bandwidth may be undesirable, and the simplest solution is to slightly decrease the pole frequency in the TIA feedback. In the following macromodel design simulations, the feedback capacitor C_{TIA} is increased from 15.91 pF to 20 pF. This moves the real pole in the TIA feedback from 10 MHz down to about 8 MHz, but keeps the actual -3 dB bandwidth of the overall filter at 10 MHz.

3.3.2 Macromodel Simulation Results

The design procedure is now used to design filters for advanced processes, and then the circuits are simulated using macromodel amplifiers. Macromodels are useful for approximating the first order response of amplifiers designed in any technology. Three different macromodel circuits are simulated and the results are shown on the following pages. The component values used are summarized in Table 3.1.

The first macromodel amplifier has $GBW = 1$ GHz. In this circuit, the amplifier specifications are relaxed for a 90 nm process. The gain bandwidth products of both the TIA and additional filter amplifiers are set to $GBW = 1$ GHz with a DC gain $A_v = 1000$ and one parasitic pole at $f_p = 1$ MHz.

The second macromodel has $GBW = 3$ GHz. In this circuit, the amplifier specifications match approximately what is reported for a 90 nm process [4]. The gain bandwidth products of both the TIA and additional filter amplifiers are set to $GBW = 3$ GHz with a DC gain $A_v = 3000$ and one parasitic pole at $f_p = 1$ MHz.

Finally, the last macromodel has $GBW = 5$ GHz. In this circuit, the amplifier specifications anticipate what may be achievable in advanced processes beyond 90 nm. The gain bandwidth products of both the TIA and additional filter amplifiers are set to $GBW = 5$ GHz with a DC gain $A_v = 5000$ and one parasitic pole at $f_p = 1$ MHz.

Table 3.1 – Summary of Components in Macromodel Simulations.

GBW	1 GHz	3 GHz	5 GHz
DC Gain	1000	3000	5000
R	500 Ω	500 Ω	500 Ω
C	3.54 pF	3.74 pF	3.74 pF
C_{in}	4 pF	3.5 pF	3 pF
C_x	650 fF	200 fF	100 fF
C_{fb}	35 pF	40 pF	45 pF
C_{TIA}	20 pF	20 pF	20 pF

Macromodel simulations are of transimpedance gain (Fig. 3.21), total filter input impedance (Fig. 3.22), and transient step response (Fig. 3.23).

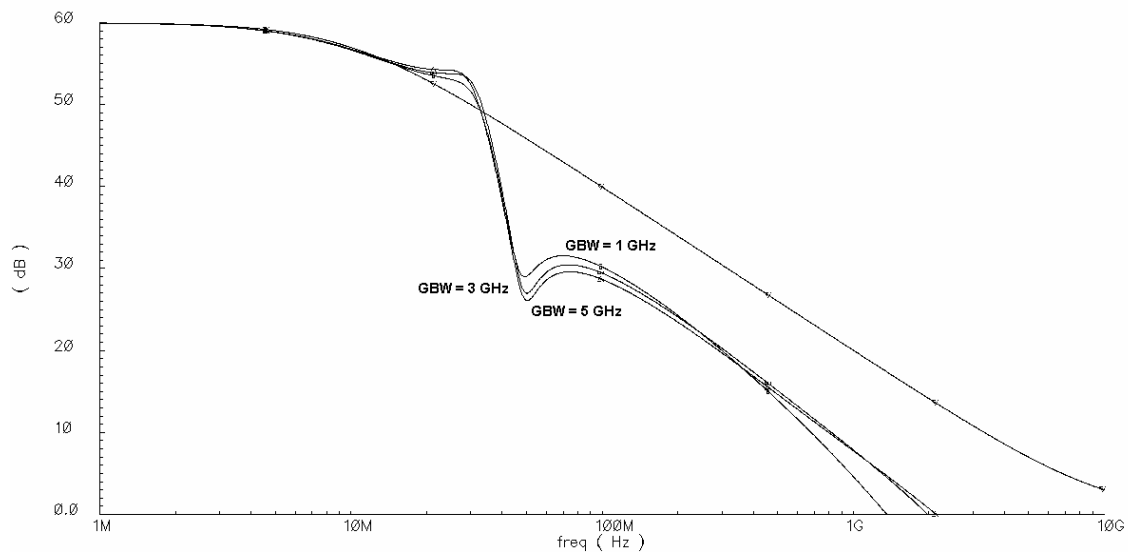


Fig. 3.21 Transimpedance gain. Rejection is slightly improved for larger GBW. Better rejection (but higher noise) could be achieved by increasing C_{fb} . For the cases where $GBW = 3$ GHz and $GBW = 5$ GHz, the value of $f_{RC} = 85$ MHz. For $GBW = 1$ GHz, $f_{RC} = 90$ MHz.

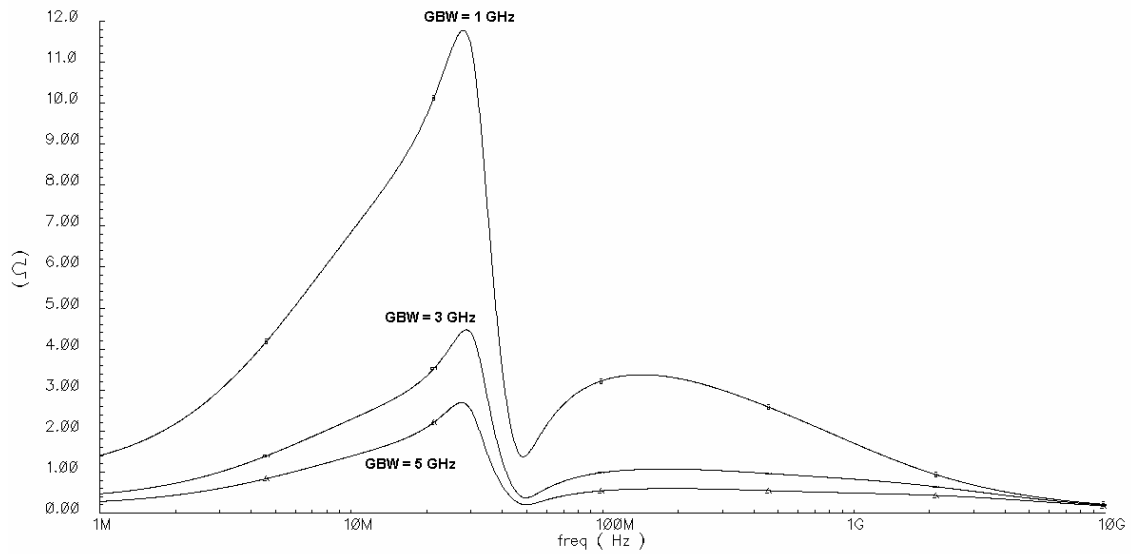


Fig. 3.22 Total filter input impedance $Z_{i,tot}$. Overall input impedance is reduced for larger GBW.

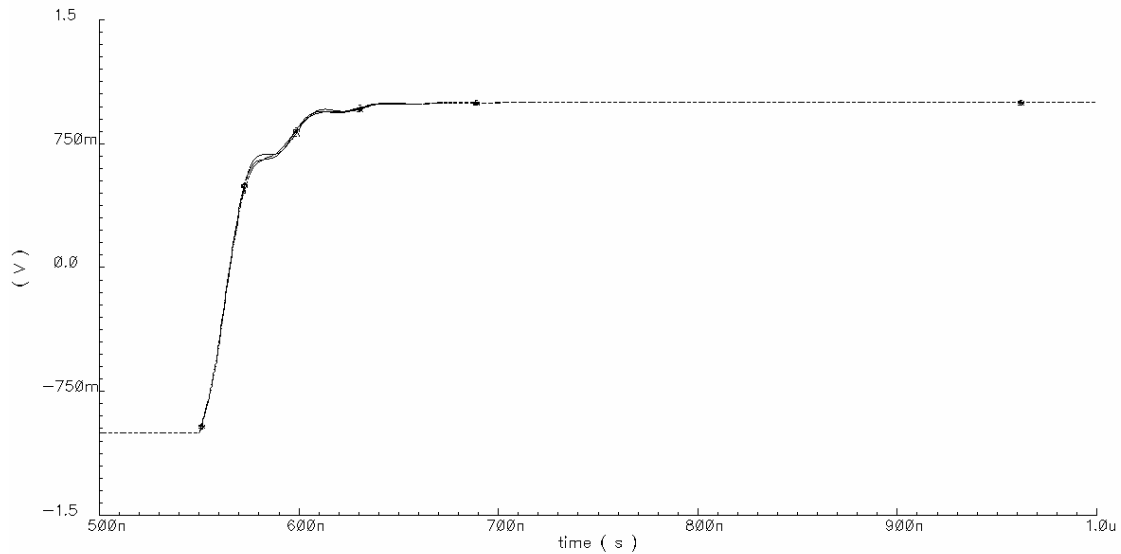


Fig. 3.23 Transient response to 1 mA current step for all three GBW. There is slight ringing in all cases. Settling time for each is around 90 ns.

Figs. 3.24 – 3.26 show how f_{RC} and component values are determined for the case where the amplifier GBW = 3 GHz.

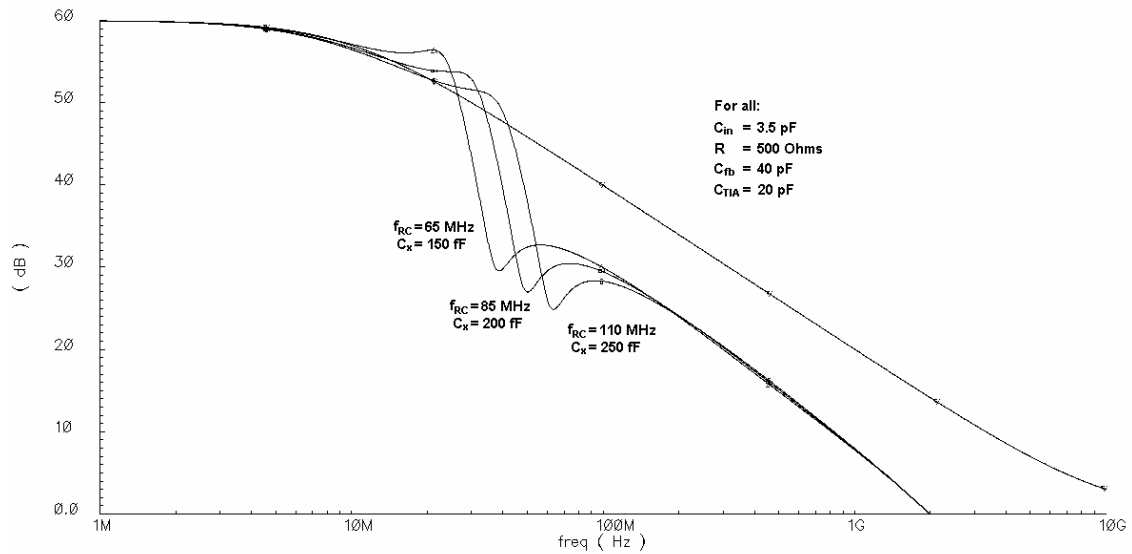


Fig. 3.24 Transimpedance gain for GBW = 3 GHz. Sweep of f_{RC} with appropriate values of C_{in} and C_x to give small transient ringing while still attaining large rejection. Values of f_{RC} are 65 MHz, 85 MHz, and 110 MHz. Sharper roll-off is achieved for smaller f_{RC} but the attenuation at and just after the notch is worse. Smooth transient response is also more difficult to achieve as f_{RC} is reduced. Notice that the actual position of the notch occurs at lower frequencies than f_{RC} (in this case at 39 MHz, 50 MHz, and 64 MHz).

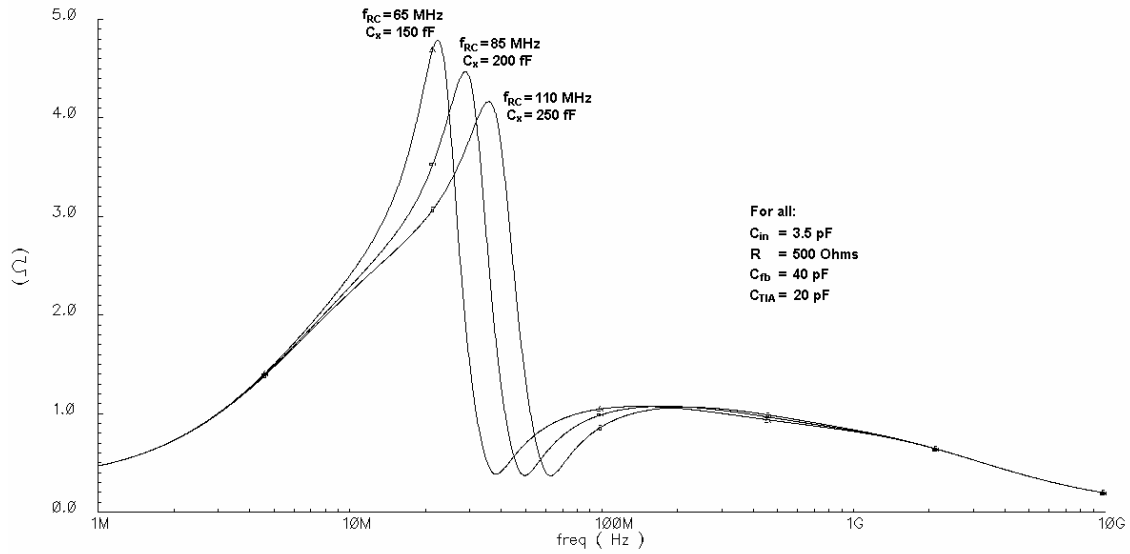


Fig. 3.25 Total filter input impedance $Z_{i,tot}$ for $f_{RC} = 65$ MHz, 85 MHz, and 110 MHz. GBW = 3 GHz.

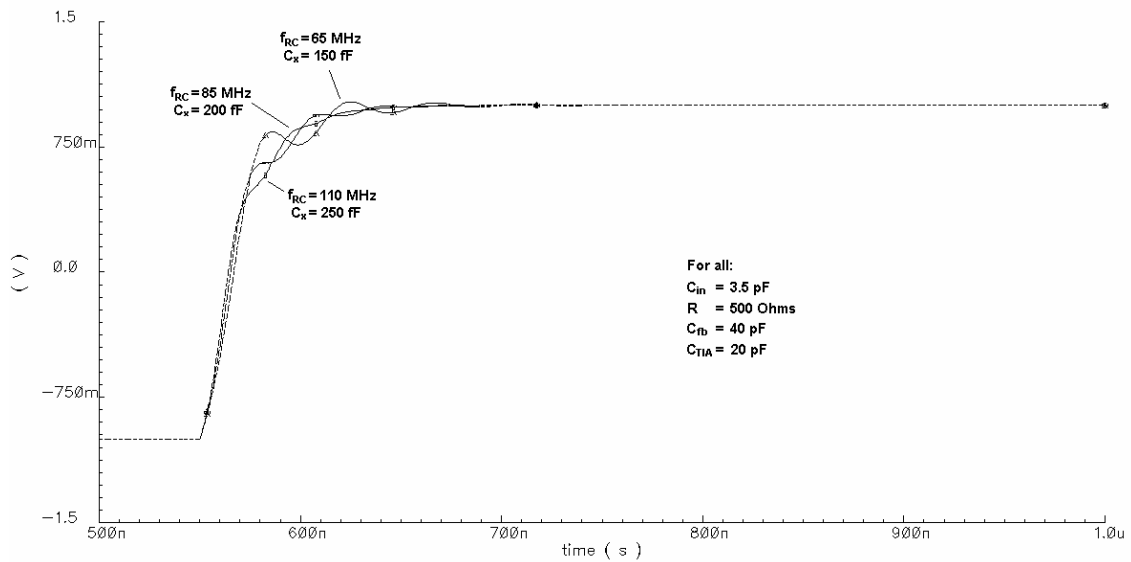


Fig. 3.26 Step response for GBW = 3 GHz. In all three cases, slight ringing is found in the step response with $f_{RC} = 65$ MHz showing the most, and $f_{RC} = 110$ MHz showing the least. For $f_{RC} = 85$ MHz and $f_{RC} = 110$ MHz, the settling time is about 90 ns, and for $f_{RC} = 65$ MHz, the settling time is around 120 ns.

CHAPTER IV

TRANSISTOR LEVEL DESIGN

The macromodel simulations presented in the previous chapter approximate how the filter may operate in advanced technologies. But the single-pole amplifier macromodels are very simplistic and do not take into account many real effects such as non-dominant poles, output resistance, and slewing. The only way to accurately determine the impact of these higher-order effects on the filter is to design and fabricate the transistor level circuit. The final circuit in this thesis is designed and laid out in Jazz Semiconductor 0.18 μm CMOS process, but an initial design has been done in TSMC 0.18 μm . Simulation results from both processes are included in this chapter. Both of these processes are twice the size of the 90 nm process used in [4]. Therefore, it is naturally expected that the amplifiers in 0.18 μm technology will have lower GBW, and thus larger TIA input impedance, than what can be achieved in a 90 nm process.

4.1 Higher Order Effects

In the transistor level simulations, zeros in the transimpedance AC response, which are due to finite bandwidth and output resistance of both the TIA and filter amplifiers, cause a spike at around 1 GHz. To alleviate this problem without adding complexity to the amplifiers, a small resistor R_{fb} is placed in series with the feedback capacitor C_{fb} and another small resistor R_z is placed in series with C_{TIA} . The effect of these components is to smooth out the high frequency AC response. To show how a

resistor in series with the capacitor can help the circuit, a sweep of R_z is performed on a macromodel circuit that includes amplifier output resistance. For simplicity, only the original 10 MHz TIA filter is present, as shown in Fig. 4.1. The values used in the simulation are $C_{hf} = 1$ pF, $R_o = 20$ Ω , $R_{TIA} = 1$ k Ω , and $C_{TIA} = 15.91$ pF with R_z swept from 1 Ω to 1 k Ω in one decade steps. Amplifier gain and bandwidth values are shown in Fig. 4.1. Fig. 4.2 illustrates the effect of the series resistor R_z .

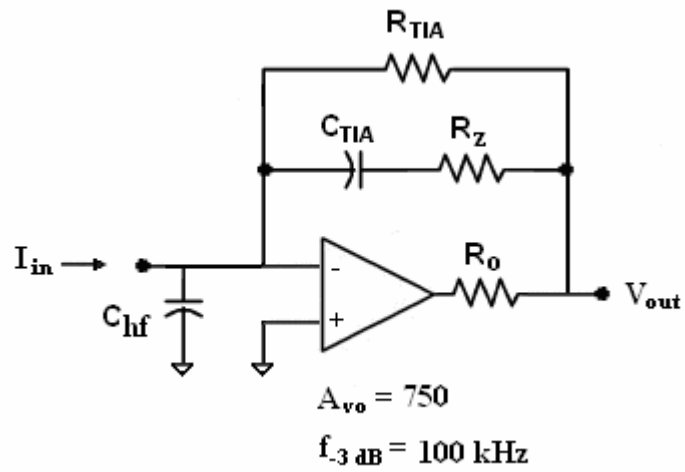


Fig. 4.1 Effect of the zero created by R_o , dampened by R_z .

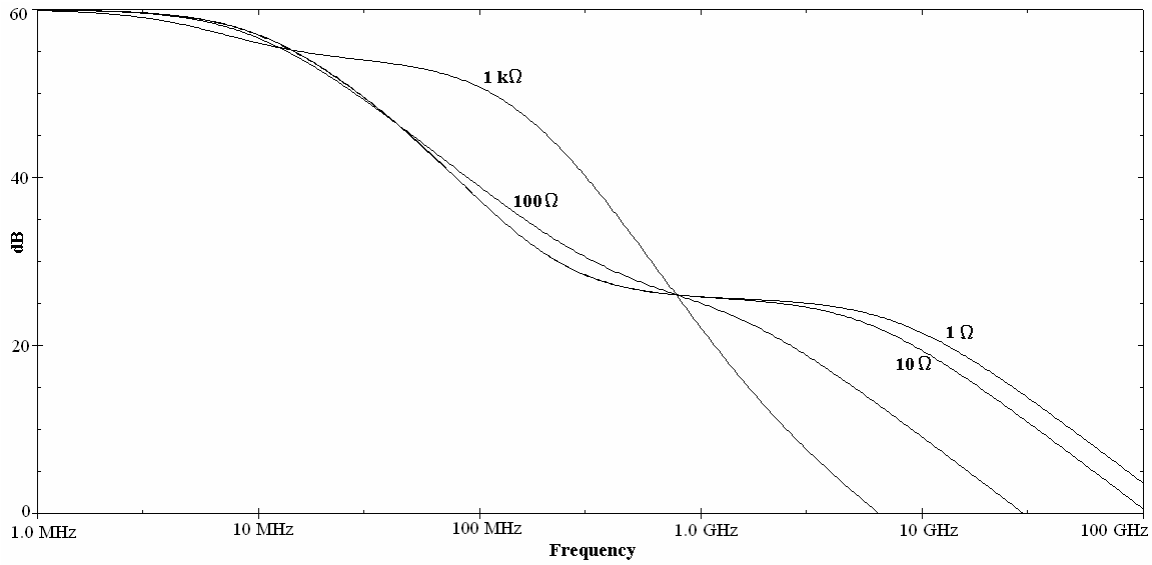


Fig. 4.2 Sweep of R_z for the circuit in Fig. 4.1.

It is observed from Fig. 4.2 that there is a crossover frequency at which point R_z has no effect on the gain. At frequencies higher than the crossover, R_z increases attenuation, while at frequencies between the 10 MHz pole and the crossover point, R_z has the undesirable effect of reducing the filter rejection. As R_z is increased at first, it greatly improves the high frequency rejection while only slightly reducing the attenuation at middle frequencies. However, as R_z gets even larger, it severely reduces the attenuation between the 10 MHz bandwidth and the crossover frequency. Since there is a trade-off for increasing R_z , it is up to the designer to determine its optimum value.

In addition to series resistors, another way to help improve attenuation at high frequencies is to increase the size of the capacitor C_{hf} . Figs. 4.3 and 4.4 show the

improvement in AC response and input impedance for increasing values of C_{hf} . Both plots are transistor level simulations of the filter in designed in TSMC 0.18 μm .

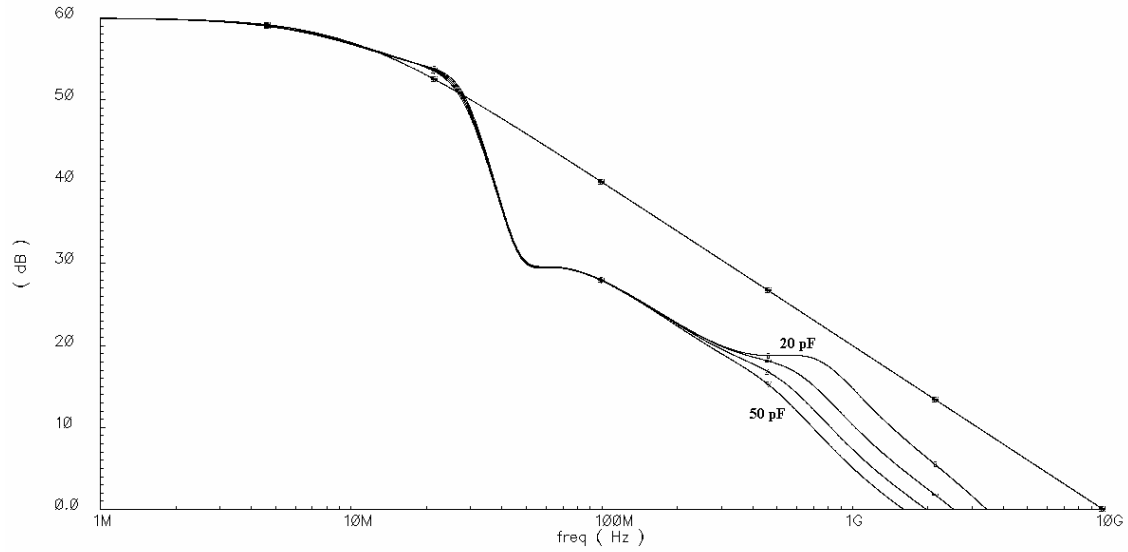


Fig. 4.3 Transimpedance gain in TSMC 0.18 μm . Sweep of C_{hf} from 20 pF to 50 pF in 10 pF increments.

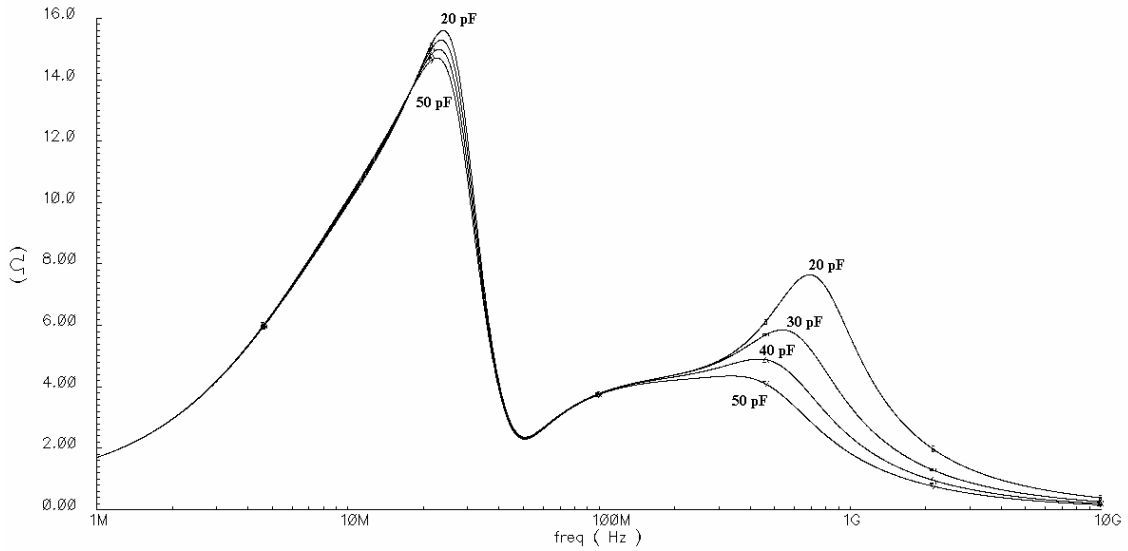


Fig. 4.4 Total filter input impedance, $Z_{i,tot}$, for sweep of C_{hf} from 20 pF to 50 pF.

Note that in Fig. 4.3, the response is nearly the same for all values of C_{hf} until around 300 MHz. At this point the larger capacitor has better attenuation and a flatter response. In Fig. 4.4, larger capacitor size slightly reduces input impedance around 20 MHz, but a much larger reduction is observed between 400 MHz and 2 GHz. From these plots, the designer must decide the trade-off between added area consumption and better high frequency attenuation. These changes in C_{hf} have a negligible effect on filter linearity or in-band noise.

4.2 Filter Design

The filter topology shown in Fig. 3.20 is designed in the transistor level. The design procedure previously outlined is used to determine optimum component values. The first step is determining C_{fb} . The absolute maximum voltage swing V_{sw} is equal to the 1.8 V supply voltage, and the largest expected interferer I_{int} is about 10 mA. At the very least, the filter should be able to process I_{int} at 50 MHz. From equation (3.20), the smallest feedback capacitor C_{fb} is 17.7 pF. While selecting this value minimizes the area consumption of the filter, a linear rail-to-rail filter output stage is necessary to handle the large voltage swing required on C_{fb} , and it is not at all possible to filter I_{int} at any frequency below 50 MHz. If however, C_{fb} is chosen so that only half the supply voltage is used for the output voltage swing ($V_{sw} = 0.9$ V), then the minimum C_{fb} is about 35 pF. Choosing the larger C_{fb} value does increase area consumption, but it enables much more relaxed specifications for the filter amplifier's output stage. Lower voltage swing usually increases the linearity of the amplifier as well. Larger C_{fb} also makes it possible

to reject even lower frequency interferers. For example, if C_{fb} is 35 pF, then the V_{sw} required to reject a 10 mA 40 MHz interferer is 1.14 V. For a 10 mA 30 MHz interferer, V_{sw} is still only 1.5 V. This means it is possible to filter both of these frequencies, given the 1.8 V supply.

The second step is to determine the component ratios. The notch frequency f_{RC} of the twin-T circuit should be higher than the actual desired notch point because the finite bandwidth of the filter amplifier tends to make the notch or local minimum drift to lower frequencies. This effect is visible in Fig. 3.24. The best way to determine f_{RC} is to run a parametric sweep of the twin-T RC product. Similar sweeps should be run to determine the optimum values of N (3.23) and M (3.26).

To determine the absolute values of the components, it is necessary to balance the trade-off of added noise as the twin-T resistors increase with the added power consumption and rising capacitor area as the resistors decrease. Once the circuit is designed up to this point and the frequency response in the range of 10 MHz to 100 MHz is acceptable, attention should be paid to the circuit response at high frequencies. R_{fb} , R_z , and C_{hf} can be increased to compensate for any peaking or reduction in the roll-off. Fig. 4.5 shows the component values used in the design of the circuit in Jazz 0.18 μm .

Once the passive component values are determined, the last step is to design the TIA amplifier and the filter amplifier. The following sections outline the design, topology, and specifications of the transistor amplifiers.

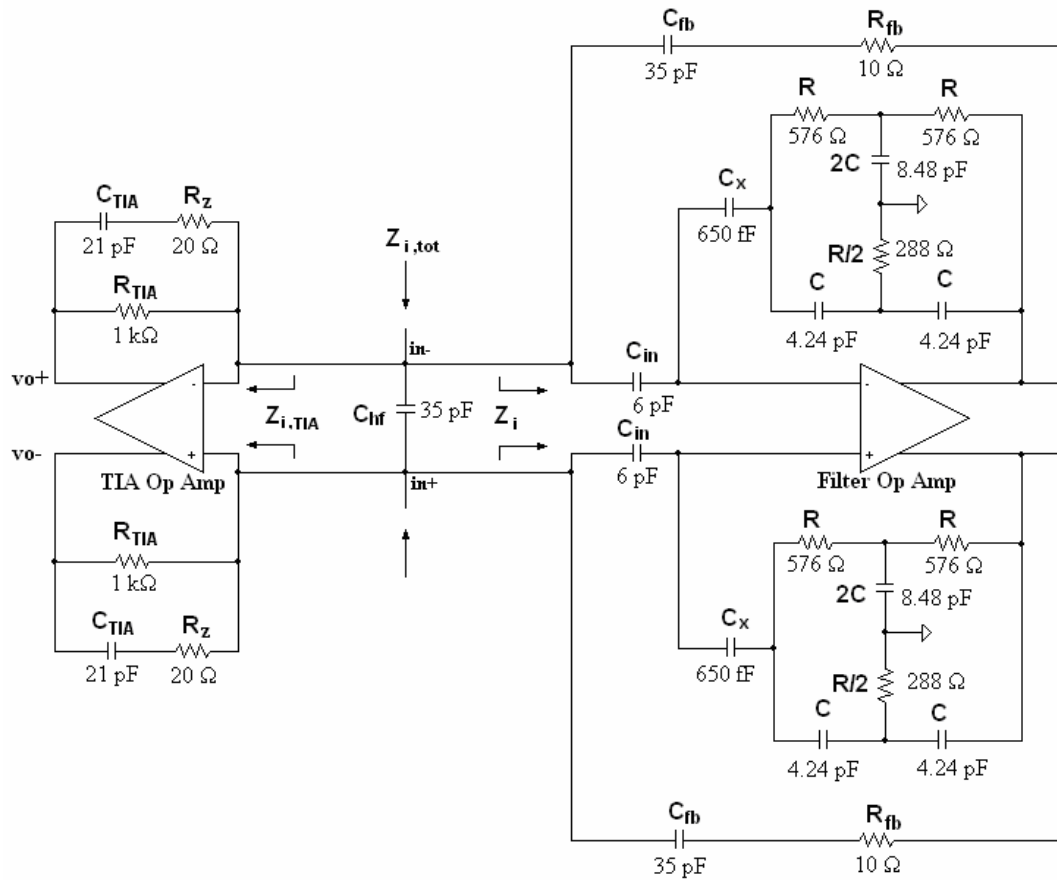


Fig. 4.5 Filter with component values.

4.2.1 Filter Op Amp Folded-Cascode Gain Stage

The filter op amp is a two-stage amplifier consisting of a single gain stage and an output buffer. The buffer will be required to handle the large 10 mA interferers. Because of the inclusion of the buffer in the filter amplifier, only one gain stage is used to conserve power. The gain stage does not necessarily need to have an extremely large DC gain since its only function is to operate at frequencies greater than 10 MHz.

Instead, the main requirement of the filter amplifier is to have a large GBW, such that it has reasonably high gain at very high frequencies.

A simple single gain stage op amp is the NMOS differential pair with active PMOS load. The fully differential version of this circuit is shown in Fig. 4.6. The differential pair is symmetrical around the vertical center; that is, $M1 = M2$ and $M3 = M4$ in terms of size and DC bias.

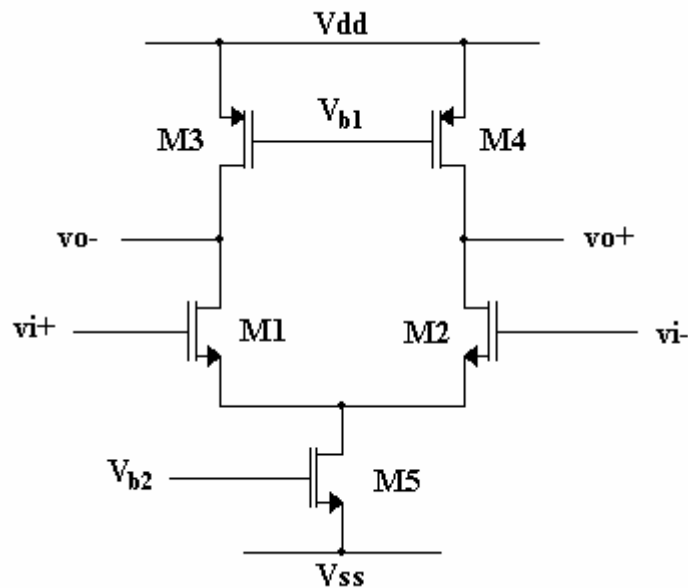


Fig. 4.6 Simple NMOS differential pair with fully-differential PMOS load.

The DC differential voltage gain of the differential pair is:

$$A_{vo} = -g_{m1}r_o \quad (4.1)$$

where the output resistance r_o is given by:

$$r_o = \frac{1}{g_{ds1} + g_{ds3}} \quad (4.2)$$

The dominant pole in the differential pair is generally located at the output node. The pole at this node is given by:

$$\omega_{-3dB} = \frac{1}{r_o C_{out,eq}} \quad (4.3)$$

where:

$$C_{out,eq} \approx C_{db1} + C_{gd1} + C_{db3} + C_{gd3} \quad (4.4)$$

Equation (4.1) suggests that since the voltage gain of the differential pair is directly proportional to the output resistance, increasing r_o will improve the operation of the circuit. While increased output resistance improves the DC voltage gain, it does not increase GBW because the location of the dominant pole is inversely proportional to r_o as shown in (4.3). In fact, GBW is just the product of equations (4.1) and (4.3):

$$GBW = \frac{g_{m1}}{C_{eq,out}} \quad (4.5)$$

From (4.5), it is evident that the way to increase GBW is to either reduce the equivalent output capacitance $C_{out,eq}$ or increase the input transistor transconductance g_{m1} . Generally for a simple differential pair, the bandwidth found in equation (4.3) can be very large because the output resistance and capacitance are both relatively small.

The voltage headroom at the output of the simple differential pair is fairly large. It is limited only by the overdrive voltages of the three vertical transistors. The voltage headroom of the differential pair is given by:

$$V_{hr} = (V_{DD} - V_{SS}) - (V_{DSAT,1} + |V_{DSAT,3}| + V_{DSAT,9}) \quad (4.6)$$

Though the simple differential pair has a large bandwidth, it may not provide enough gain for the filter to function properly. As observed from (4.1) and (4.5), higher output resistance can increase gain without affecting GBW. High gain can be achieved in one stage by using a cascode topology [6]. Fig. 4.7 shows a telescopic cascode circuit. The approximate output resistance and capacitance of the cascode circuit are given by the equations:

$$r_{o,cas} \approx \left(\frac{1}{g_{ds1}} + \frac{1}{g_{ds3}} + \frac{g_{m3}}{g_{ds1}g_{ds3}} \right) \parallel \left(\frac{1}{g_{ds5}} + \frac{1}{g_{ds7}} + \frac{g_{m5}}{g_{ds5}g_{ds7}} \right) \quad (4.7)$$

$$C_{out,eq} \approx C_{db5} + C_{gd5} + C_{db3} + C_{gd3} \quad (4.8)$$

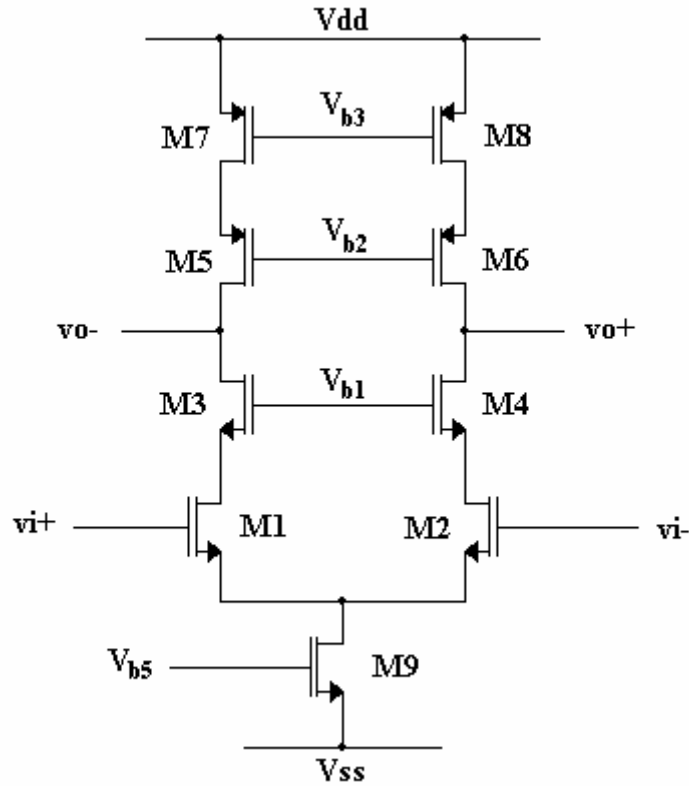


Fig. 4.7 Fully differential cascode op amp.

The voltage gain of the cascode amplifier is improved over that of the simple differential pair because the output resistance from (4.7) is much larger than r_o found in (4.2). The main disadvantage of the telescopic cascode amplifier is its reduced voltage headroom. The output headroom of the amplifier in Fig. 4.7 is:

$$V_{hr,cas} = (V_{DD} - V_{SS}) - (V_{DSAT,1} + V_{DSAT,3} + |V_{DSAT,5}| + |V_{DSAT,7}| + V_{DSAT,9}) \quad (4.9)$$

Improved voltage swing can be realized with the folded-cascode topology, shown in Fig. 4.8. From equation (3.20), large voltage headroom is important for keeping the size of C_{fb} reasonably small. The gain, output resistance, and bandwidth of the folded-cascode amplifier are the same as that of the telescopic cascode. The voltage headroom of the folded-cascode op amp is increased by one overdrive voltage over the telescopic cascode:

$$V_{hr,fc} = (V_{DD} - V_{SS}) - (V_{DSAT,7} + V_{DSAT,5} + |V_{DSAT,3}| + |V_{DSAT,9}|) \quad (4.10)$$

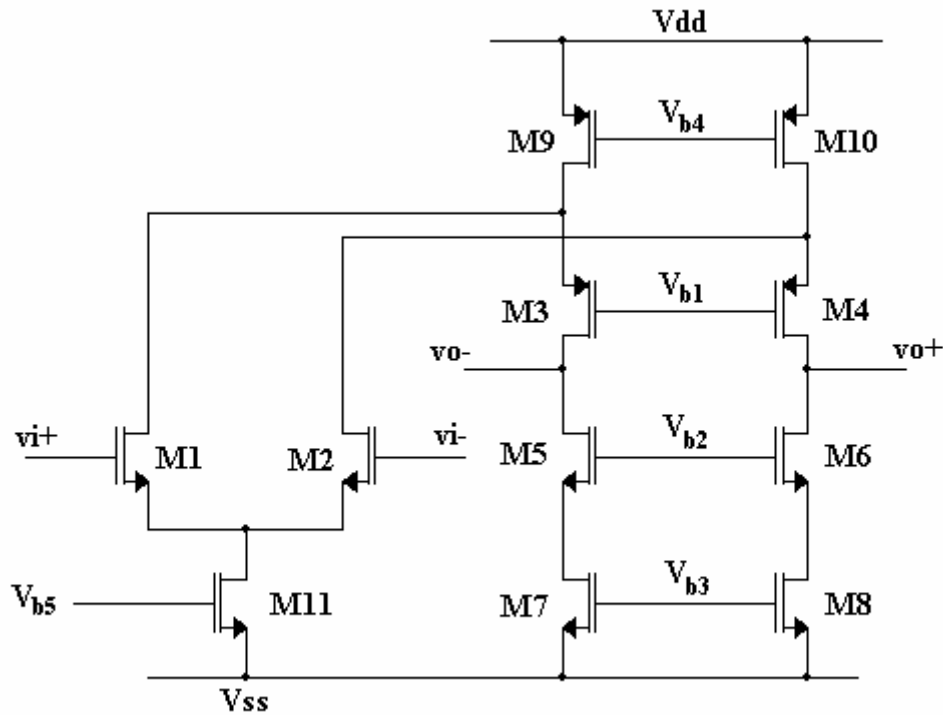


Fig. 4.8 Fully differential folded-cascode op amp.

Assuming the dominant pole of the filter op amp is located at the folded-cascode output, the stability of the circuit can be controlled by placing a small capacitor C_c between the amplifier output nodes as shown in Fig. 4.9. The effect of C_c is to increase the equivalent capacitance at the output node. The equivalent output capacitance becomes:

$$C_{out,eq} \approx C_{db5} + C_{gd5} + C_{db3} + C_{gd3} + 2C_c \quad (4.11)$$

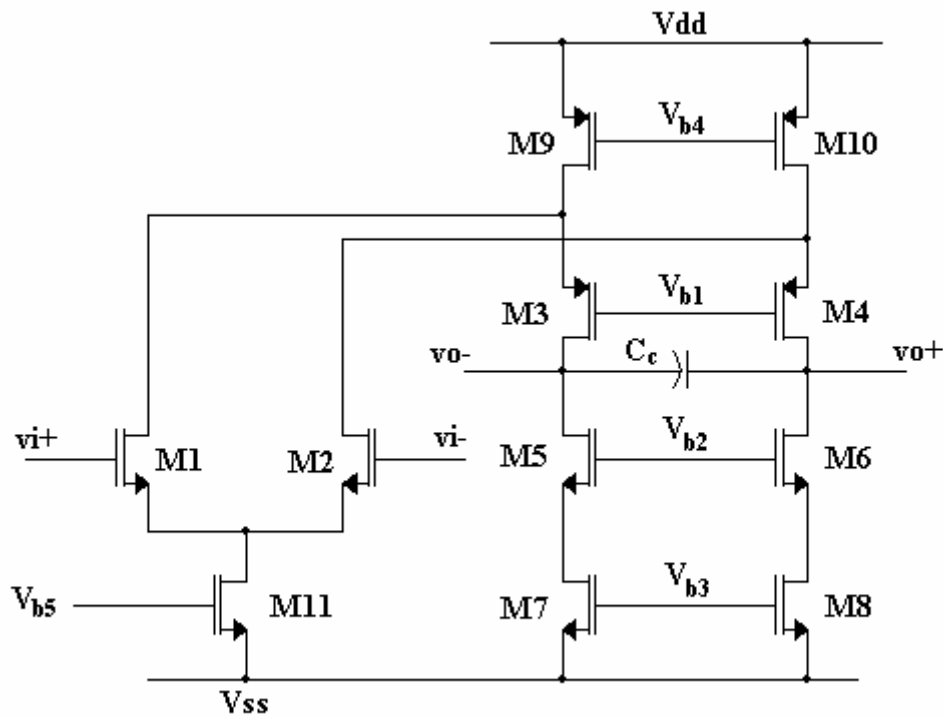


Fig. 4.9 Fully differential folded-cascode op amp with compensation.

Because of its high gain and reasonable output voltage swing, the folded-cascode amplifier is utilized as the gain stage of the filter op amp. Bias voltages V_{b1} , V_{b2} , V_{b4} , and V_{b5} are generated by DC current mirrors, while V_{b3} is controlled by a common mode feedback circuit. Table 4.1 lists the capacitor value and the dimensions, overdrive voltage, and bias current of each transistor in the folded-cascode amplifier.

Table 4.1 – Folded Cascode Component Operating Points.

Transistor/ Capacitor	Width [μm]/ Capacitance [pF]	Length [μm]	V_{DSAT} [mV]	I_{bias} [mA]
M1	180	0.2	94.7	1.62
M2	180	0.2	94.7	1.62
M3	400	0.2	-149	2.35
M4	400	0.2	-149	2.35
M5	180	0.2	114	2.35
M6	180	0.2	114	2.35
M7	180	0.2	110	2.35
M8	180	0.2	110	2.35
M9	800	0.2	-136	3.98
M10	800	0.2	-136	3.98
M11	360	0.2	99.3	3.25
Cc	0.61	-	-	-

Because the folded-cascode circuit is fully differential and contains a high impedance output node, it requires a common mode feedback (CMFB) error amplifier to maintain a proper bias. Without a CMFB circuit, slight mismatch between the operating points of the NMOS and PMOS transistors could force either the top or bottom half of the circuit into the triode region. The basic CMFB circuit is composed of a common mode detection circuit, reference voltage detection, and feedback to a controlling node in

the fully differential amplifier. Fig. 4.10 shows a low distortion CMFB topology used to bias the folded-cascode stage:

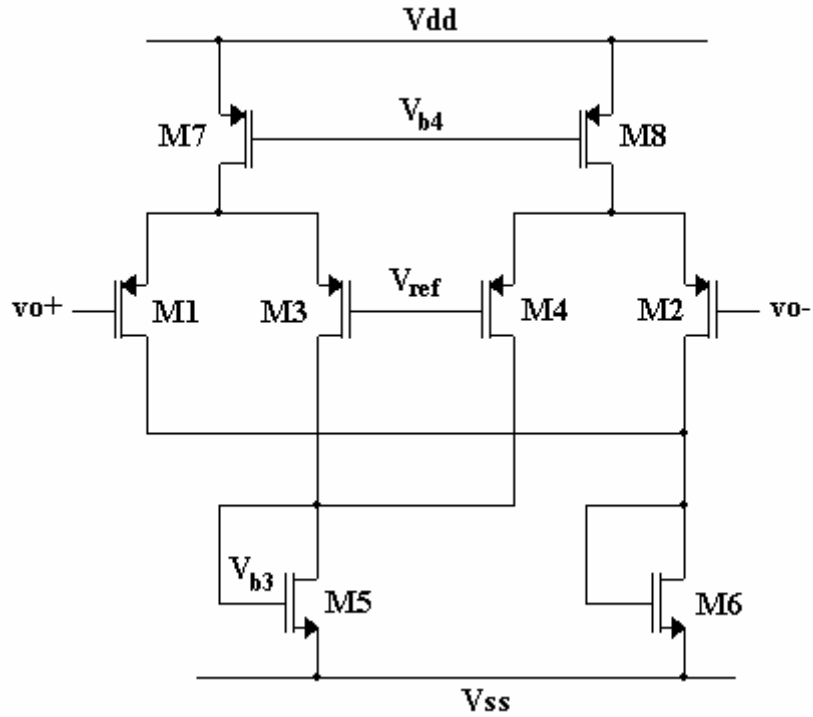


Fig. 4.10 CMFB common-mode detector and error amplifier.

This topology similar to one proposed in [7]. The common mode output voltage is detected by M1 and M2 and the reference voltage is detected by M3 and M4. The diode connected load M5 returns the CMFB control signal to the folded cascode at the node V_{b3} . The current sources M7 and M8 share the same bias voltage as the M9 and M10 from the folded-cascode amplifier, thus eliminating the need for an extra current mirror. Table 4.2 shows the CMFB transistor dimensions and operating points.

Table 4.2 – Folded Cascode CMFB Transistor Operating Points.

Transistor	Width [μm]	Length [μm]	V_{DSAT} [mV]	I_{bias} [mA]
M1	400	0.2	-92.7	0.783
M2	400	0.2	-94.3	0.820
M3	400	0.2	-105	1.09
M4	400	0.2	-104	1.05
M5	160	0.2	111	2.14
M6	160	0.2	100	1.60
M7	400	0.2	-134	1.87
M8	400	0.2	-134	1.87

4.2.2 Filter Op Amp Class AB Output Buffer

The folded-cascode amplifier requires an output buffer for a couple of reasons. The first is that if the large feedback capacitor C_{fb} is directly connected to the output node, it would kill the bandwidth of the amplifier, rendering it useless for this high frequency application. The second reason the amplifier requires a buffer is that even if it could tolerate the reduced bandwidth caused by C_{fb} , it would not be able to supply the current necessary to sink 10 mA interferers away from the TIA filter because its bias current is not that large. Finally, even if its bias current were increased enough to process a 10 mA signal, it would operate extremely inefficiently, requiring well over 10 mA DC bias current for both positive and negative output branches. The requirements of the buffer then are to efficiently drive the feedback capacitor C_{fb} , introduce minimal capacitance and conductance to the folded-cascode output nodes, and be very linear even for large signals.

The selection of the class of amplifier for the buffer stage is very important. The first thing to consider is the efficiency. The efficiency of an output stage is given as:

$$\eta = \frac{P_{Load}}{P_{Dissipated}} \times 100\% \quad (4.12)$$

P_{Load} is the power delivered to the load and $P_{Dissipated}$ is the average power consumed by the buffer. Class A buffers, which operate with continuous current flow, achieve no more than 25% efficiency. Class B buffers on the other hand, operate with no bias current under quiescent conditions and only consume current when current is being delivered to the load. A source-follower Class B buffer is shown in Fig. 4.11.

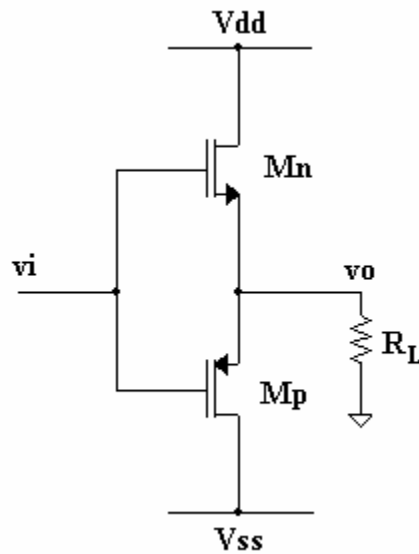


Fig. 4.11 Class B source-follower buffer.

Class B buffers can achieve maximum efficiency of 78.5%. Unfortunately, they suffer from an effect called crossover distortion. Illustrated in Fig. 4.12, crossover distortion is a result of both PMOS and NMOS transistors operating in the cutoff region in the quiescent state. As the input voltage rises slightly, both transistors remain in cutoff, causing no current to flow to the load. As the input voltage rises further such that $v_i - v_o > V_{TH,N}$, then the NMOS transistor turns on and current can flow to the load. The same thing occurs to the PMOS device as the input voltage falls.

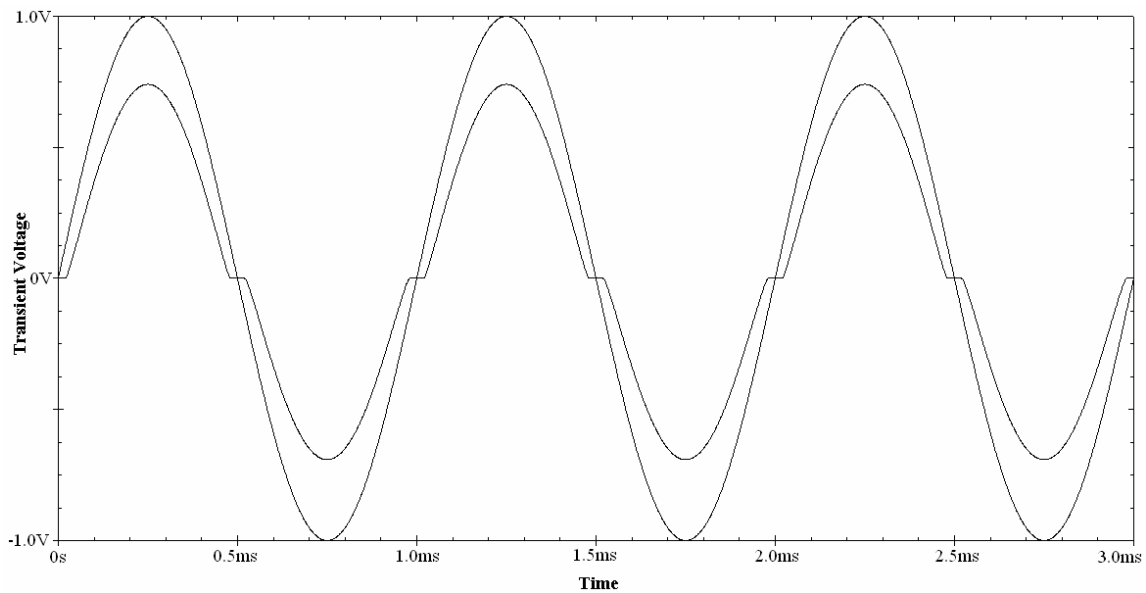


Fig. 4.12 Crossover distortion in class B buffer.

The class AB buffer is similar to the class B except that some bias current flows in the quiescent state. This reduces the efficiency of the amplifier, but it eliminates the crossover distortion. A source-follower class AB buffer is shown in Fig. 4.13. The

circuit is the same as the class B buffer except that gate voltage of the NMOS is shifted up by a threshold voltage and the PMOS gate voltage is shifted down a threshold voltage. This causes both transistors to operate at the edge of the saturation region. Therefore any small change in input voltage causes current to flow to the load.

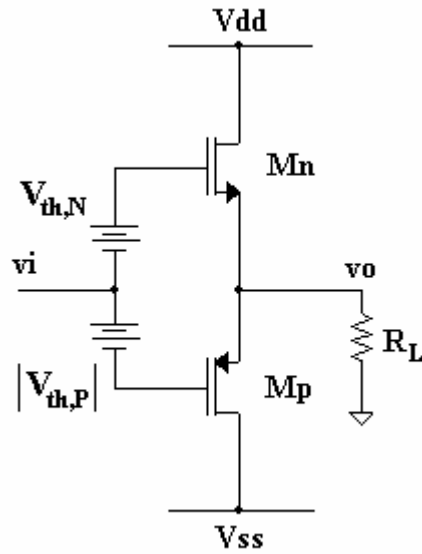


Fig. 4.13 Class AB source-follower buffer.

The common source buffer, shown in Fig. 4.14, is an alternative to the source-follower buffer. The output resistance of the source-follower buffer is:

$$r_{o,sf} = \frac{1}{g_{m,p} + g_{m,n}} \quad (4.13)$$

The output resistance of the common source buffer is:

$$r_{o,cs} = \frac{1}{g_{ds,p} + g_{ds,n}} \quad (4.14)$$

In general, the source-follower circuit has the benefit of lower output resistance than a similar common source buffer. However, the common source buffer in Fig. 4.14 has a number of advantages over the source-follower that make it desirable for use in this application. First, the voltage headroom of the source-follower is reduced by the threshold voltages of both the NMOS and PMOS, while the common source buffer is only reduced by the overdrive voltages of its NMOS and PMOS. Second, for an N-well technology, the source-follower NMOS transistor suffers from distortion due to the body effect, whereas in the common source configuration, both transistors' source-bulk voltages are zero.

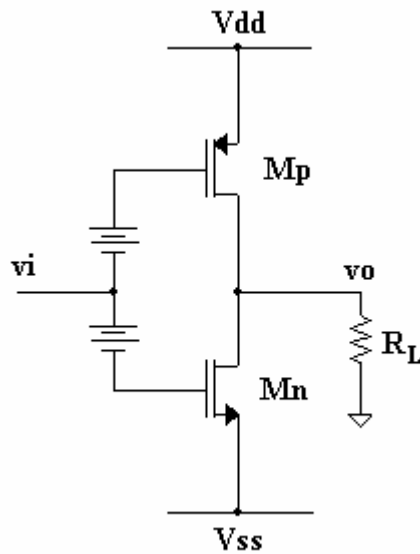


Fig. 4.14 Class AB common source buffer.

Fig. 4.15 shows a method for reducing the output resistance of the common source buffer by using negative feedback error amplifiers to control the gate voltages of the buffer transistors [8]:

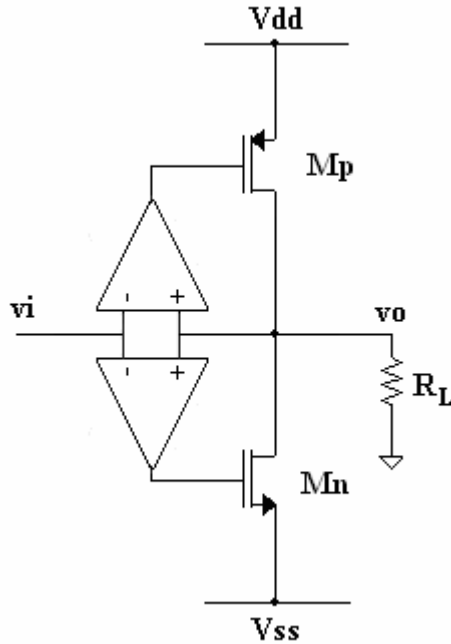


Fig. 4.15 Buffer output resistance reduced by error amplifiers.

If each amplifier in Fig. 4.15 has a gain A_v , the output resistance of the buffer is:

$$r_{o,csa} = \frac{1}{g_{ds,p} + g_{ds,n} + A_v(g_{m,n} + g_{m,p})} \quad (4.15)$$

From (4.15) it is evident that large transconductance and amplifier gain significantly reduce the output resistance of the amplifier. The amplifiers cannot just be designed

with high gain in mind. Since they are configured in closed loop with active transistors which have gain of their own, the error amplifiers must also be carefully designed so as to maintain loop stability. Therefore, an amplifier with moderate gain and high bandwidth, such as a single-ended differential pair, is desired. Fig. 4.16 shows the buffer schematic with error amplifiers.

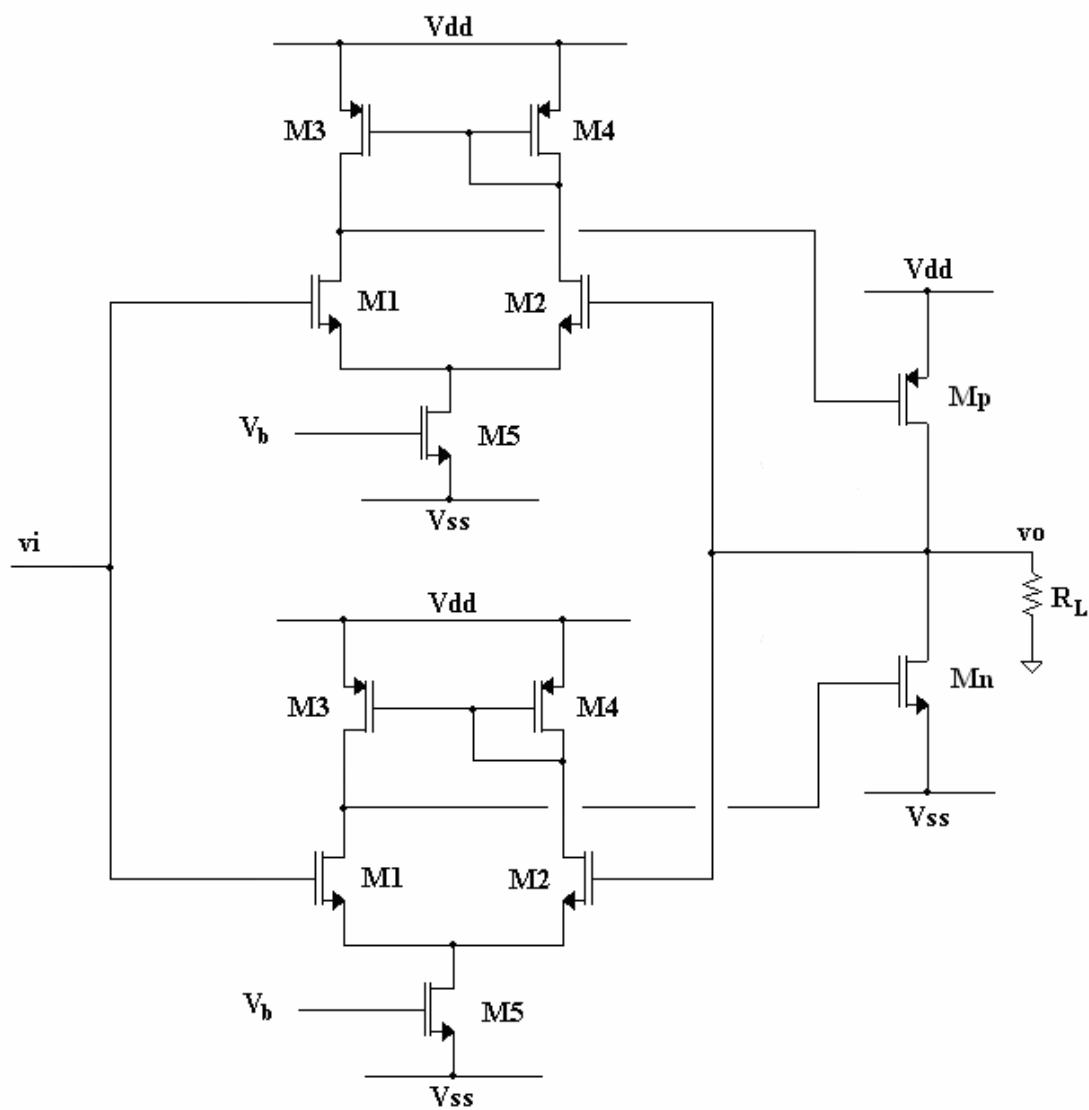


Fig. 4.16 Output buffer with single-ended error amplifiers.

Two buffers, one for each output, are needed for the filter amplifier since it is a fully differential circuit. This means a total of four error amplifiers are required, which could consume a large amount of power unless the amplifiers are specifically designed for low power operation. Table 4.3 shows the operating points of each device in Fig. 4.16.

Table 4.3 – Output Buffer Transistor Operating Points.

Transistor	Width [μm]	Length [μm]	V_{DSAT} [mV]	I_{bias} [mA]
M1	80	0.18	94.6	0.811
M2	80	0.18	91.0	0.761
M3	80	0.18	-170	0.811
M4	80	0.18	-167	0.761
M5	160	0.18	96.7	1.57
Mn	100	0.18	274	4.18
Mp	30	0.18	-339	4.12

4.2.3 TIA Op Amp

For a more consistent comparison between the operation of the original TIA filter and the filter proposed in this thesis, the TIA amplifier is designed with the same topology as in [4]. The op amp is a two stage fully-differential operational transconductance amplifier (OTA) as shown in Fig. 4.17. The CMFB network in [4] senses the common mode voltage at the output nodes and returns the common mode control signal to node V_{b2} . The topology of the CMFB is not reported in [4], so the same topology that was used for the filter amplifier CMFB is utilized for the TIA. The only difference is that the common mode control voltage is taken from the drain of M6 instead of M5. The reason for this is that since the OTA in Fig. 4.17 has two gain stages,

there is one more inversion than in the filter amplifier. In order to keep the loop in negative feedback, the output has to be taken at the other load transistor.

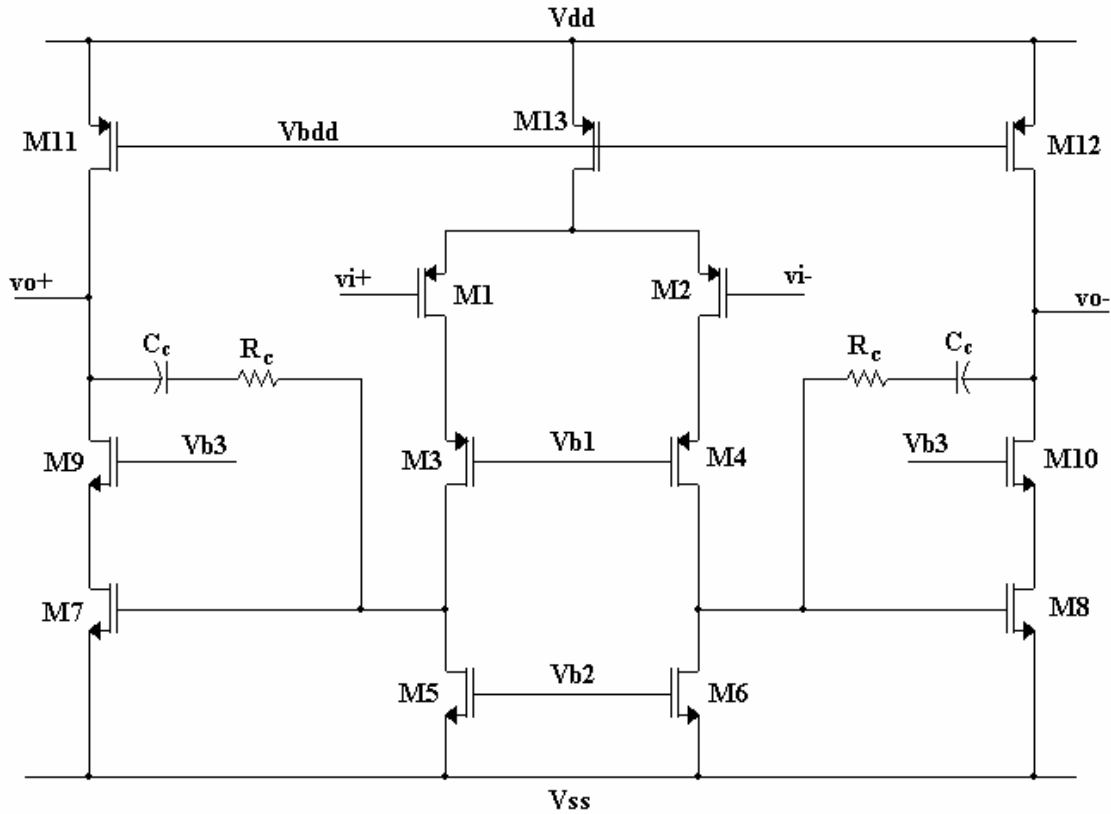


Fig. 4.17 Fully-differential OTA from [4].

Linearity of the amplifier is improved by making GBW large. Because of the large GBW, non-dominant poles can cause stability problems. Miller capacitor C_c splits the dominant and non-dominant poles to maintain good phase margin, and the resistor R_c is used to cancel the feedforward zero created by C_c . While noise is not a concern in the filter op amp because it only interacts with the filter in the stop-band, the TIA op amp

processes in-band signals and must therefore be a low noise device. In fact, because the current mode passive mixer has such low flicker noise, the TIA op amp is the main contributor of this low frequency noise. The input differential pair M1 and M2 is composed of very large transistors to reduce flicker noise as much as possible [9]. Additionally, PMOS transistors are used because they have a lower flicker noise coefficient. A summary of TIA op amp components is shown in Table 4.4. Common mode feedback components are shown in Table 4.5.

Table 4.4 – TIA Component Operating Points.

Transistor/ Capacitor/ Resistor	Width [μm]/ Capacitance [pF]/ Resistance [Ω]	Length [μm]	V_{DSAT} [mV]	I_{bias} [mA]
M1	432	0.18	-175	3.90
M2	432	0.18	-175	3.90
M3	432	0.18	-163	3.90
M4	432	0.18	-163	3.90
M5	240	0.18	112	3.90
M6	240	0.18	112	3.90
M7	240	0.18	122	4.41
M8	240	0.18	121	4.31
M9	240	0.18	119	4.41
M10	360	0.18	118	4.31
M11	360	0.18	-184	4.37
M12	360	0.18	-183	4.30
M13	810	0.18	-176	7.81
C_c	4	-	-	-
R_c	50	-	-	-

Table 4.5 – TIA CMFB Transistor Operating Points.

Transistor	Width [μm]	Length [μm]	V_{DSAT} [mV]	I_{bias} [mA]
M1	180	0.18	-163	1.67
M2	180	0.18	-189	2.29
M3	180	0.18	-170	1.84
M4	180	0.18	-145	1.28
M5	252	0.18	102	3.12
M6	252	0.18	111	3.96
M7	360	0.18	-176	3.50
M8	360	0.18	-177	3.57

Table 4.6 is a summary of the specifications of the filter amplifier, including folded-cascode gain stage with output buffer and the TIA amplifier.

Table 4.6 – Amplifier Specifications.

Specification	Filter Amplifier	TIA Amplifier
Current Consumption	56 mA	24.7 mA
DC Gain	43.5 dB	53 dB
GBW	882 MHz	1.02 GHz
Phase Margin	49°	71.5°
Buffer Output Resistance	5 Ω up to 1 GHz	N/A
Settling Time	110 ns	80 ns

4.3 Layout Considerations

Ideally, the fabricated circuit should show the same response as the schematic level design. Unfortunately, parasitics such as substrate capacitance and metal trace resistance can cause significant worsening of the response, especially at high frequencies. The layout of the circuit must be carefully designed to reduce parasitics and to ensure good matching of differential components. Interconnecting blocks are placed

physically close to each other to minimize metal trace length. Also, metal wires conducting large currents such as power supply connections are made wide to reduce current density and resistive voltage drop, whereas wires carrying small bias currents and high frequency signals are made narrow to reduce the metal-to-substrate capacitance.

4.3.1 Passive Components

Common centroid techniques are employed on differential components where possible. Capacitors are broken up into fractions and then interspersed in a checkered fashion with similar capacitors. For example, there are two 35 pF capacitors C_{fb} in the filter. Each C_{fb} is broken up into 8 different 4.375 pF capacitors and then combined with the other C_{fb} as shown in Fig. 4.18. This technique minimizes mismatch due to gradients on the surface of the wafer. All capacitors in this filter design that have a matching component utilize the common centroid technique.

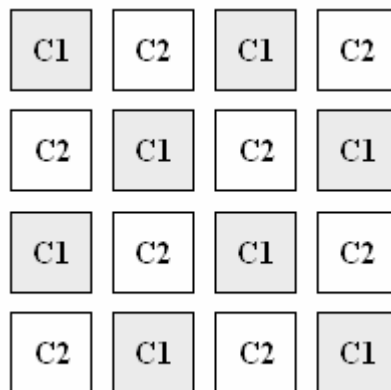


Fig. 4.18 Capacitors with common centroid.

Resistors generally consume much smaller area than capacitors, which means surface gradients tend to affect them with less intensity. Instead of using the common centroid technique, matching resistors are simply placed directly adjacent to each other and in the same orientation. This provides good matching without increasing the complexity of the resistor layout.

4.3.2 Active Components

For transistors, multi-finger design is used to reduce polysilicon gate resistance. However, more fingers mean larger source/drain area and thus larger source-to-substrate and drain-to-substrate parasitic capacitances. Therefore, a compromise can be reached between gate resistance and substrate capacitance. Also, like the capacitors, common centroid technique is used for matching transistors. In addition, dummy transistors are used to reduce variation at the edges of the transistor blocks. Fig. 4.19 shows an example of matching transistors. Each transistor M1 and M2 has a gate width of $3.6 \mu\text{m} \times 4 \text{ fingers} \times 2 \text{ multiplier} = 28.8 \mu\text{m}$. Where possible, transistors in the filter that have a matching component utilize the common centroid technique and dummy transistors. All transistors with widths larger than $10 \mu\text{m}$ are split into multi-finger devices.

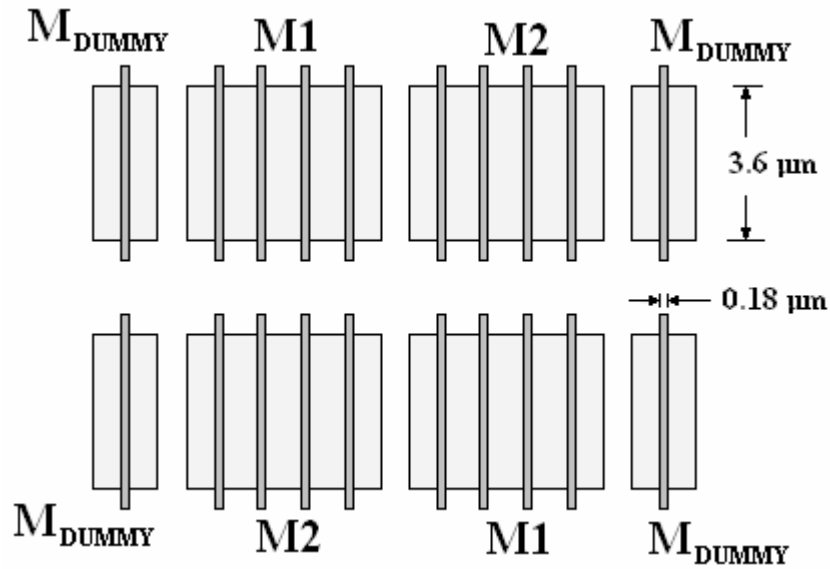


Fig. 4.19 Multi-finger common centroid matched transistors with dummy elements.

To reduce the body effect, all PMOS devices are placed in an N-well biased to the same potential as the transistor source terminal. This means matching PMOS devices that do not share the source node cannot be made common centroid since they must be in separate N-wells. The bulk nodes of all NMOS devices are connected to the lowest supply potential and not the source nodes, so all NMOS devices utilize the common centroid technique.

4.3.3 Chip Layout

The overall layout of the chip is shown in Fig. 4.20. The upper portion of the layout is the original TIA filter combined with the filter proposed in this thesis. Below it is the original TIA filter without the proposed filter. Both versions of the filter are

included on the test chip so that fair testing and analysis can be done on the chip after fabrication.

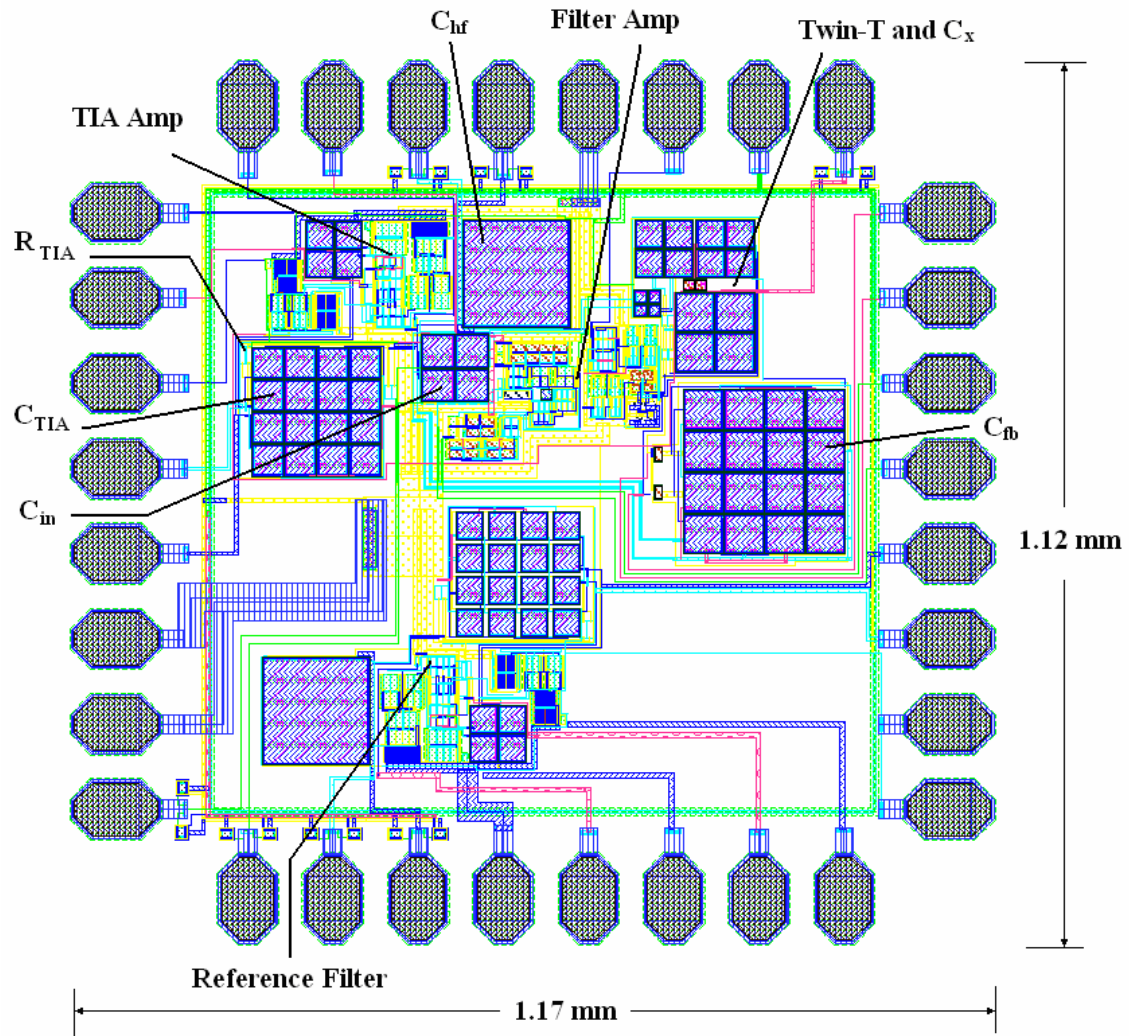


Fig. 4.20 Filter layout in Jazz 0.18 μm .

CHAPTER V

SIMULATION RESULTS

The results of the designed filter designed in Jazz 0.18 μm are compared with those of the original TIA filter also designed in Jazz 0.18 μm . Where applicable, these results are also compared with the ideal single-pole low-pass transfer function.

5.1 Schematic Level Simulation Results

Fig. 5.1 shows the AC response of the designed filter along with the original filter and the single pole low-pass transfer function. As expected in the new filter, slight bandwidth extension occurs up to about 20 MHz at which point the filter response quickly falls to below 30 dB for the rest of the frequency spectrum. In the final schematic level design, the series feedback resistor R_{fb} is designed to be 5 Ω instead of 10 Ω because it is expected that in the layout of the circuit the wire traces will add extra series resistance which will degrade the circuit performance in the lower stop-band frequencies. The trade-off is that the schematic level simulation includes the large bump in response around 900 MHz. The consequence of this bump is increased input resistance and lost rejection at high frequencies. It does not significantly affect stability or transient response.

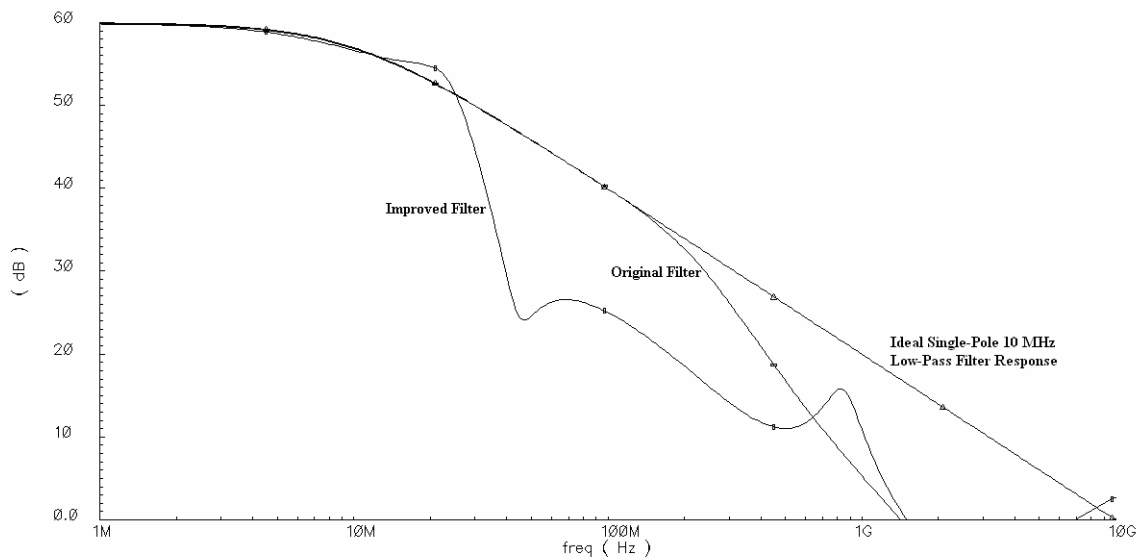


Fig. 5.1 AC response of filter.

Fig. 5.2 shows the small signal input impedance of the filter. The input impedance remains below $15\ \Omega$ over all frequencies and below $8\ \Omega$ in the high frequency stop-band. Most importantly, the input impedance between 40 MHz and 400 MHz is kept well below $4\ \Omega$, which is very low. While the $13\ \Omega$ peak input impedance of the original filter is lower than that of the new filter, the original filter input impedance is at this peak throughout the critical 40 MHz to 400 MHz range. It is in the range that large interferers threaten the linearity of the filter.

Fig. 5.3 is the transient response to a 1 mA input current pulse. Slight ringing in the new filter is observed due to the additional filter network, while the original filter shows a first order response. The ringing in the new filter is expected and was observed in the macromodel simulations.

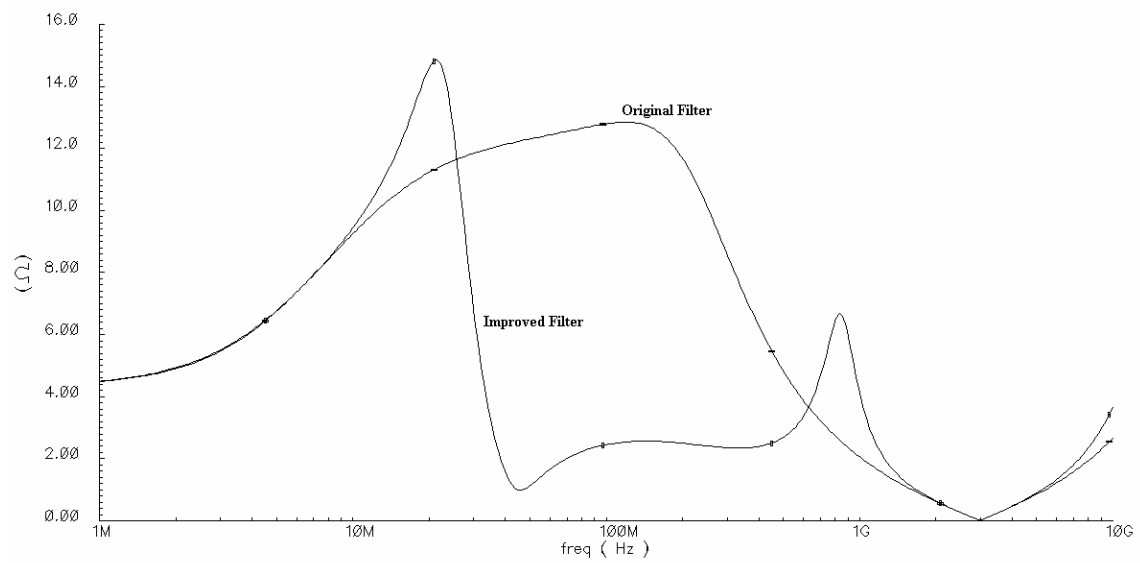


Fig. 5.2 Small signal input impedance of filter.

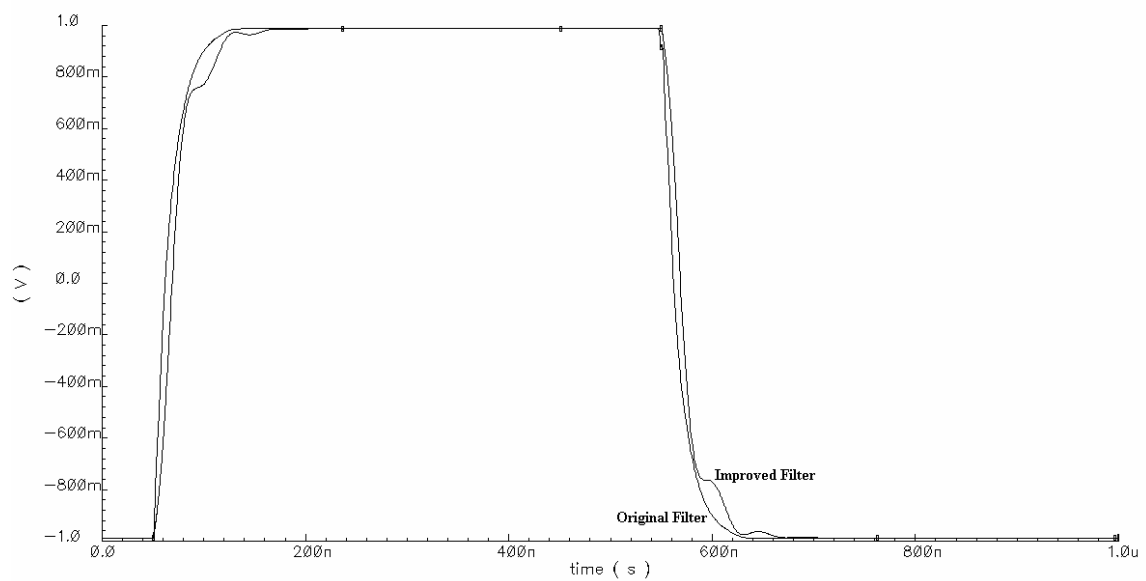


Fig. 5.3 Filter transient response to 1 mA current pulse.

Fig. 5.4 shows the transient response of the new filter to a 10 MHz 100 μ A signal along with a 50 MHz 1 mA interferer, and Fig. 5.5 shows the response of the original filter to the same 10 MHz signal and 1 mA 50 MHz interferer.

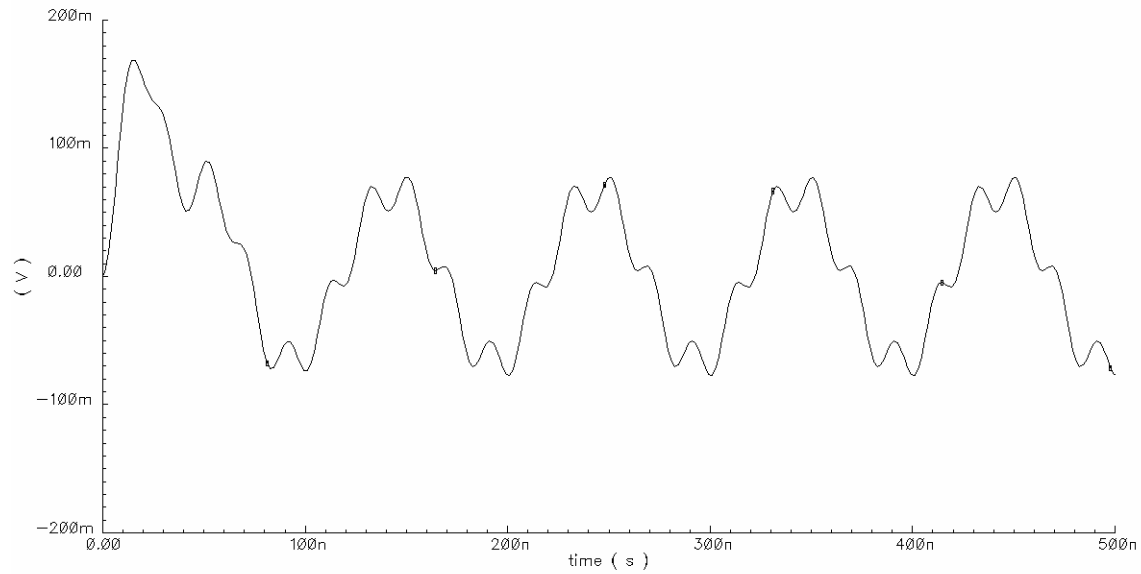


Fig. 5.4 New filter response to 10 MHz 100 μ A and 50 MHz 1 mA signals.

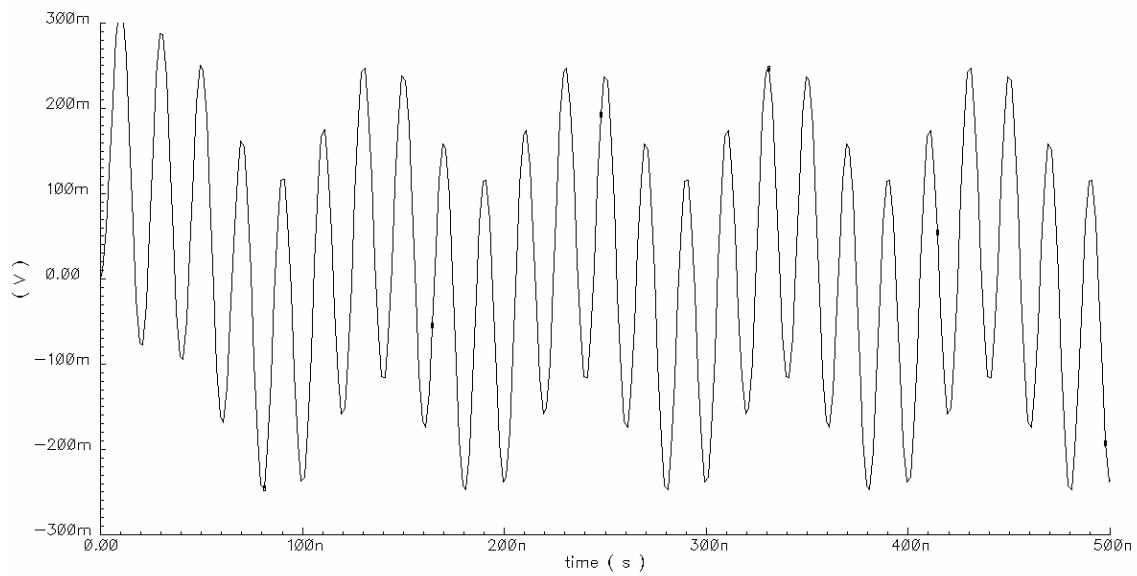


Fig. 5.5 Original filter response to 10 MHz 100 μ A and 50 MHz 1 mA signals.

Fig. 5.6 and Fig. 5.7 show the responses to 10 MHz 100 μ A and 50 MHz 10 mA signals of the new and original filters, respectively. Notice that the 0-to-peak voltage of the 50 MHz signal for the new filter is around 350 mV, whereas the 0-to-peak voltage of original filter is 1.6 V. Fortunately, the supply voltage for Jazz 0.18 μ m is 1.8 V so this signal does not saturate the TIA filter, but if the supply was 1 V, then the filter would be very saturated.

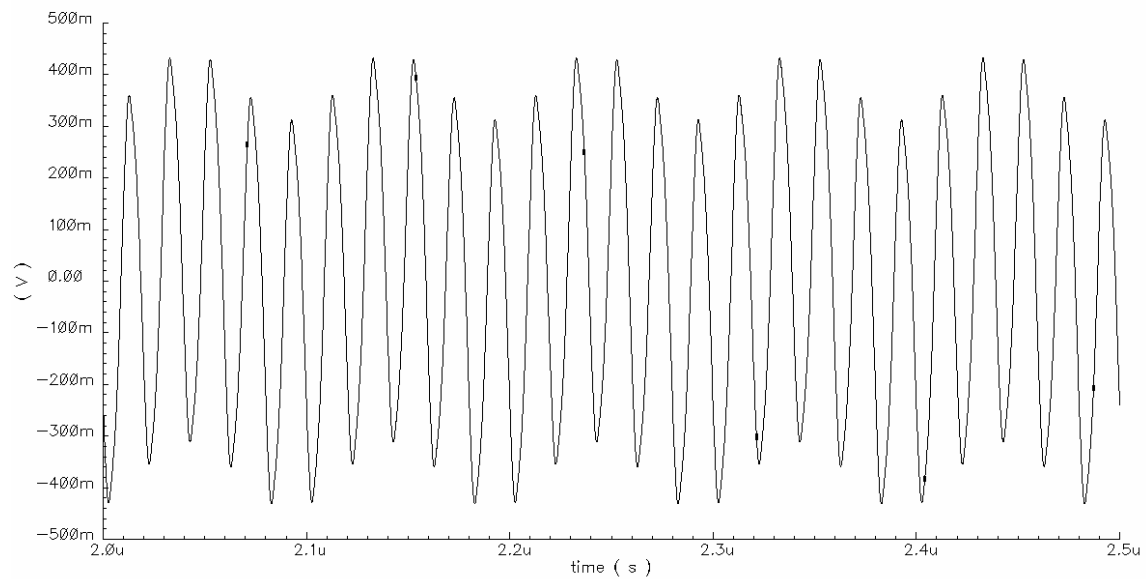


Fig. 5.6 New filter response to 10 MHz 100 μ A and 50 MHz 10 mA signals.

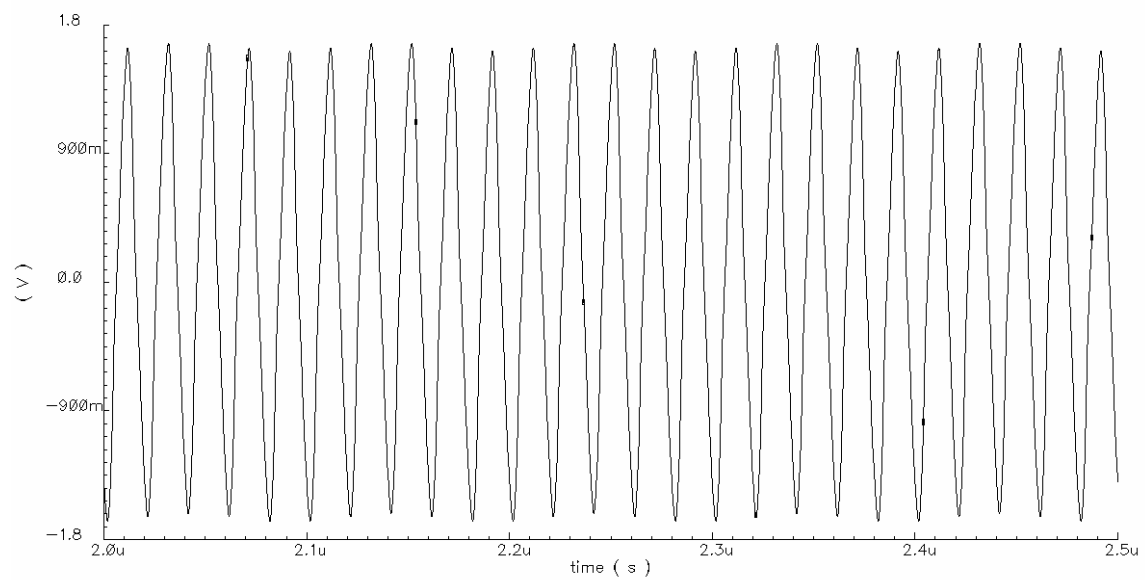


Fig. 5.7 Original filter response to 10 MHz 100 μ A and 50 MHz 10 mA signals.

Fig. 5.8 and Fig. 5.9 show the discrete Fourier transform (DFT) of the waveform in Figs. 5.6 and 5.7, respectively. The DFT window is rectangular with a width of 500 ns, and $N = 512$ samples. A comparison of Figs. 5.8 and 5.9 shows that the 10 mA 50 MHz signal response of the new filter is attenuated 12 dB more than the original filter. The new filter also shows less harmonic distortion than the original filter. Notice on both plots the intermodulation harmonics at 30 MHz, 70 MHz, 90 MHz, etc. The largest harmonic, at 150 MHz, is 16 dB lower for the new filter. In any case, the 150 MHz harmonic is not a big issue because it is far beyond the 10 MHz bandwidth and will be filtered by the DSP.

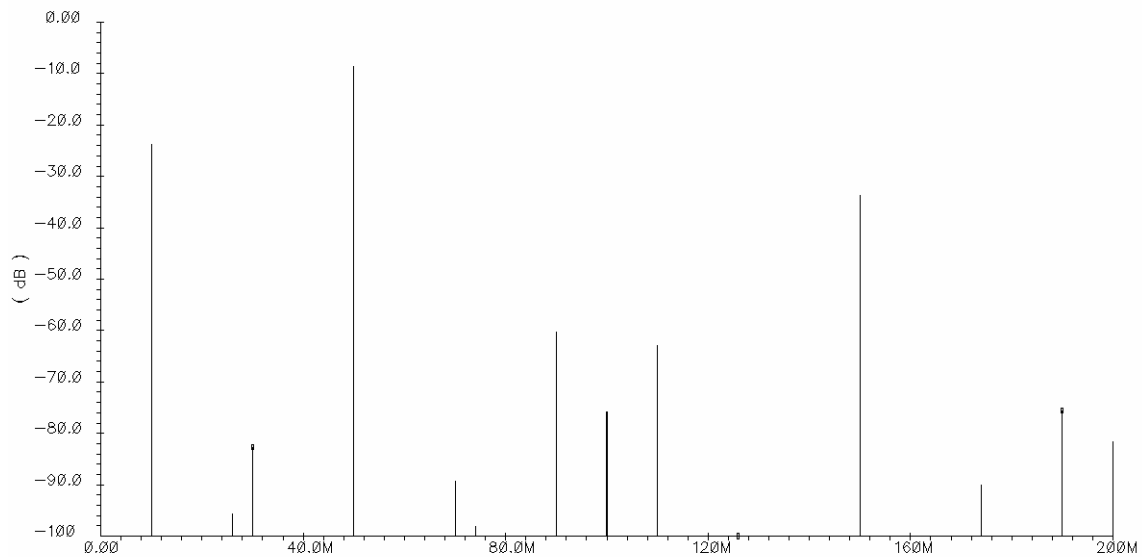


Fig. 5.8 DFT for new filter 10 MHz 100 μ A signal and 50 MHz 10 mA interferer.

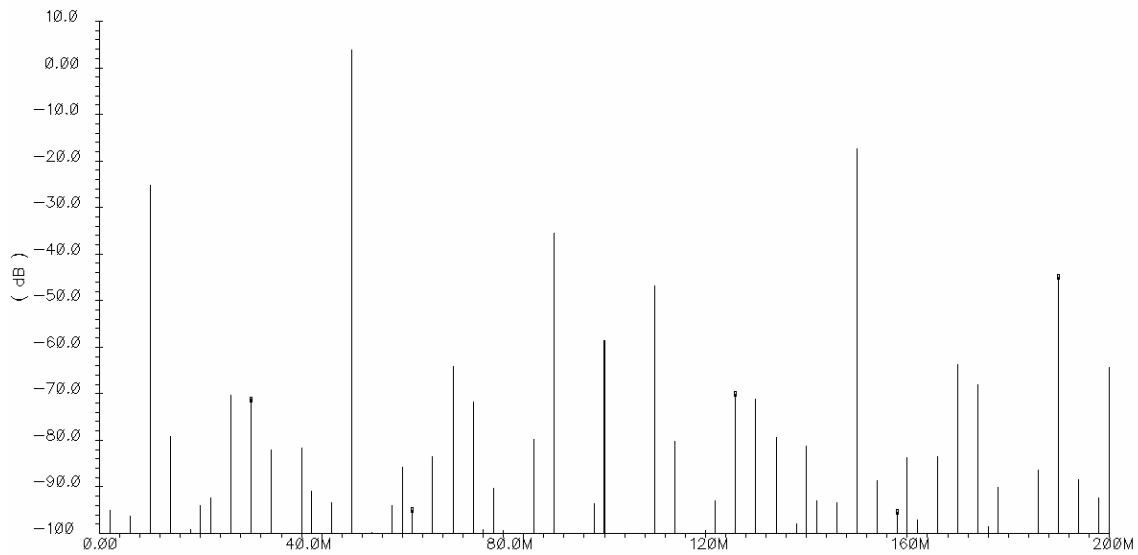


Fig. 5.9 DFT for original filter 10 MHz 100 μ A signal and 50 MHz 10 mA interferer.

The DFT of the response of the new filter to 50 MHz 5 mA and 90 MHz 5 mA signals is shown in Fig. 5.10. The DFT window is rectangular with a width of 500 ns, and $N = 512$ samples. The concern with these two interferers is the intermodulation product $2f_1 - f_2$. For $f_1 = 50$ MHz and $f_2 = 90$ MHz, the result is 10 MHz. This in-band harmonic is very problematic because it will not be filtered by the DSP. Comparing Figs. 5.10 and 5.11, the 10 MHz harmonic in the new filter response is nearly 10 dB below the 10 MHz harmonic in the original filter. This result is due to the fact that the input impedance of the original filter at these frequencies is much larger than the input impedance of the new filter, so the voltage level at the amplifier inputs is much larger for the simple TIA filter.

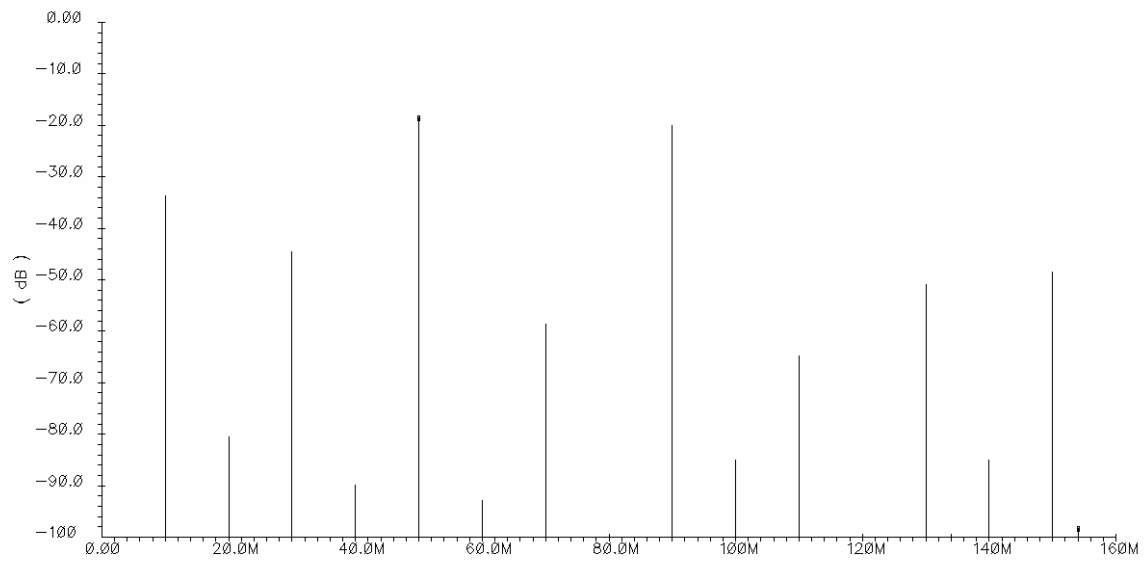


Fig. 5.10 DFT of new filter response for 50 MHz and 90 MHz 5 mA signals.

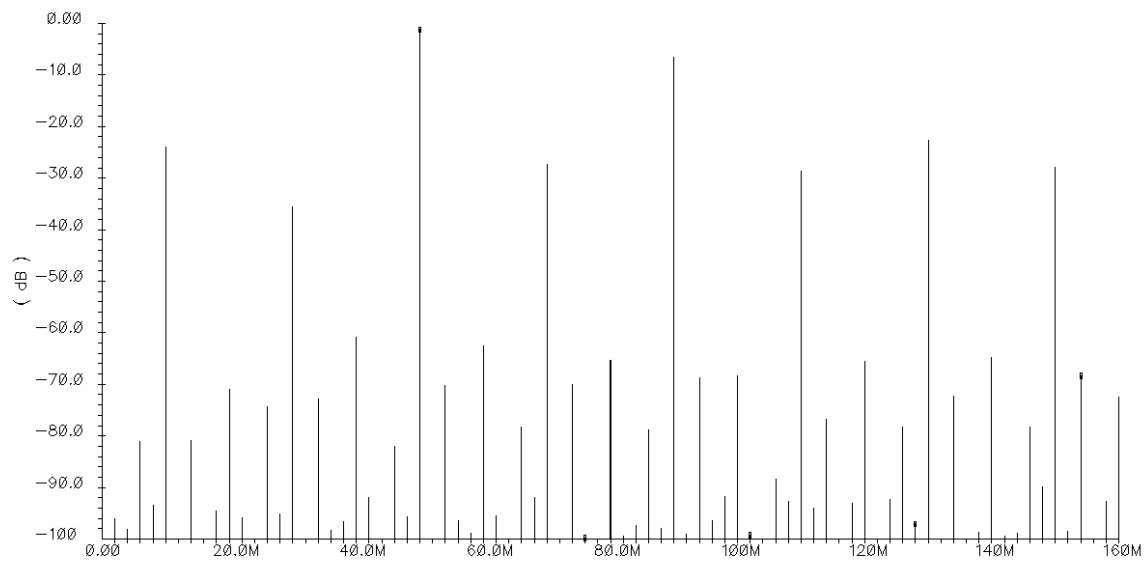


Fig. 5.11 DFT of original filter response for 50 MHz and 90 MHz 5 mA signals.

Fig. 5.12 and Fig. 5.13 show the DFT of the new filter and original filter response to 9 MHz and 10 MHz 500 μ A input signals. The DFT window is rectangular with a width of 1 μ s, and $N = 512$ samples. Intermodulation distortion is similar for both filters, and in-band harmonics are at least 60 dB below the input tones.

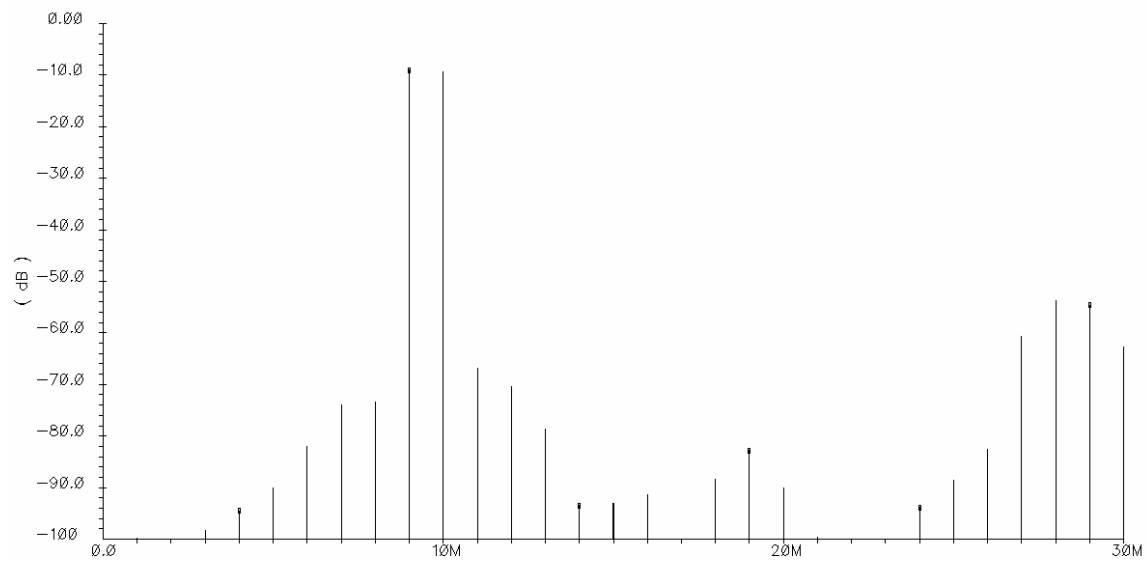


Fig. 5.12 New filter DFT for 9 MHz and 10 MHz 500 μ A signals.

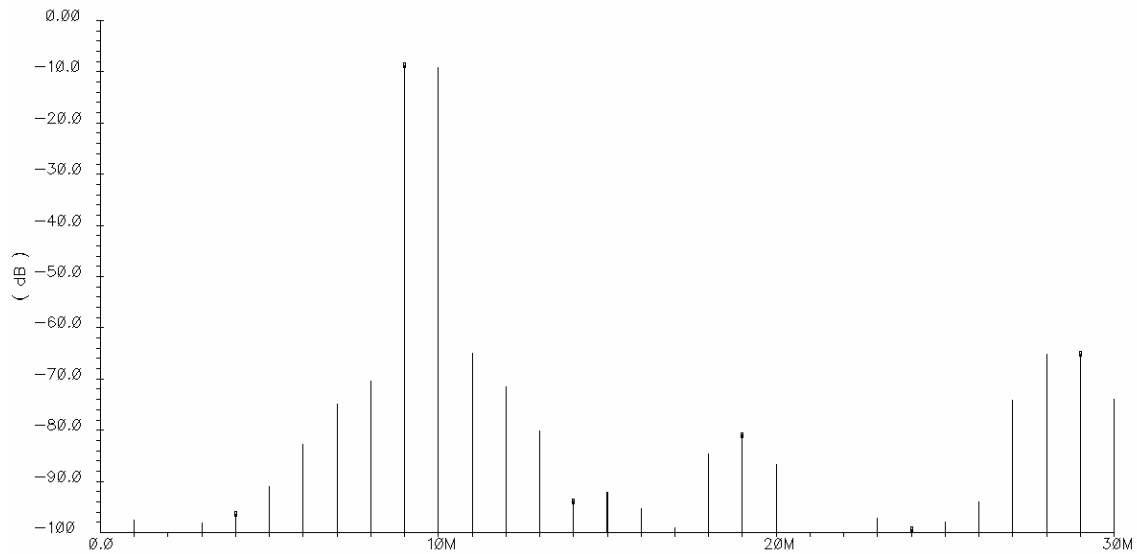


Fig. 5.13 Original filter DFT for 9 MHz and 10 MHz 500 μ A signals.

Fig. 5.14 shows the input referred spot noise current density for the new filter and the original filter. The noise of the new filter is higher than the original, which is expected since more circuitry has been added to the system. However, only the noise in the 10 MHz bandwidth is of concern, so the large noise density of the new filter in the stop-band does not pose a problem. In fact, Fig. 5.14 is only correct up to 10 MHz, since at higher frequencies most of the input current noise is diverted into the new filter and does not appear at the real output. The noise summary is shown in Table 5.1.

Table 5.1 – Noise Summary.

Filter	Integrated Noise (1 kHz – 10 MHz) [nA]
New Filter	211
Original Filter	58.9

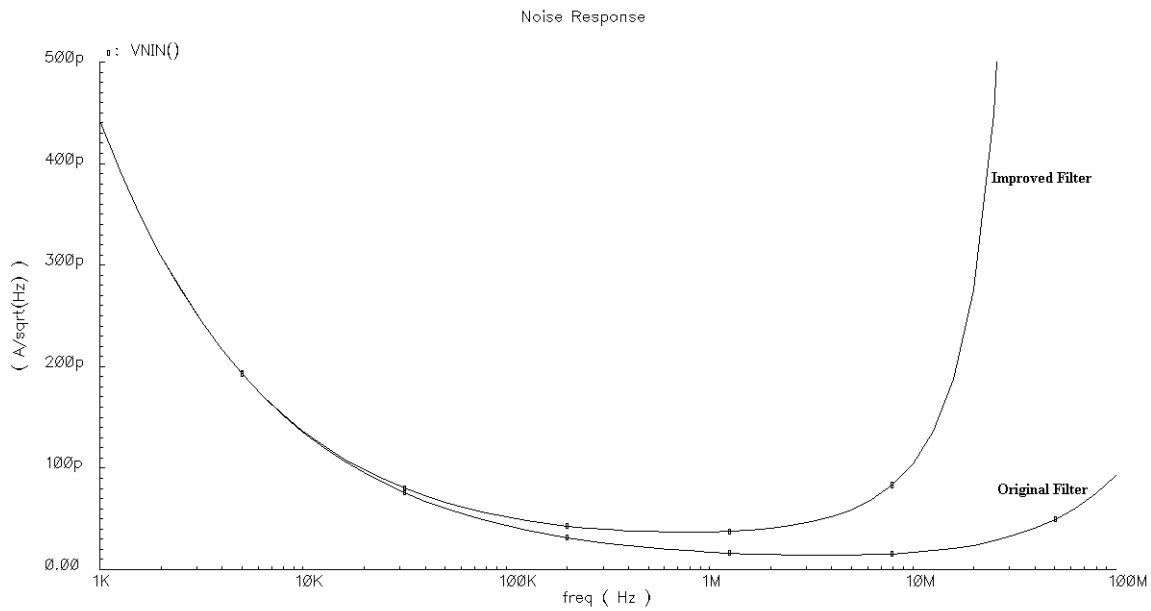


Fig. 5.14 Input referred spot noise current density.

5.2 Post-Layout Simulation Results

Layout results are somewhat degraded from those of the schematic level simulations. It is already very difficult to achieve GBW above 1 GHz in 0.18 μm technology, but the bandwidth is further reduced by metal wire resistance and parasitic capacitance. The AC plot is shown in Fig. 5.15. Rejection between 30 MHz and 300 MHz is up to 13 dB worse than in the schematic level. The response of the original filter is also worse because of its limited bandwidth. Fig. 5.16 compares the small signal input impedance of the new and old filters. The minimum input impedance of the improved filter is 5.2 Ω compared to 1 Ω in pre-layout simulations.

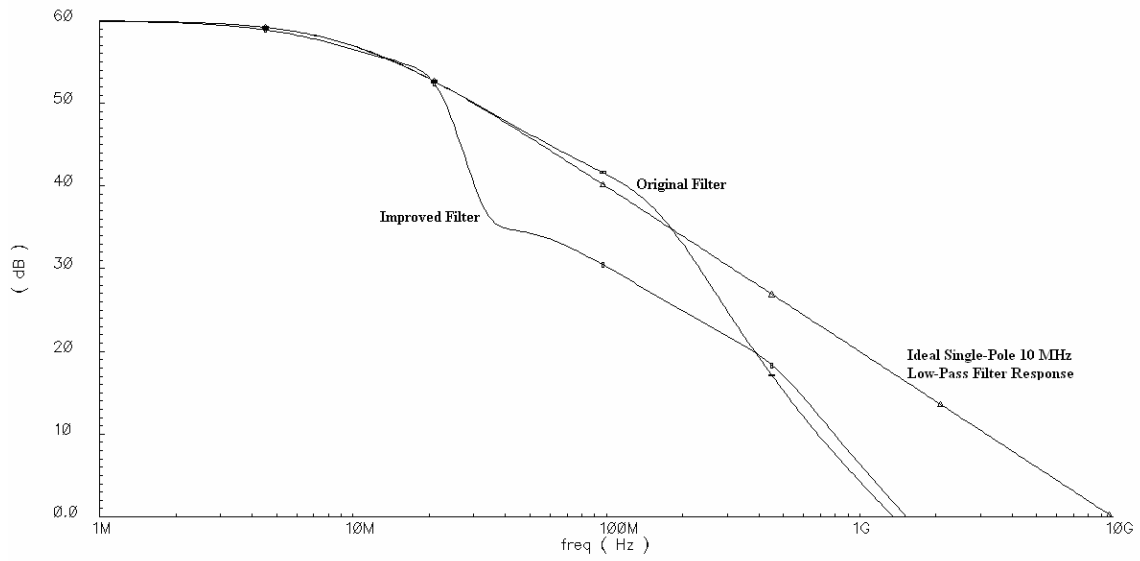


Fig. 5.15 Post-layout AC simulation results.

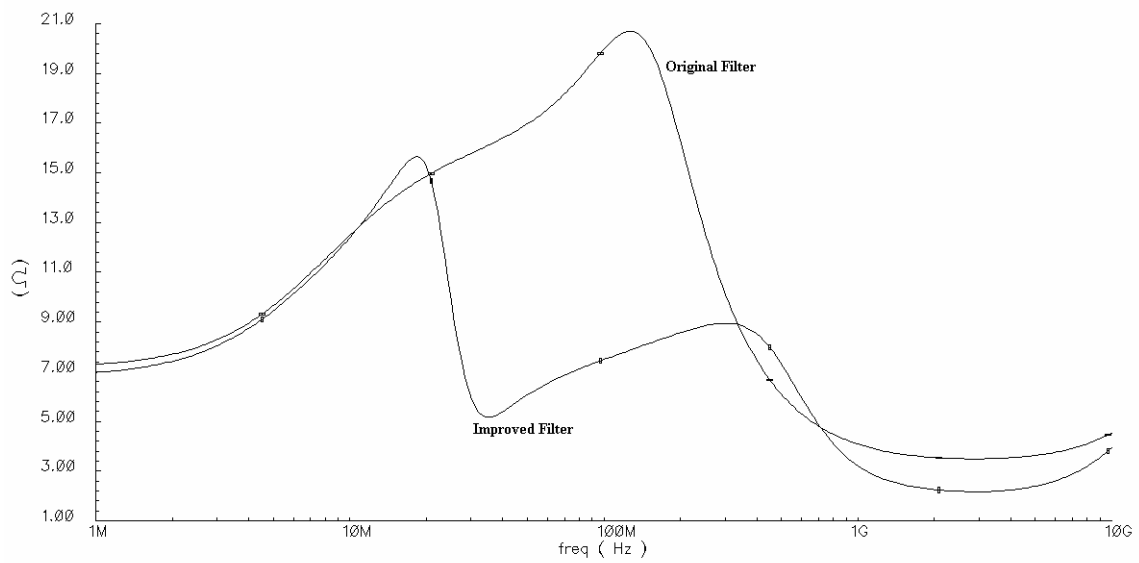


Fig. 5.16 Post-layout small signal input impedance.

The transient step response to 1 mA current pulses is shown in Fig. 5.17. The ringing that appeared in the pre-layout simulations of the improved filter is further dampened by parasitics.

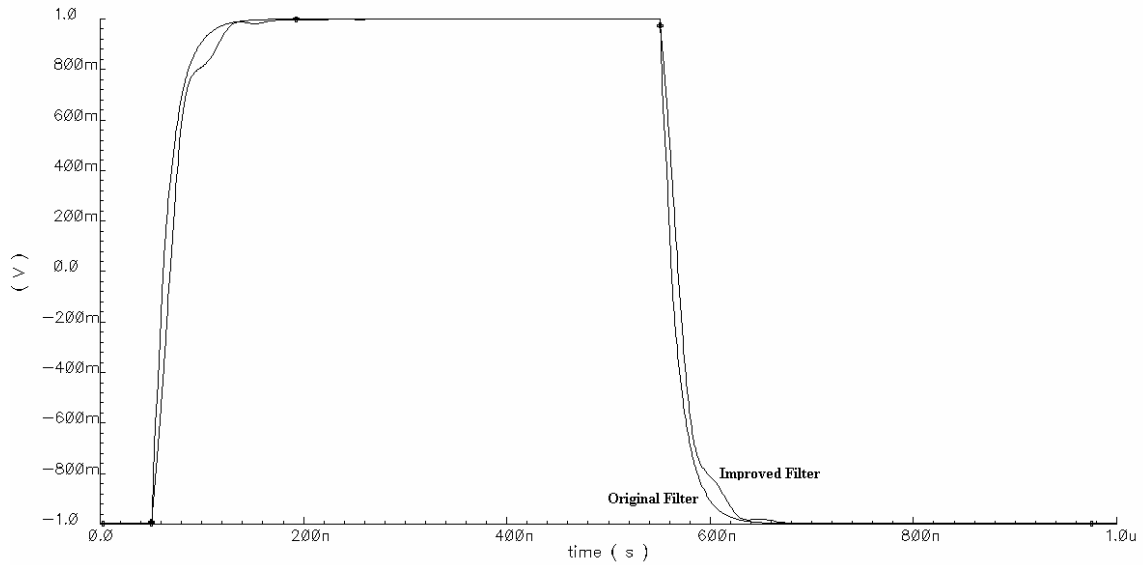


Fig. 5.17 Post-layout transient step response.

Figs. 5.18 and 5.19 show the transient response of the old and new filters to 10 MHz 100 μ A and 50 MHz 1 mA inputs. While post-layout simulations show that the rejection of the improved filter is not as good as the schematic level simulations in Fig. 5.4, it is still much better than the post-layout simulations of the old filter response in Fig. 5.19.

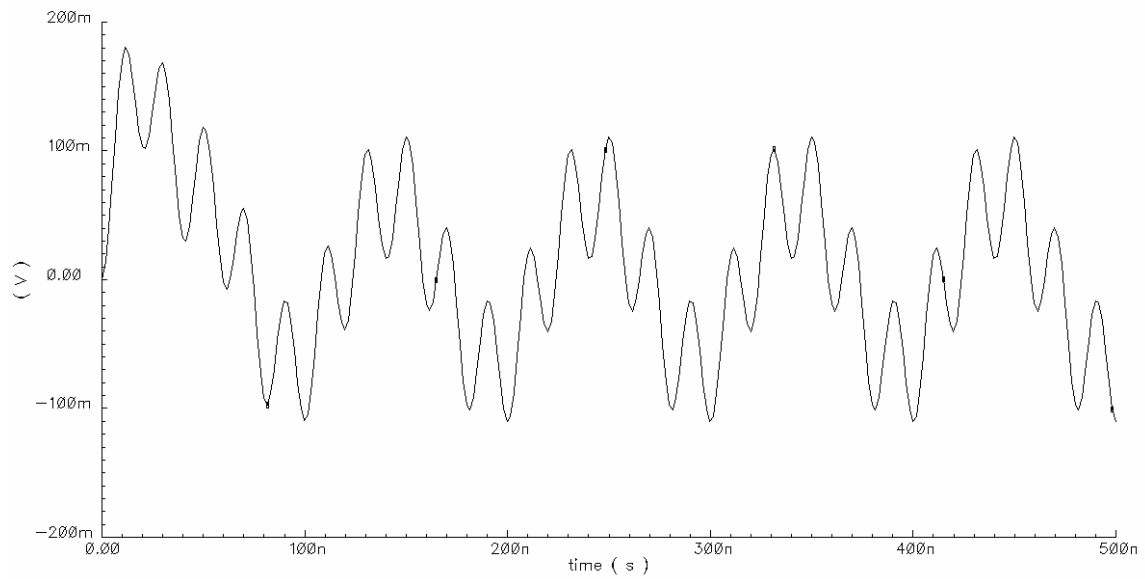


Fig. 5.18 Post-layout transient response of new filter to 10 MHz 100 μ A and 50 MHz 1 mA signals.

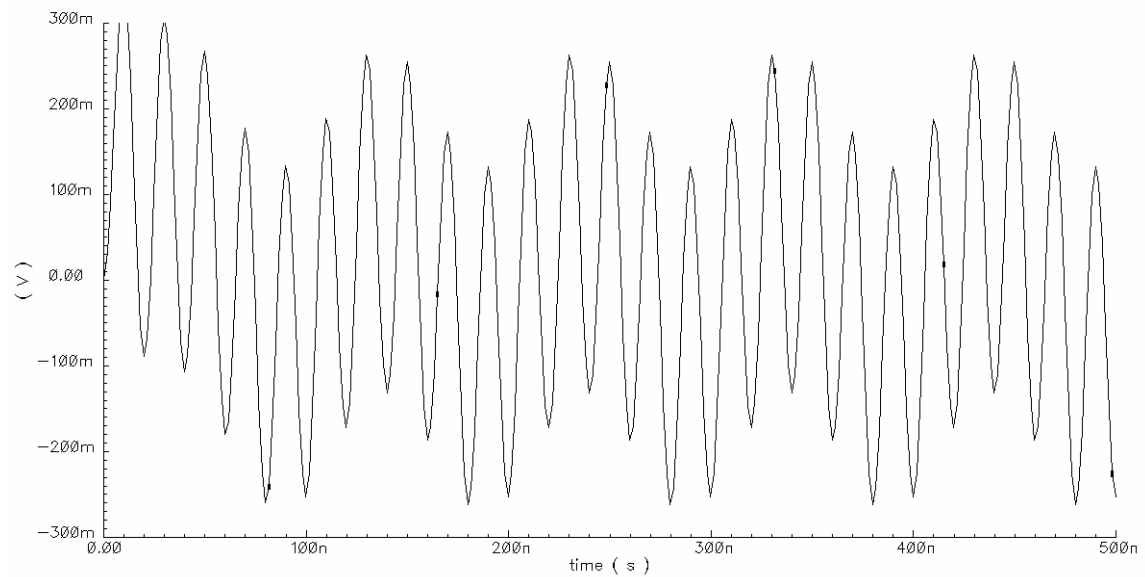


Fig. 5.19 Post-layout transient response of original filter to 10 MHz 100 μ A and 50 MHz 1 mA signals.

To illustrate the impact of reduced input impedance, the input voltage waveforms associated with Figs. 5.18 and 5.19 are displayed in Fig. 5.20. The larger input voltage is indicative of larger input impedance. This larger voltage swing not only reduces the linearity of the filter amplifiers, but it also decreases mixer channel resistance linearity.

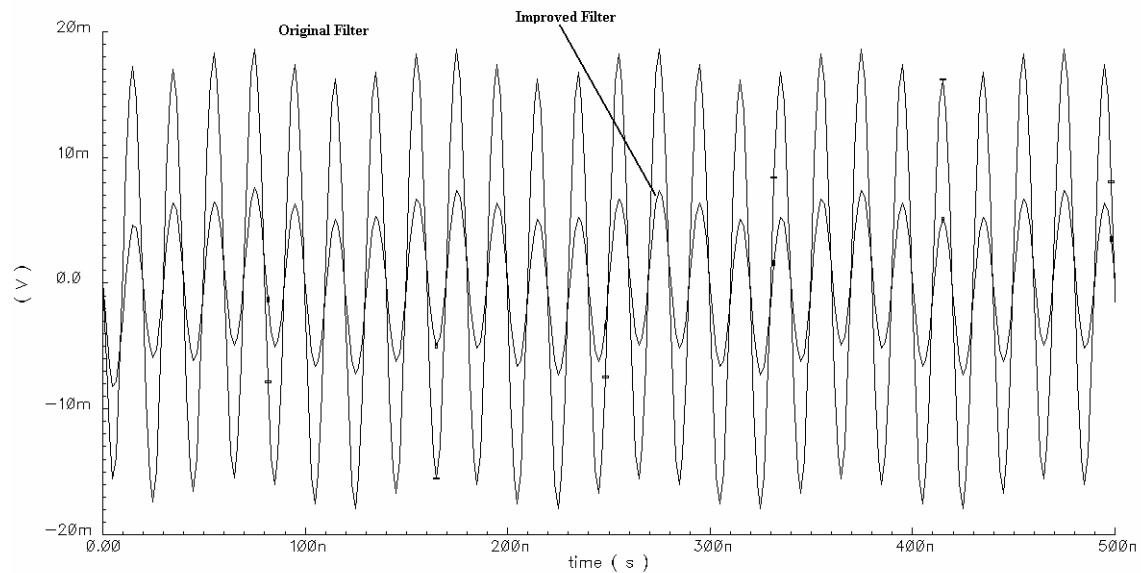


Fig. 5.20 Transient input voltage waveform in the presence of 10 MHz 100 μ A and 50 MHz 1 mA signals.

Figs. 5.21 and 5.22 show the transient response of the old and new filters to 10 MHz 100 μ A and 50 MHz 10 mA inputs.

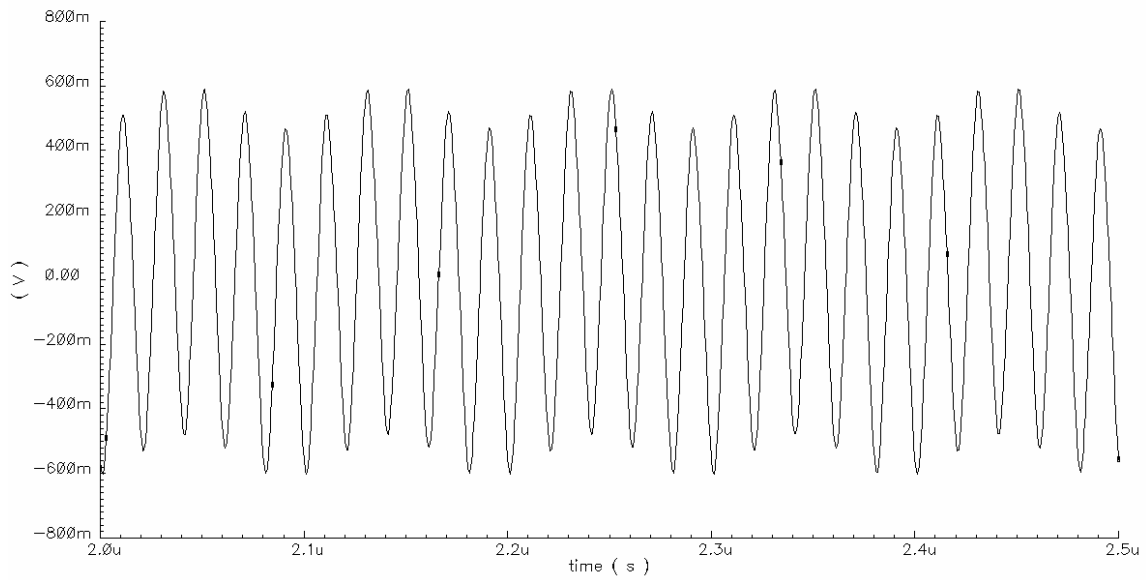


Fig. 5.21 Post-layout transient response of new filter to 10 MHz 100 μ A and 50 MHz 10 mA signals.

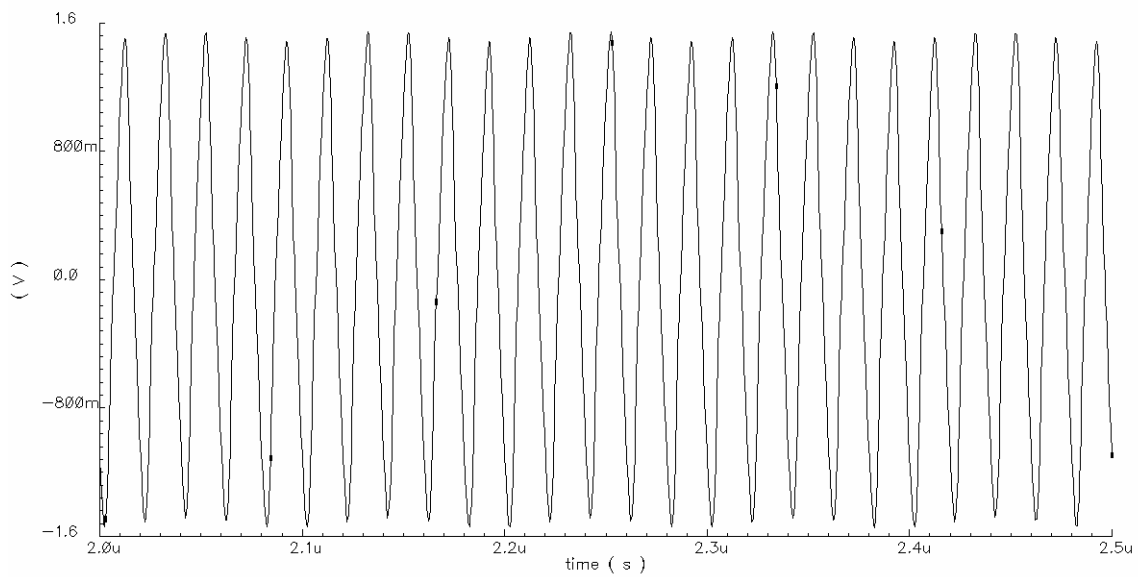


Fig. 5.22 Post-layout transient response of original filter to 10 MHz 100 μ A and 50 MHz 10 mA signals.

The frequency components of Figs. 5.21 and 5.22 are displayed in Figs 5.23 and 5.24, respectively. The DFT window is rectangular with a width of 500 ns, and $N = 512$ samples. The 50 MHz tone of the original filter response is about 7 dB larger than that of the new filter.

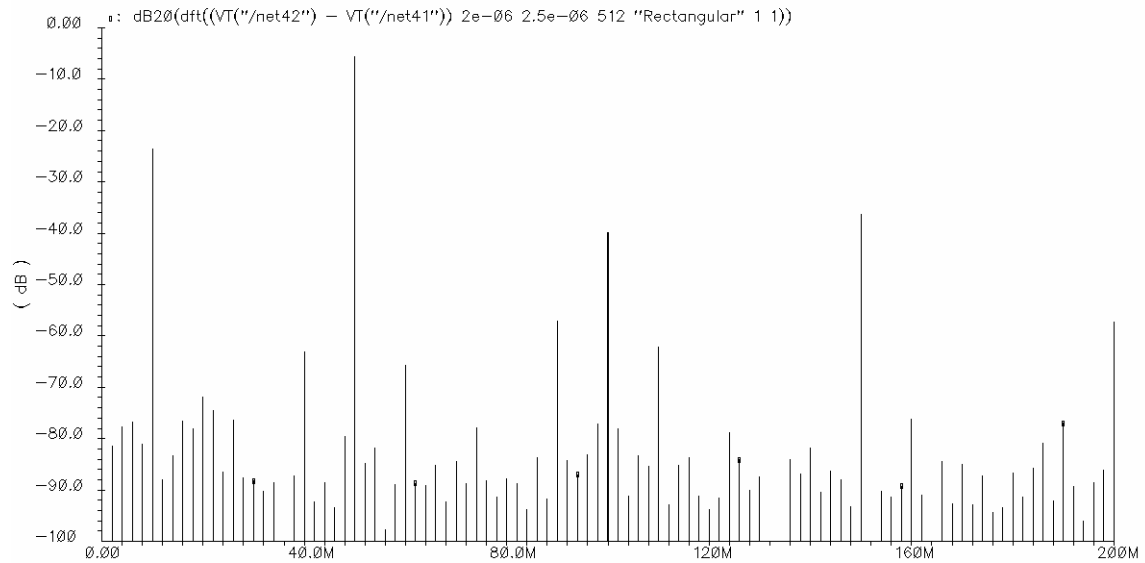


Fig. 5.23 Post-layout DFT of response of new filter to 10 MHz 100 μ A signal and 50 MHz 10 mA interferer.

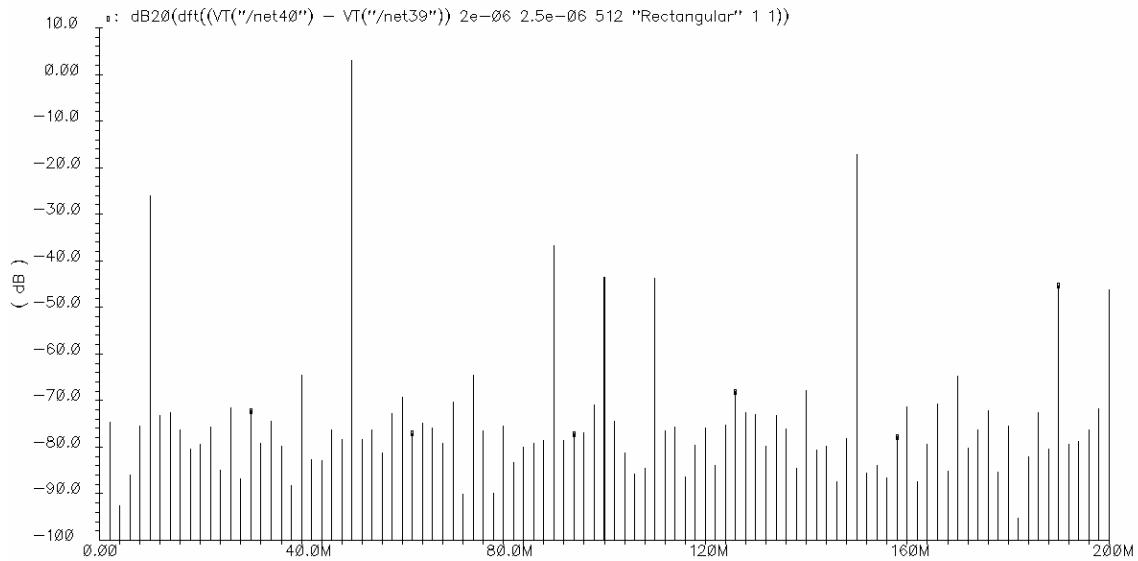


Fig. 5.24 Post-layout DFT of response of original filter to 10 MHz 100 μ A and 50 MHz 10 mA interferer.

Fig. 5.25 shows the input referred spot noise current density for the new filter and the original filter. As in the pre-layout simulations, the noise of the new filter is larger than the original. Also, Fig. 5.25 is only valid from 1 kHz to 10 MHz, since after 10 MHz, most of the input noise current is diverted to the new filter and does not show up at the original filter output. The noise summary is shown in Table 5.2.

Table 5.2 – Post-Layout Noise Summary.

Filter	Integrated Noise (1 kHz – 10 MHz) [nA]
New Filter	242
Original Filter	56.3

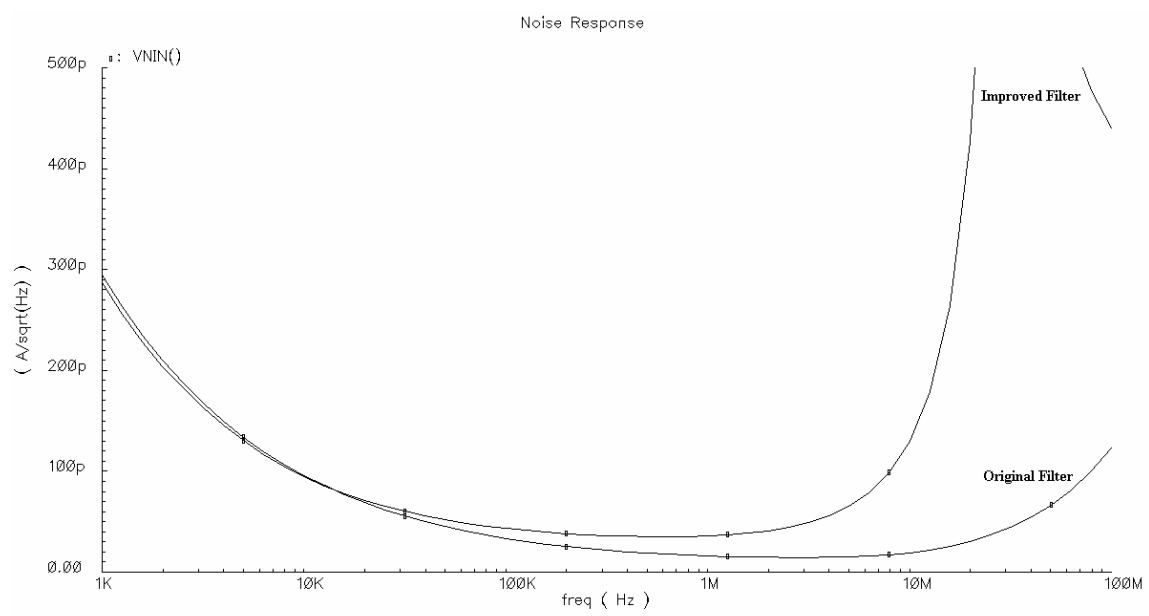


Fig. 5.25 Post-layout simulation of input referred spot noise current density.

CHAPTER VI

CONCLUSION

In this thesis, an improved low-pass transimpedance filter is designed in Jazz 0.18 μm process. The original one-pole low pass filter from [4] is also designed in Jazz 0.18 μm , and the simulation results of both are compared. Since the input to a transimpedance circuit is current, the designed filter utilizes the current divider concept to attenuate stop-band interferers. The new circuit is placed in parallel with the existing TIA filter and draws current signals away from the TIA filter by shaping a passive impedance. The passive impedance is a large capacitor which is multiplied at high frequencies by way of a sharp high pass filter. Capacitive multiplication is based on Miller's well-known theorem [5].

The existing one pole filter with 10 MHz bandwidth has less than 15 dB attenuation of interferers at 50 MHz, which may not be enough to prevent the filter from saturating if supply voltage is low and the interferer is very large. The designed filter sinks the large interfering current away from the TIA filter which prevents saturation and relaxes requirements on the digital filtering blocks. In schematic level simulations, interferers at 40 MHz and 50 MHz are rejected by 30 dB and 35 dB, respectively. In post-layout simulations, 40 MHz and 50 MHz attenuations are greater than 25 dB.

In addition to improved rejection, by sinking the large interferers away from the filter, the voltage swing at the input, and thus in the input impedance, is significantly reduced. Reduced input voltage swing increases the linearity of both the transimpedance

filter and the preceding mixer block. It has been shown that in-band intermodulation harmonics can be reduced by 10 dB.

Improvements can be made to the filter as technology size is reduced. Smaller parasitics increase the bandwidth of the new filter amplifier making it better able to process large currents at higher frequencies. This will increase attenuation of stop-band tones and reduce the overall filter input impedance.

Even if amplifiers with extremely high GBW are employed, there are still some issues that arise because of the nature of the passive RC network which defines the filter response. One disadvantage of the design in this thesis is the small ringing that is observed in the transient step response. Another disadvantage is the large capacitor sizes that must be used to meet the low-voltage high-current requirements of the receiver. Finally, the power consumption of the filter amplifier is around twice that of the original TIA. Increased power consumption is to be expected since the filter amplifier is required to process much larger signals at much higher frequencies than the TIA. However, future research should be devoted to finding improvements and solutions to these drawbacks.

REFERENCES

- [1] B. Razavi, *RF Microelectronics*, Upper Saddle River, NJ: Prentice Hall, 1998.
- [2] J. Tsividis, *Operation and Modeling of the MOS Transistors*, 2nd ed., Boston, MA: McGraw-Hill, 1999.
- [3] S. Zhou and M.-C. F. Chang, “A CMOS passive mixer with low flicker noise for low-power direct conversion receiver,” *IEEE J. Solid-State Circuits*, vol. 40, pp. 1084 – 1093, May 2005.
- [4] J-H C. Zhan, B. R. Carlton, and S. S. Taylor, “A broadband low-cost direct-conversion receiver front-end in 90 nm CMOS,” *IEEE J. Solid-State Circuits*, vol. 43, pp. 1132 – 1137, May 2008.
- [5] J. M. Miller, “Dependence of the input impedance of a three-electrode vacuum tube upon the load in the plate circuit,” *Scientific Papers of the Bureau of Standards*, vol. 15, pp. 367 – 385, 1920.
- [6] B. Razavi, *Design of Analog CMOS Integrated Circuits*, New York: McGraw-Hill, 2001.

- [7] J. F. Duque-Carillo, “Control of the common-mode component in CMOS continuous-time fully differential signal processing,” *Analog Integrated Circuits and Signal Processing*, vol. 4, pp. 131 – 140, 1993.
- [8] P. E. Allen and D. R. Holberg, *CMOS Analog Circuit Design*, New York: Oxford University Press, 2nd ed., 2001.
- [9] M. Valla, G. Montagna, R. Castello, R. Tonietto, and I. Bietti, “A 72-mW CMOS 802.11a direct conversion front-end with 3.5-dB NF and 200-kHz 1/f noise corner,” *IEEE J. Solid-State Circuits*, vol. 40, pp. 970 – 977, April 2005.

APPENDIX A

ADDITIONAL TRANSIMPEDANCE AND INPUT IMPEDANCE EQUATIONS

The input impedance of the TIA block can be expressed by the following equation:

$$Z_{i,TIA} = \frac{R_{TIA} (s + \omega_p)}{s^2 R_{TIA} C_{TIA} + s(1 + A_v' \omega_p R_{TIA} C_{TIA}) + A_v' \omega_p} \quad (A.1)$$

where A_v is the gain of the existing TIA op amp, $A_v' = 1 + A_v$, ω_p is the TIA op amp dominant pole, and R_{TIA} and C_{TIA} are the feedback impedances. (It is assumed that the first non-dominant pole is at much higher frequencies than ω_p and thus does not affect $Z_{i,TIA}$ very much at frequencies below GBW). Then putting $Z_{i,TIA}$ in parallel with Z_i (3.21) gives the full equation for the total input impedance:

$$Z_{i,tot} = \frac{R_{TIA} (s^3 (R^2 C^2) + s^2 (R^2 C^2 \omega_p) + s + \omega_p)}{s^4 (R_{TIA} R^2 C^2 (C_{TIA} + C_{fb} (C + N(C + 2C_x))))} \quad (A.2)$$

$$+ s^3 \left(R^2 C^2 (1 + A_v' \omega_p R_{TIA} C_{TIA}) + \omega_p R^2 C R_{TIA} C_{fb} (C + N(C + 2C_x)) \right)$$

$$+ 2 R R_{TIA} C_{fb} N (2C + C_x)$$

$$+ s^2 (R_{TIA} C_{TIA} + A_v' \omega_p R^2 C^2 + 2 R C_{fb} \omega_p R_{TIA} N (2C + C_x) + R_{TIA} C_{fb} (N + 1))$$

$$+ s (\omega_p R_{TIA} C_{fb} (N + 1) + 1 + A_v' \omega_p R_{TIA} C_{TIA})$$

$$+ A_v' \omega_p$$

Equation (A.2) represents the total input impedance $Z_{i,tot}$ neglecting C_{hf} . The equation for the overall transfer function is:

$$\frac{v_o}{i_i} = -\frac{A_v R_{TIA}}{s((1 + A_v)R_{TIA}C_{TIA} + C_{hf}R_{TIA}) + ((1 + A_v) + (R_{TIA}/Z_i))} \quad (A.3)$$

where $R_{TIA} = 1 \text{ k}\Omega$, $C_{TIA} = 15.91 \text{ pF}$ and A_v is the gain of the existing TIA op amp.

If $A_v \rightarrow \infty$, then (A.3) reduces to the expected first order equation:

$$\frac{v_o}{i_i} = -\frac{R_{TIA}}{s(R_{TIA}C_{TIA}) + 1} \quad (A.4)$$

If the existing TIA's dominant parasitic pole at ω_p is included, then equation (A.3) becomes:

$$\begin{aligned} \frac{v_o}{i_i} = & -\frac{A_v R_{TIA}}{s^2 \left(\frac{1}{\omega_p} (R_{TIA}C_{TIA} + C_{hf}R_{TIA}) \right)} \\ & + s \left((1 + A_v)R_{TIA}C_{TIA} + C_{hf}R_{TIA} + \frac{1}{\omega_p} \left(1 + \frac{R_{TIA}}{Z_i} \right) \right) \\ & + \left((1 + A_v) + \left(\frac{R_{TIA}}{Z_i} \right) \right) \end{aligned} \quad (A.5)$$

Putting (3.21) into (A.3) gives the following transimpedance transfer function:

$$\begin{aligned}
\frac{v_o}{i_i} = & - \frac{s^2 (R^2 C^2 A_v R_{TIA} \omega_p) + A_v R_{TIA} \omega_p}{s^4 (R^2 C R_{TIA} (C(C_{TIA} + C_{hf}) + C_{fb} (C + N(C + 2C_x)))) +} \\
& s^3 \left(\omega_p R^2 C^2 (A_v' R_{TIA} (C_{TIA} + C_{hf})) + R^2 C^2 + 2 R R_{TIA} C_{fb} N(2C + C_x) \right) + \\
& s^2 \left(R_{TIA} (C_{TIA} + C_{hf}) + R_{TIA} C_{fb} (1 + N) + \omega_p A_v' R^2 C^2 \right) + \\
& s \left(1 + \omega_p (A_v' R_{TIA} C_{TIA} + C_{hf} R_{TIA} + R_{TIA} C_{fb} (N + 1)) \right) + \\
& A_v' \omega_p
\end{aligned} \tag{A.6}$$

where N is found in (3.23) and:

$$A_v' = 1 + A_v \tag{A.7}$$

APPENDIX B

OPEN LOOP TRANSFER FUNCTION OF AUXILIARY FILTER

The open loop transfer function of the circuit shown in Fig. B.1 is:

$$\frac{v_o}{v_i} = - \frac{s^2 \left(\frac{R^2 C_{in} C}{C_x} (C + 2C_x) \right) + s \left(\frac{2RC_{in}}{C_x} (2C + C_x) \right) + \frac{C_{in}}{C_x}}{s^2 (R^2 C^2) + 1} \quad (\text{B.1})$$

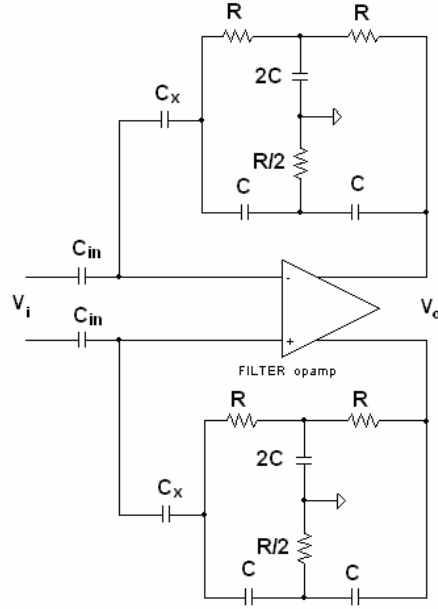


Fig. B.1 Open loop high-pass filter with ideal amplifier.

Substituting N from (3.23) into (B.1), then the reduced equation is:

$$\frac{v_o}{v_i} = -\frac{s^2(R^2CN(C+2C_x)) + s(2RN(2C+C_x)) + N}{s^2(R^2C^2) + 1} \quad (\text{B.2})$$

APPENDIX C

PARAMETRIC, CORNER, MONTE CARLO, AND PARASITIC SIMULATIONS

All simulations in Appendix C were done on a circuit designed in TSMC 0.18 μm . Results show the impact of process and temperature variations on filter performance.

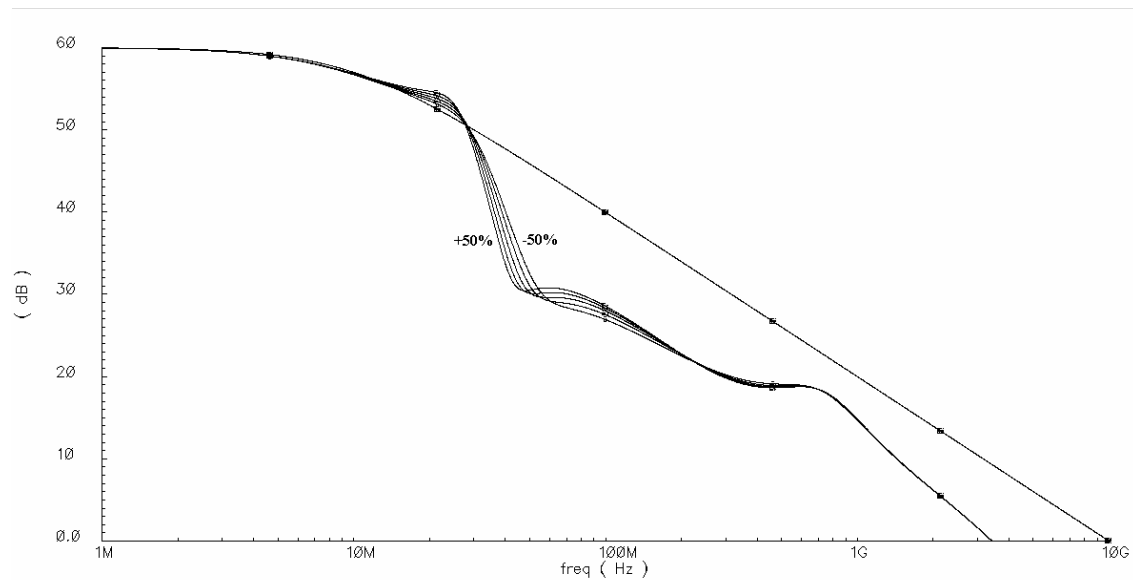
Part 1: Parametric Sweeps

Fig. C.1 $\pm 50\%$ variation in one R in twin-T (same R for both sides of differential circuit).

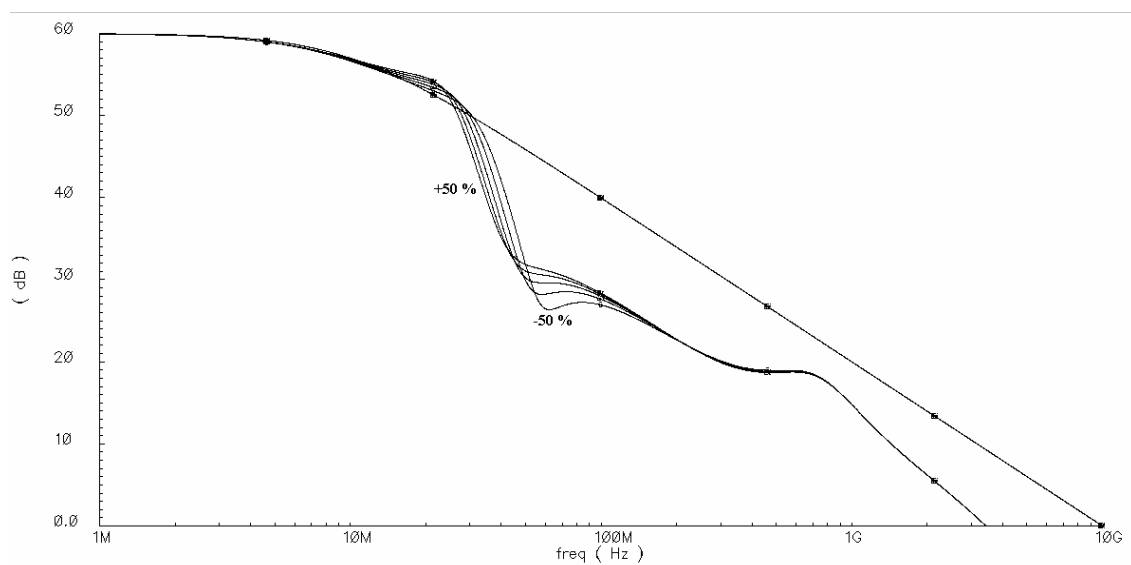


Fig. C.2 $\pm 50\%$ variation in one C in twin-T (same C for both sides of differential circuit).

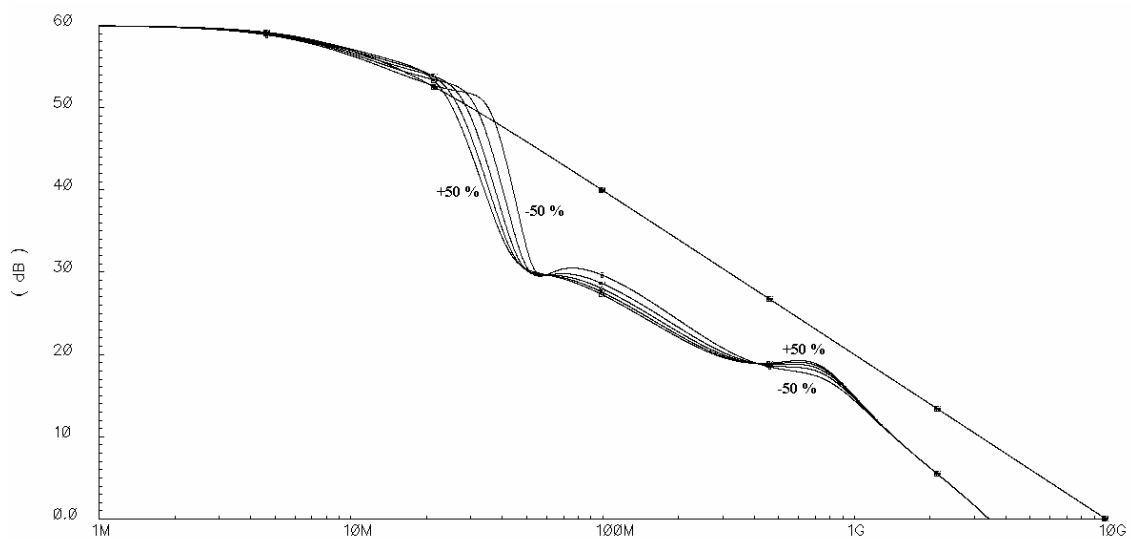


Fig. C.3 $\pm 50\%$ variation in C_{in} (same for both sides of differential circuit).

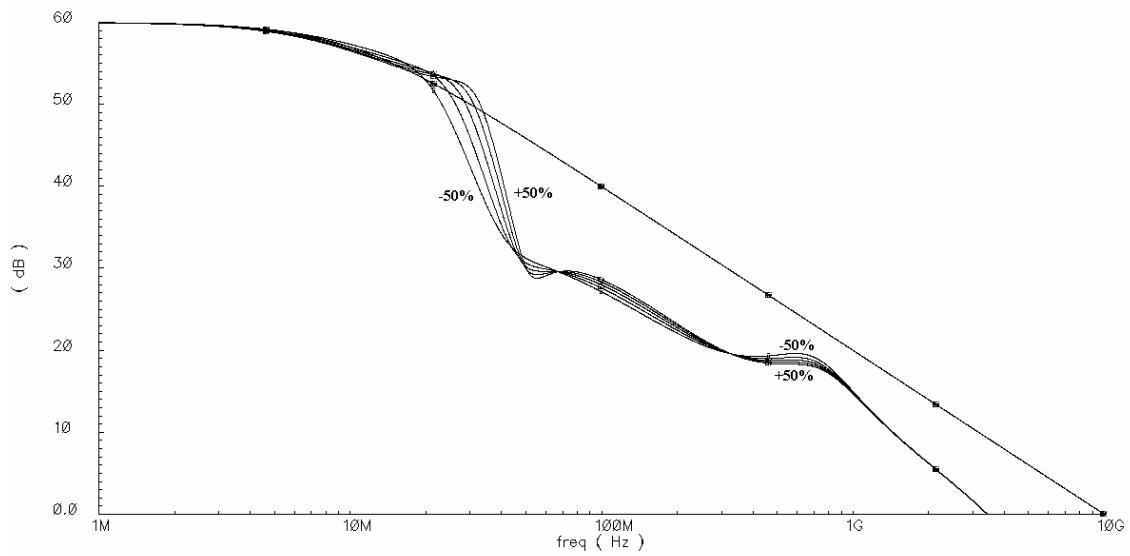


Fig. C.4 $\pm 50\%$ variation in C_x (same for both sides of differential circuit).

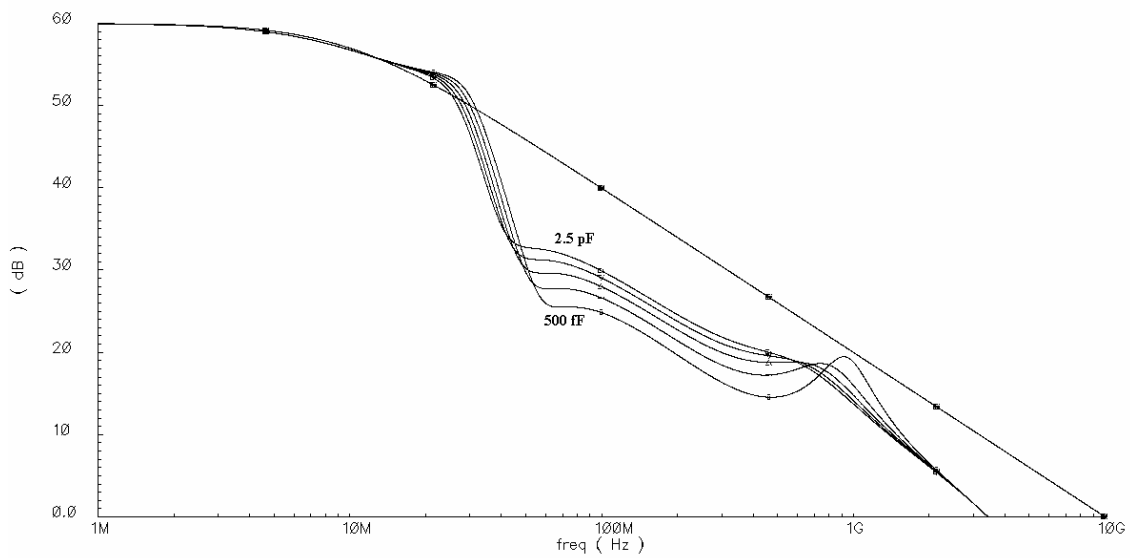


Fig. C.5 Variation in C_{TIA} . Larger value reduces TIA bandwidth which increases rejection.

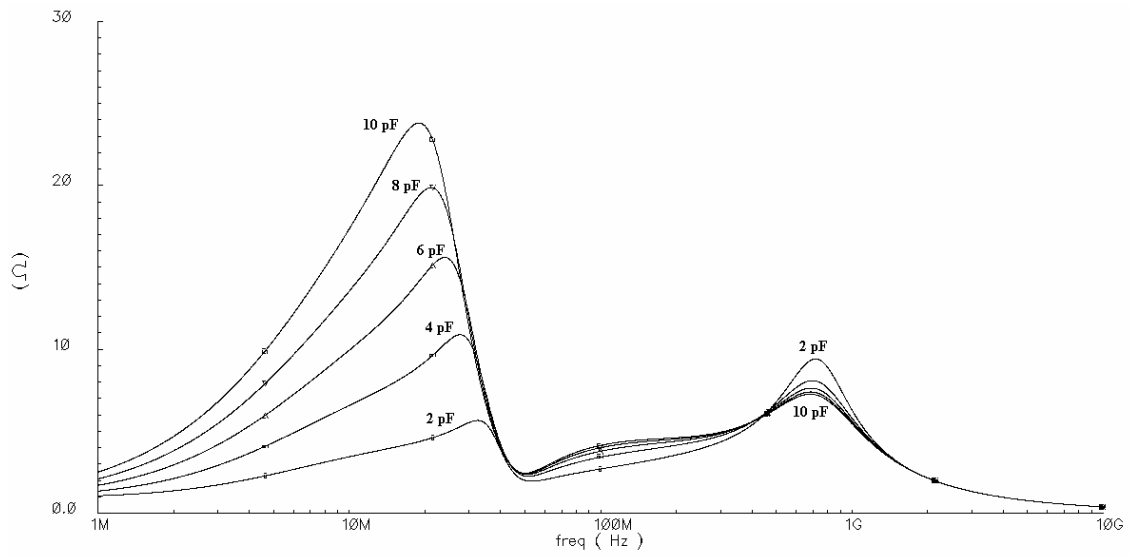


Fig. C.6 Variation in $C_{C,TIA}$. Larger value reduces TIA bandwidth which increases circuit input impedance.

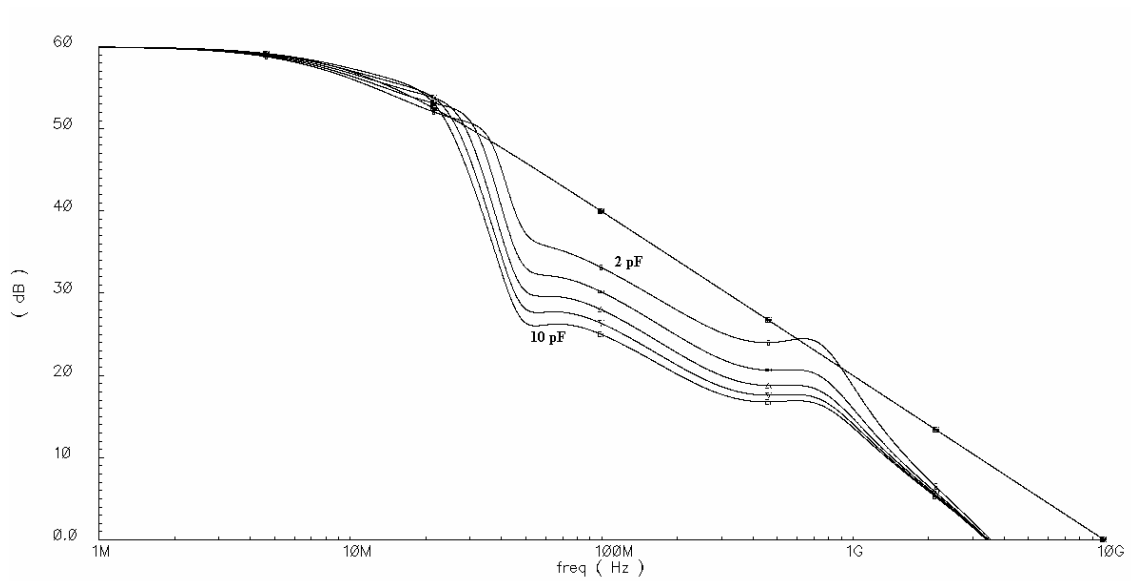


Fig. C.7 Variation in $C_{C,FilterAmp}$. Larger value reduces filter amplifier bandwidth which decreases rejection.

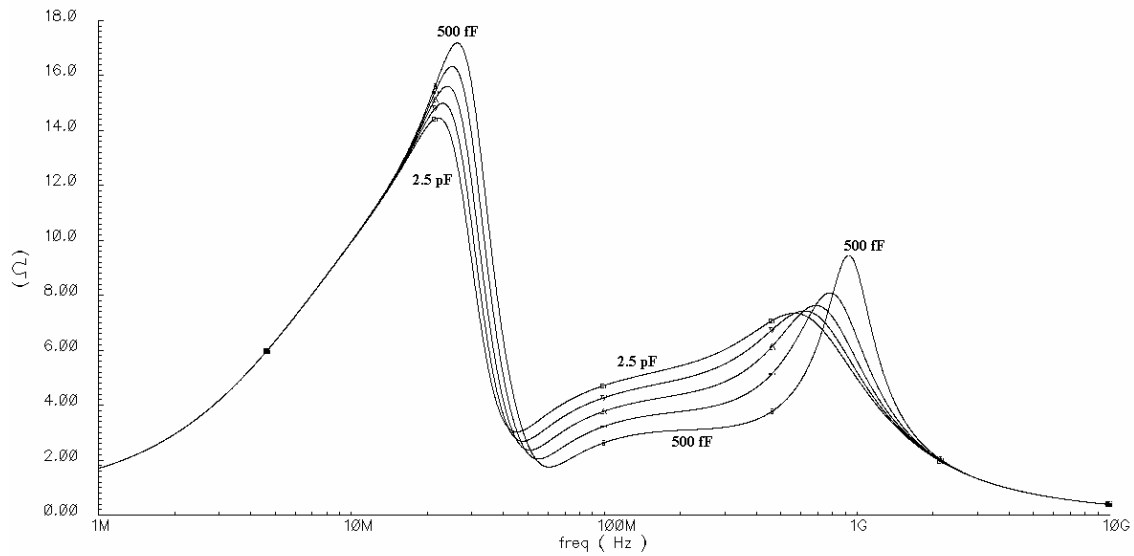


Fig. C.8 Variation in $C_{C,FilterAmp}$.

In Fig. C.8, larger $C_{C,FilterAmp}$ reduces input impedance before “notch”, but increases it after “notch”, though high frequency spike in impedance may occur for small values if C_{hf} is not large enough.

Part 2: Corner Simulations

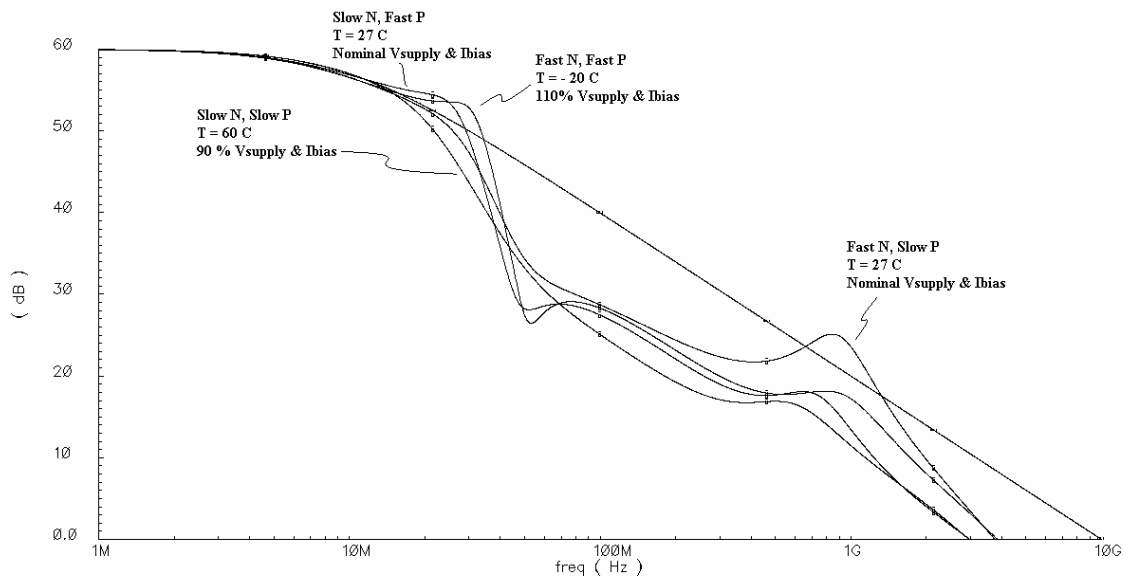


Fig. C.9 AC results of corner simulations. Curves for fast/slow and slow/fast are run with nominal supply voltage and current and at $T = 27^\circ\text{C}$. Fast/fast corner is run with 110% supply voltage and current and at $T = -20^\circ\text{C}$. Slow/slow corner is run with 90% supply voltage and current and at $T = 60^\circ\text{C}$.

In Fig. C.9, the high frequency bump for the fast/slow corner does not have a significant effect on transient response, but does reduce rejection and increase input impedance. It can be improved with larger C_{hf} as shown in Fig. C.10.

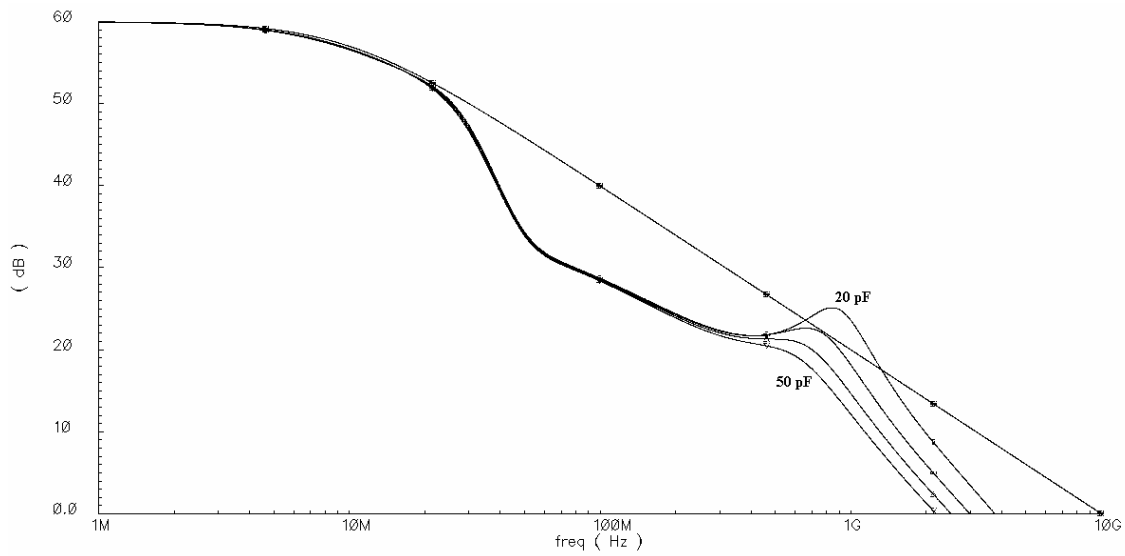


Fig. C.10 AC result for fast/slow corner and sweep of C_{hf} . The high frequency bump is reduced for larger C_{hf} .

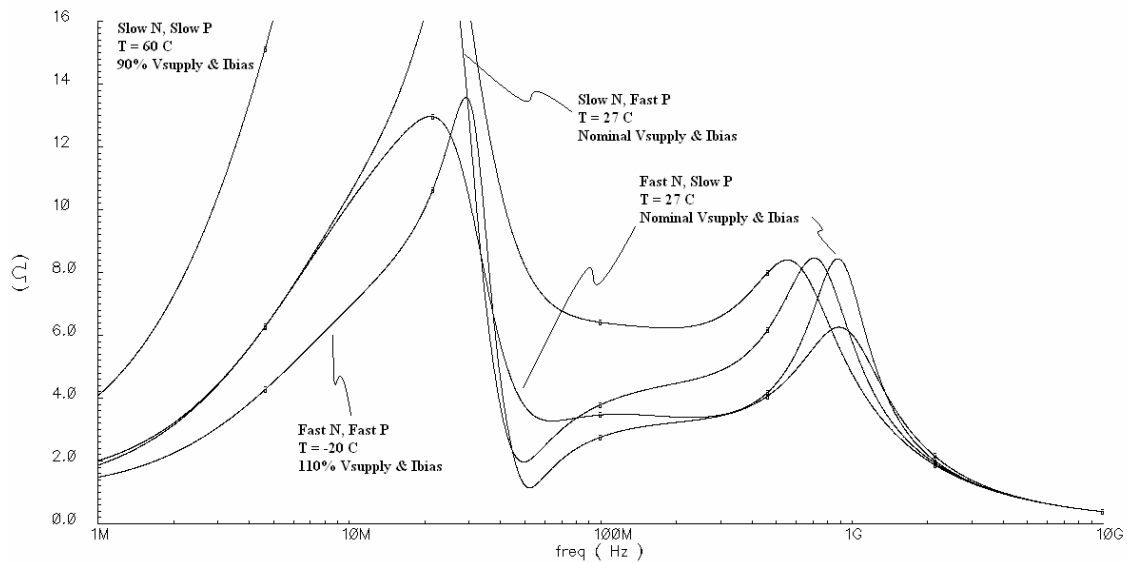


Fig. C.11 Input impedance corner simulations. Curves for fast/slow and slow/fast are run with nominal supply voltage and current and at $T = 27^\circ\text{C}$. Fast/fast corner is run with 110% supply voltage and current and at $T = -20^\circ\text{C}$. Slow/slow corner is run with 90% supply voltage and current and at $T = 60^\circ\text{C}$. The slow/fast corner peaks at $18\ \Omega$, and the slow/slow corner peaks at $28\ \Omega$.

Part 3: Monte Carlo Simulations

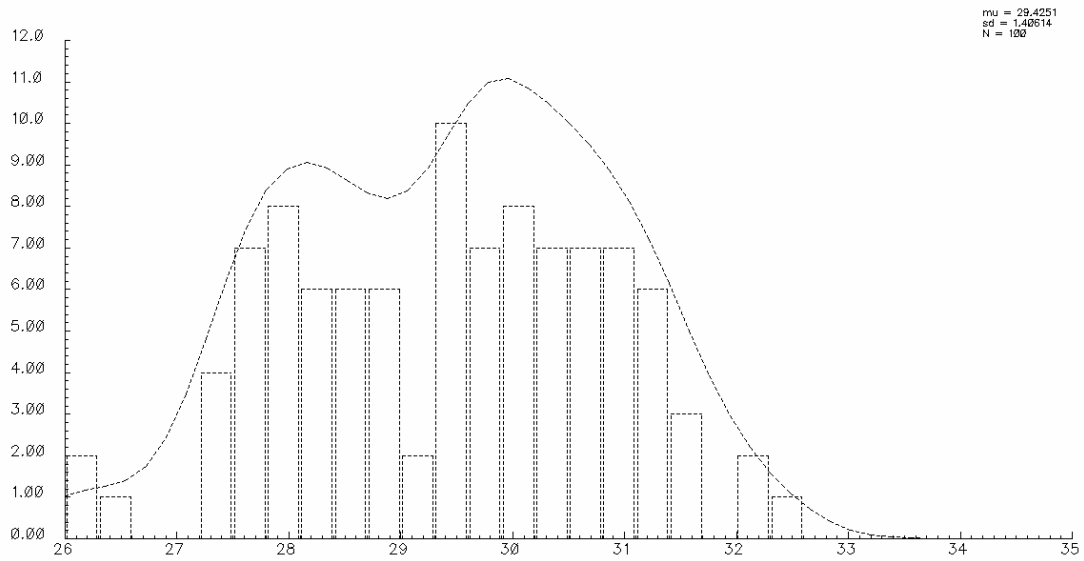


Fig. C.12 Histogram showing filter rejection at 50 MHz. Average rejection (from 60 dB) is 29 dB with a standard deviation of 1.4 dB.

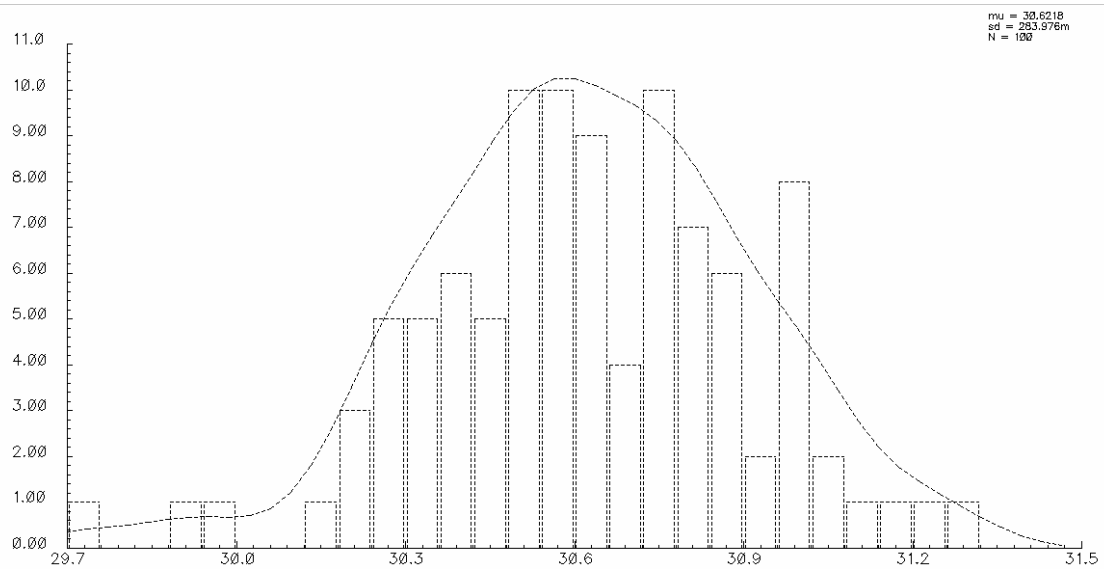


Fig. C.13 Histogram showing filter rejection at 75 MHz. Average rejection (from 60 dB) is 31 dB with a standard deviation of 0.3 dB.

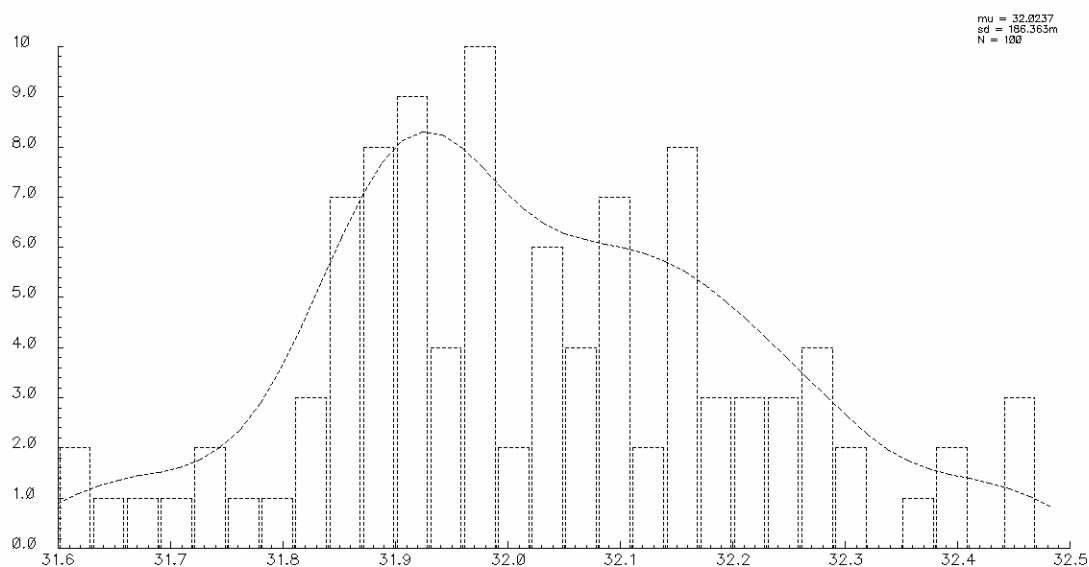


Fig. C.14 Histogram showing filter rejection at 100 MHz. Average rejection (from 60 dB) is 32 dB with a standard deviation of 0.2 dB.

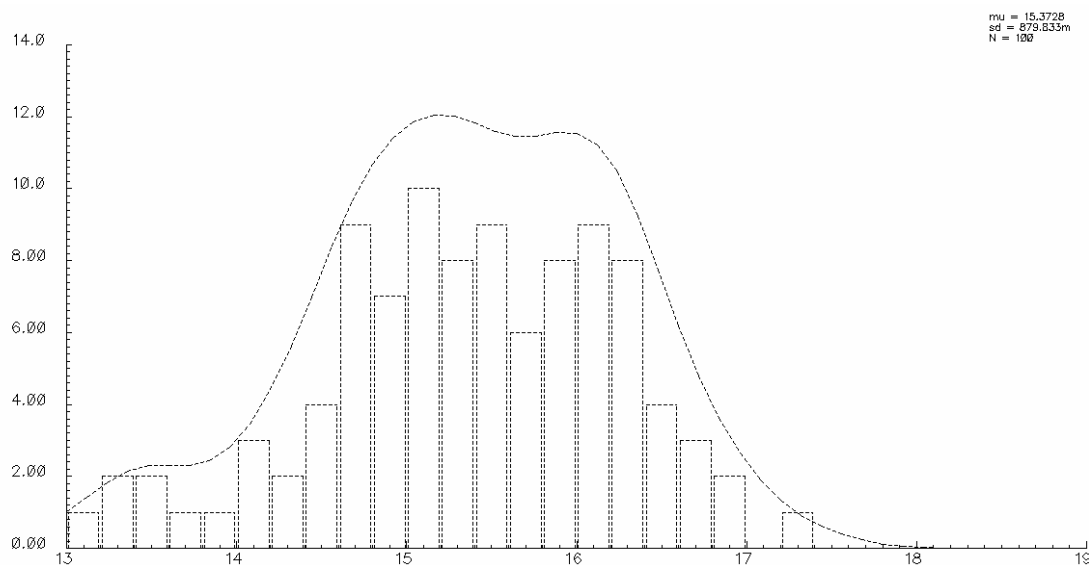


Fig. C.15 Histogram showing maximum input impedance. Average maximum input impedance is 15.4 Ω with a standard deviation of less than 1 Ω .

Part 4: Parasitic Simulations

Grounded parasitic capacitors at each node are defined in terms of percent of the total capacitance connected to that particular node. Sweeps are done from 1% to 100%. From Fig. C.16, more parasitics reduce the rejection from edge of bandwidth up to about 300 MHz, at which point the parasitic capacitors tend to increase rejection.

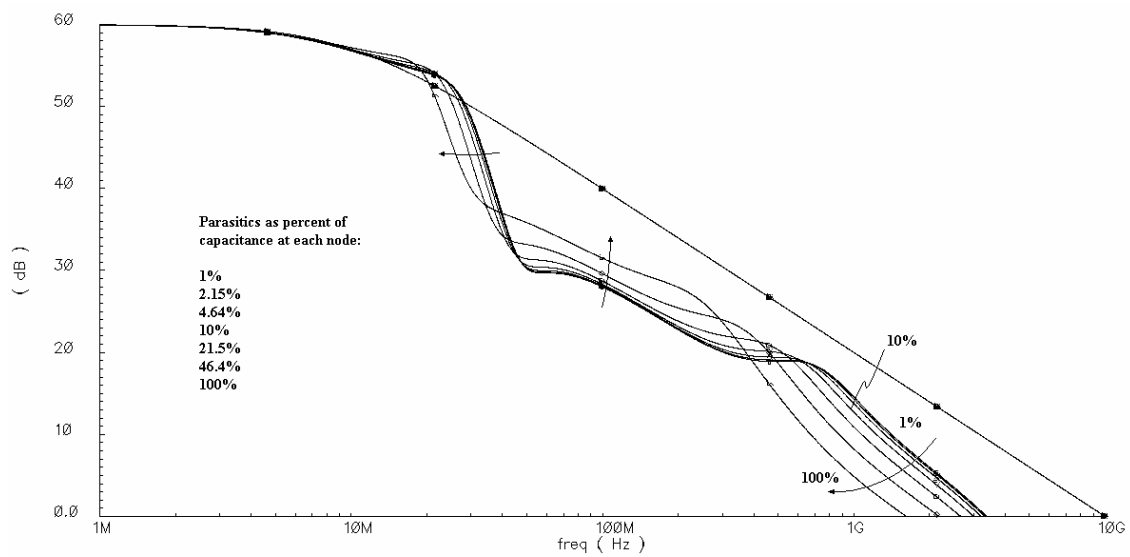


Fig. C.16 Transimpedance gain for parasitic sweep.

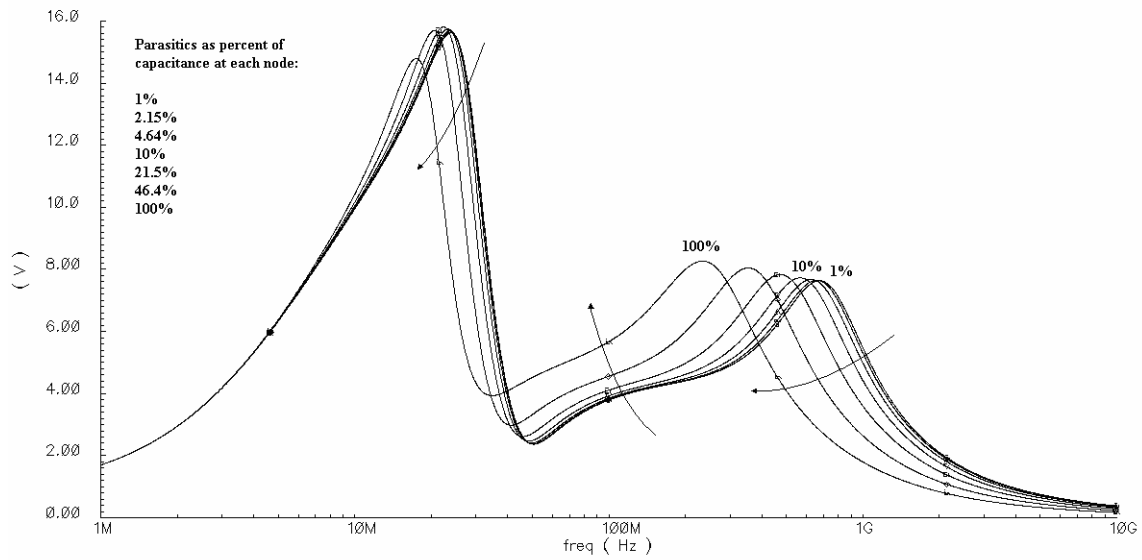


Fig. C.17 Input impedance for parasitic sweep.

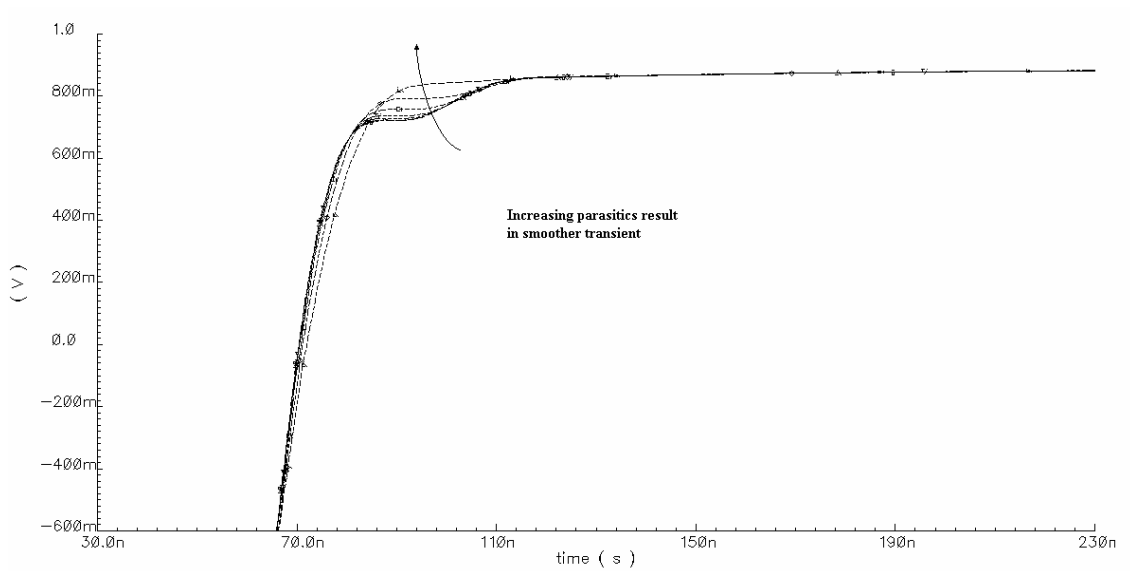


Fig. C.18 Transient step response for parasitic sweep.

In Fig. C.17, more parasitics reduce Z_i from edge of bandwidth up to the notch, increase Z_i from notch to about 300 MHz, then once again reduce Z_i . In Fig C.18, more

parasitics reduce ringing in the step response. Fig. C.19 shows more parasitics increase in-band noise levels.

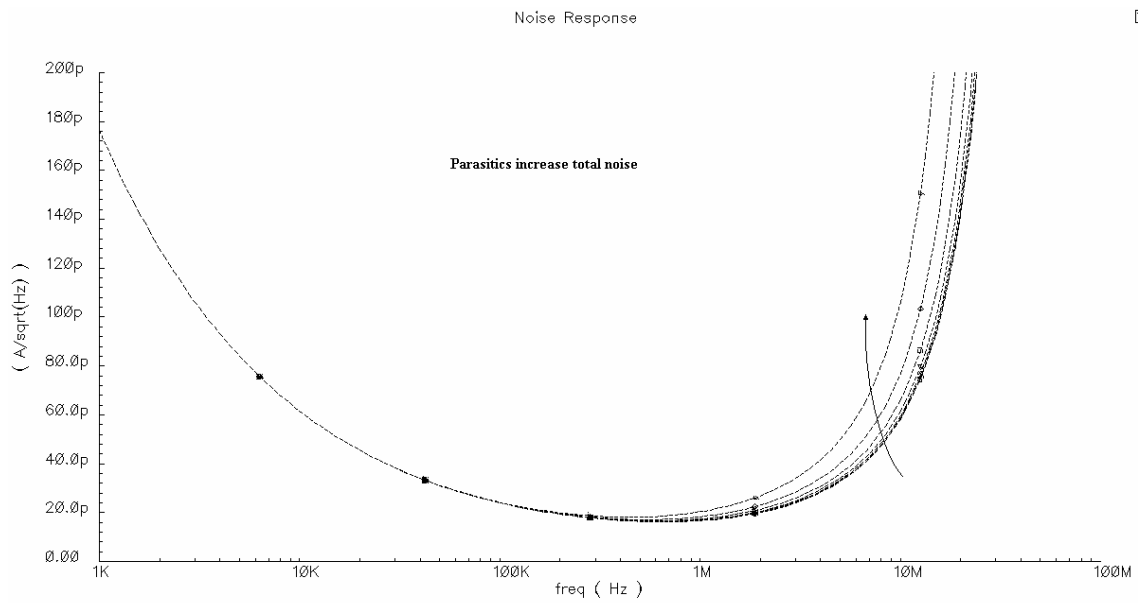


Fig. C.19 Input referred spot noise current for parasitic sweep.

VITA

Name: James Keith Hodgson

Address: Department of Electrical and Computer Engineering,
Texas A&M University
214 Zachry Engineering Center
TAMU 3128
College Station, TX 77843-3128

Email Address: keith.hodgson@gmail.com

Education: B.S., Electrical Engineering, Texas A&M University, 2005
M.S., Electrical Engineering, Texas A&M University, 2009